Control of Workplace Diesel Exhaust Particulate

Final Progress Report

October 28, 2009

Alfredo J. Armendariz, Ph.D., Principal Investigator
Ali Farnoud, Ph.D., Co-Investigator

Southern Methodist University
3101 Dyer Street, Rm. 203
Dallas, TX 75205
214-768-1890
aja@lyle.smu.edu

submitted to:

Mary Pat Shanahan
Contract Specialist
National Institute of Occupational Safety and Health
Centers for Disease Control and Prevention
Procurement and Grants Office, Field Branch V
626 Cochrans Mill Road
Pittsburgh, PA 15236-0070

Project Starting Date: 8/1/2005
Project Ending Date: 7/31/2009

TABLE OF CONTENTS

LIST OF TERMS AND ABBREVIATIONS

a	Wire diameter
b	Plate-to-plate distance in an electrostatic precipitator
A	A parameter of Peek's model for onset voltage which has the unit of electric field (V/m)
B	A parameter of Peek's model for onset voltage ($V/m^{1/2}$)
E_0	Onset electric field
δ	Relative density of the gas
V_0	Onset voltage
V_s	Sparkover voltage
T	Absolute temperature
P	Absolute pressure
i	Current per length of wire
K	Mobility of the ions $m^2/v.sec$
M	Empirical constant to calculate current in an ESP
V	Applied voltage
k	Boltzmann constant
e	Electron charge equals $1.6 * 10^{-19}$ C
$\bar{c}_i$	Average thermal velocity
N_i	Number concentration of the particle
τ	Dimensionless parameter representing time
d_p	Particle diameter$q(t)$ Charge on the particle at a time t
t	Time
E	Applied electric field
K_E	A constant in Coulomb's equation of electrostatic force which equals $9*10^9$ Nm^2/C^2
ξ_p	Dielectric constant of the particle. Infinite for conductive particles.
ξ_0	Vacuum permittivity. Equals $8.85 * 10^{-12}$ C/Nm^2
λ	Mean free path of air molecules
C_D	Drag coefficient
L	Length of the ESP collection plates

w	Particle migration velocity
F	Electrostatic force
q	Charge on the particle (Coulomb)
n_F	Number of imparted electron charges due to the electric field
n_E	Number of imparted electron charges due to diffusion
V_{TE}	Terminal electrical velocity
C_c	Cunningham correction factor
ρ	Density
Q	Flow rate
w_e	Effective migration velocity
Eff	Efficiency of the ESP

ABSTRACT

Diesel engines are the most efficient internal combustion engines. The exhaust from these engines, however, has been linked to occupational cancers in workers who spend significant amounts of time near diesel vehicles or diesel machinery. Methods developed so far to reduce exposures to the particulate matter (PM) found in diesel exhaust emissions have focused on the use of mechanical filters. Some of these systems have shown good performance in occupational applications, but even the most advanced mechanical filters have limitations. Many can create a backpressure which will cause increased fuel consumption. In addition, mechanical filters need to be regenerated periodically to reduce back pressure and prevent plugging, which can be a complex process.

The primary objective of this study was to lower the incidence of occupational lung cancers through the development of a technique to reduce diesel particulate matter emissions into the workplace. This study focused on a novel electrostatic precipitation (ESP) technique to capture diesel particulate matter. Large-scale electrostatic precipitators have been widely used in heavy industry and utilities for more than a century, but they have not been successfully miniaturized for particulate removal from mobile sources or diesel powered machinery.

Fundamental studies were performed in the laboratory to understand the important electrostatic properties of small-scale ESPs. A small-scale ESP was constructed and tested, and several modified versions were designed to optimize performance. Tests were performed using the exhaust generated by a stationary 5.5kW diesel-powered electric generator, using different fuel qualities and at different load conditions.

The use of the small-scale ESP on the engine exhaust resulted in average reductions in particle mass emissions of approximately 80 percent at moderate levels of power consumption that never exceeded 65 watts.

This project demonstrated the feasibility of using small-scale electrostatic precipitators to lower emissions of diesel PM. The commercial development of the prototype unit developed in this project will provide industrial hygienists and machinery vendors with another option to reduce the concentration of diesel PM in the workplace, thus lowering exposures and potentially reducing the incidence of occupational lung cancer.

LIST OF FIGURES

LIST OF TABLES

SECTION 1

HIGHLIGHTS AND SIGNIFICANT FINDINGS

Design and Power Consumption – A small-scale electrostatic precipitator (ESP) was designed and constructed to capture the particles emitted in diesel exhaust from industrial and mining machinery, to reduce exposure by workers to this pollutant. High levels of performance (80-90% removal) were achieved with power consumption at levels less than typical consumption by lighting, radio, and other common electrical components of machinery and vehicles.

Particle Collection Efficiency -- The small-scale ESP was tested under a variety of conditions to investigate particle collection efficiency and gradual improvements were made to increase performance. The ESP was able to remove approximately 80 percent of the particles in the exhaust measured on a mass basis, and 90 percent of the particles in the exhaust measured on a number basis. The mass removal efficiency of the ESP was obtained at different load conditions and the effect of fuel type on the removal efficiency was investigated.

Investigation of Electrostatic Properties of Small-Scale Units – Large-scale electrostatic precipitators have been successfully used in heavy industry and utilities for many decades. One of the highlights of this project was the development of a library of carefully collected data on the physical and electrostatic properties of small ESPs. We believe that this is the most extensive empirical data ever collected on small ESP properties, and the data should help future researchers develop the technology for exhaust cleaning in additional occupational and environmental applications. Our data indicates that while the traditional electrostatic design equations work well for predicting some of the properties of small scale units, for other properties, methodology specific to small scales is required.

TRANSLATION OF FINDINGS

This project investigated the potential for small-scale electrostatic precipitators to reduce the concentrations of particulate matter being emitted in diesel exhaust. Up until now, very little was known about the practical use of small-scale ESPs in the industrial or occupational setting,

including the potential use on diesel exhaust. This project demonstrated, through the careful design, construction, and testing of a prototype, that electrostatic precipitators can achieve high levels of performance reducing emissions of diesel particulate. In those workplace environments where the latest improvements to fuel quality and engine combustion quality cannot sufficiently reduce particle emissions to safe levels, especially for tight or confined spaces such as garages and underground mines, the use of an ESP might be the ideal solution. Future work is planned for the technology to focus on the construction and job-site testing of prototype units, to gather additional information about practical durability and use, and to evaluate changes to personal exposure. There is outstanding potential for this work to translate into commercial technology that can be employed to protect workers within 3-5 years.

OUTCOMES/RELEVANCE/IMPACT

Potential outcomes: The high concentration of particulate matter in diesel exhaust has been a concern in the occupational setting for many decades. Unfortunately, reductions in particle emissions from exhausts to date have been insufficient to bring concentrations in many workplaces to recognized safe levels. This project demonstrates to engine and control system manufacturers that electrostatic precipitators can significantly reduce particle concentrations. The prototype unit developed during this project is ready for field testing and then commercialization. If deployed, these devices could provide up to 90% reductions in diesel particle concentrations in the workplace.

In addition, there are other sources of occupational particulate matter where the use of an electrostatic precipitator could be used to reduce exposures. However, the lack of empirical data on the electrostatic properties of small-scale units hampered their design and implementation. The extensive data collected by this project on the fundamental electrostatic properties of small-scale ESPs will be a significant asset to other engineering designers. The data gives them the necessary tools to predict the performance of small scale units and to design systems to meet specific applications.

SECTION 2

SCIENTIFIC REPORT

CHAPTER 1

INTRODUCTION AND MOTIVATION

1.1 Significance and Background

There has been a tremendous amount of research on adverse health effects of air pollution since the great smog of 1952 in London accelerated the modern environmental movement and resulted in Clean Air Acts in different countries. The problem was tackled by policy makers and scientists from many different angles and the epidemiological and then toxicological effects of airborne pollutants were investigated.

Advances in the field of industrial hygiene occurred almost simultaneously with concern about ambient air pollution. The wide-publicity in the 1970's surrounding black lung disease in underground coal miners, and the diseases being linked to asbestos exposure in miners and other workers in the 1960's highlighted the problem of air contaminants in certain occupations, especially those where workers spent large amount of time in confined spaces.

Of all the air pollutants in the environmental and occupational settings, particulate matter (PM) has received special attention because of its effect on visibility, strong evidence of adverse health effects, and association with cancer. A survey by the World Health Organization (WHO) showed that 12 out of 20 mega cities in the world had serious total suspended particle (TSP) problems and five of them had moderate to heavy

TSP problems (Mage *et al*, 1996). For perspective, the levels of particulate matter in Delhi, India and Shanghai, China, occasionally spike to an annual average of 400 $\mu g/m^3$ and 250 $\mu g/m^3$, many times the U.S. ambient air quality standard of 35 $\mu g/m^3$ (Gurjar *et al*, 2007).

Epidemiological studies of the effects of particulate matter on health began in the early 20th century, but the era of robust epidemiological analysis began with studies in the 1980's. These studies showed a statistically significant relationship between mortality rates and exposure to particles across a variety of locations (Evans *et al*, 1984; Ozkaynak *et al*, 1987; Lipfert *et al*, 1988). The conclusions of studies were questioned because they did not control for confounding factors like smoking and diet, and several of them examined total mortality rates, instead of mortality linked to respiratory diseases (Vedal, 1997).

Building on the work from the 1980's, additional epidemiological studies were performed in the 1990's, including a series of the first "prospective cohort studies." The "Harvard Six Cities Study" examined 8000 people in six different metropolitan areas who were followed for 14 to 16 years and their age, sex, diet, education, and all other individual factors were recorded (Dockery *et al*, 1993). The American Cancer Society study performed the same process for more than 500,000 people in 151 metropolitan areas (Pope *et al*, 1995). The results of both studies confirmed that cardiopulmonary mortality is strongly associated with airborne PM and sulfate concentration (Pope *et al.*, 1995). Because of the controversies that these studies created, an independent team from the Health Effects Institute (HEI) re-evaluated the statistical analyses, and their work verified the studies' conclusions (Krewski *et al.*, 2000a; Krewski *et al*, 2000b; Krewski *et al*, 2000c). More recent analyses of the cohorts in these studies have been performed, the associations between particulate air pollution and health outcomes have strengthened, and results are still being published (Pope *et al*, 2002; Pope *et al*, 2004; Laden *et al*, 2006).

After these two landmark U.S. studies, numerous other prospective studies examining air pollution air pollution with respiratory and cardiovascular diseases were performed in different parts of the world (Hoek *et al*, 2002; Finkelstein *et al*, 2004; Filluel *et al*, 2005).

Particulate air pollution is a complex mixture of many different chemical compounds, and the composition at a location depends on the nature of the sources in the area, plus transport into the area from other locations. Chemical analysis, source apportionment, and receptor modeling studies indicated that internal combustion engines are a major source of particulate matter in most urban areas (Swietlicki *et al*, 1996; Artaxo *et al*, 1999; Querol *et al*, 2001). A few studies have shown higher rates of mortality and morbidity in people who live close to highways (Kim *et al*, 2004; Brugge *et al*, 2007). Harrison *et al* related a major portion of particulate matter in London to vehicles; of which the contribution of diesel vehicles was much more significant than gasoline vehicles (Harrison *et al*, 1996). Another study showed similar results for city of Houston (Fraser *et al*, 2003). Diesel engines emit high concentrations of particulate matter with diameters 1 micrometer (μm) or smaller (Kittelson, 1998). These particles are readily inhalable and evidence is accumulating that these small particles are particularly harmful to human health, compared to the larger airborne particles (Chuang *et al*, 2005; Maynard and Kuempel, 2005). In a comprehensive review article, EPA summarized most of the important studies on health effects of diesel exhaust and concluded that exposure to diesel exhaust may cause lung cancer and "the particulate phase [as opposed to toxic gases] appears to have the greatest contribution to the carcinogenic effect" (EPA, 2002). Therefore, in addition to the general concern about all types and sources of airborne particulate matter, the potential effects of diesel particulate matter (DPM) are the subject of much health and engineering research.

In addition to the people exposed to diesel particulate matter in urban areas and areas around highways, millions of workers who work in mines, shipyards, railroads, and construction sites are frequently exposed to DPM. Stayner *et al* (1998) reviewed a number of toxicological and epidemiological studies and concluded that miners have an increased risk of lung cancer when exposed to DPM for long periods of time (Stayner *et al*, 1998). In spite of the concern about health impacts, diesel engines are the power source for a large portion of the world's heavy trucks, trains, ships, and construction and mining machinery. Diesel engines are more fuel efficient than gasoline engines, by approximately 30%. The good self-ignition properties of diesel fuel allow a different design in which the compression ratio can be much higher than gasoline engines (16 to 24 for diesel engines versus 7 to 9 for gasoline engines). These properties make it possible for diesel engines to function over a wide range of air to fuel ratios while gasoline can only be properly combusted over a narrow air to fuel ratio. Diesel engines also provide greater torque output at lower engine speeds than gasoline engines. The high-torque characteristics of diesel engines, the fuel economy benefits, and concerns about climate change from CO_2 emissions suggests that diesel engines will continue to be the primary heavy duty internal combustion engines for many years to come.

In spite of these great properties, the potential adverse health effects of diesel exhaust are so serious, especially in confined spaces, that states of Ohio, Pennsylvania, and West Virginia have banned or are considering banning using diesel engines in their underground mines (MSHA, 2003). A clean diesel engine can save important benefits to visibility and the clarity of atmosphere, the public health of people that live in diesel-impacted areas, and workers in industries that use diesel-powered machinery or vehicles.

1.2 Diesel Particulate Matter Composition and Structure

DPM has a very complex structure. Its formation starts in the cylinder; where precursor molecules, produced during the incomplete combustion of diesel fuel in fuel-rich zones, form very small particles of elemental carbon of the order of 2 to 3 nm diameter (Neeft *et al*, 1996). These particles gradually agglomerate and form bigger carbon particles which are around 10 to 30 nm. These particles are abundant in diesel exhaust and the mode diameter of the number size distribution happens at this diameter (Kittelson, 1998). Further agglomeration in the exhaust line and in the atmosphere grows the particles to diameters above 100 nm. Chemical analyses indicate that in addition to the agglomerated carbon, adsorbed sulfate compounds, water, and hydrocarbon vapors can also significantly contribute to the chemical composition (Liang, 2006).

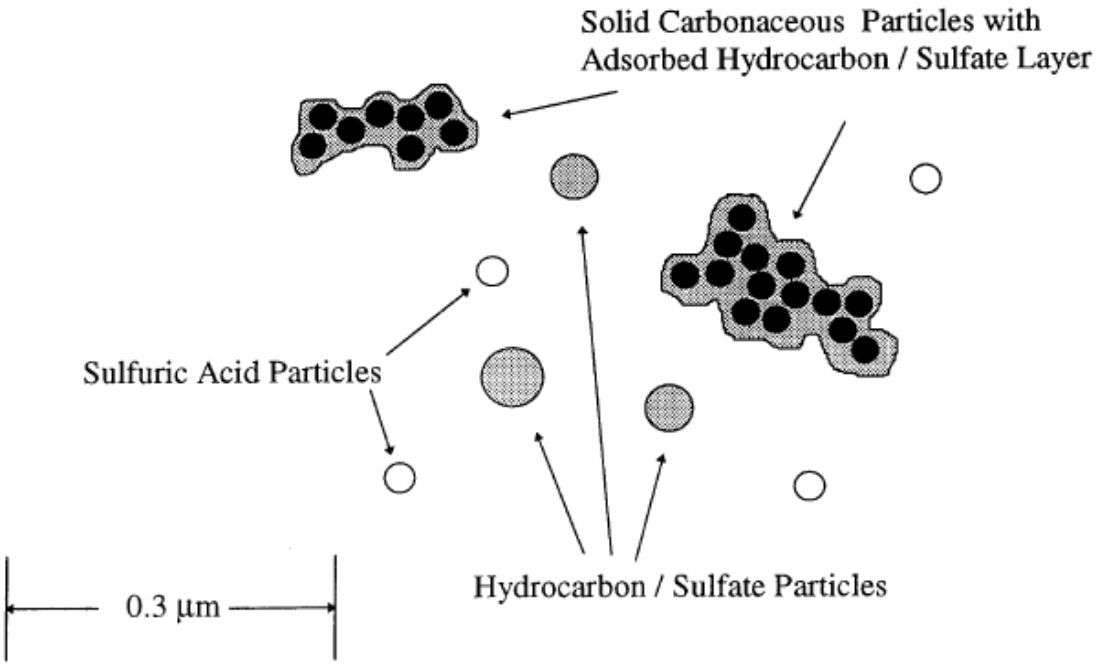

Figure 1.1 Typical composition of diesel particulate matter (Kittelson, 1998)

The hydrocarbons originate from unburned fuel and volatilized lubricating oil and are sometimes referred to as the Soluble Organic Fraction (SOF) of the diesel exhaust particles. On a

mass basis, the SOF can contribute from 10 to 90 percent of the total mass, depending on engine operating conditions. At light load conditions, the cylinder temperatures are relatively cool and insufficient to burn all the fuel vapor hydrocarbons, increasing the SOF fraction in the DPM. However, at higher loads the hydrocarbon fraction diminishes, and instead, a larger percentage of the DPM will consist of elemental carbon (Sharma *et al*, 2005). Polycyclic aromatic hydrocarbons (PAH), which are known human carcinogens, are frequently found in the SOF portion of the DPM. Therefore, the PAH content of the DPM is high at lighter loads (Tan *et al*, 2004). Regarding the sulfur present in diesel fuel, much of it will be oxidized to gaseous SO_2, but a portion of it also oxidizes to SO_3 which further nucleates into sulfuric acid and sulfate particles. Another significant component of DPM are metal oxides (a.k.a. ash) which are produced from metal compounds in the fuel and lubricating oil. All these processes will result in the complex mixture of elemental carbon, organic carbon, sulfate, sulfuric acid, and ash that forms diesel particulate matter.

On a number basis, the overwhelming number of individual DPM particles is smaller than 50 nm in diameter. On a mass basis, however, approximately 90 percent of the DPM mass at the exhaust pipe is contributed by particles in the 100-300 nm diameter range. Figure 2 shows typical size distributions of diesel particulate matter.

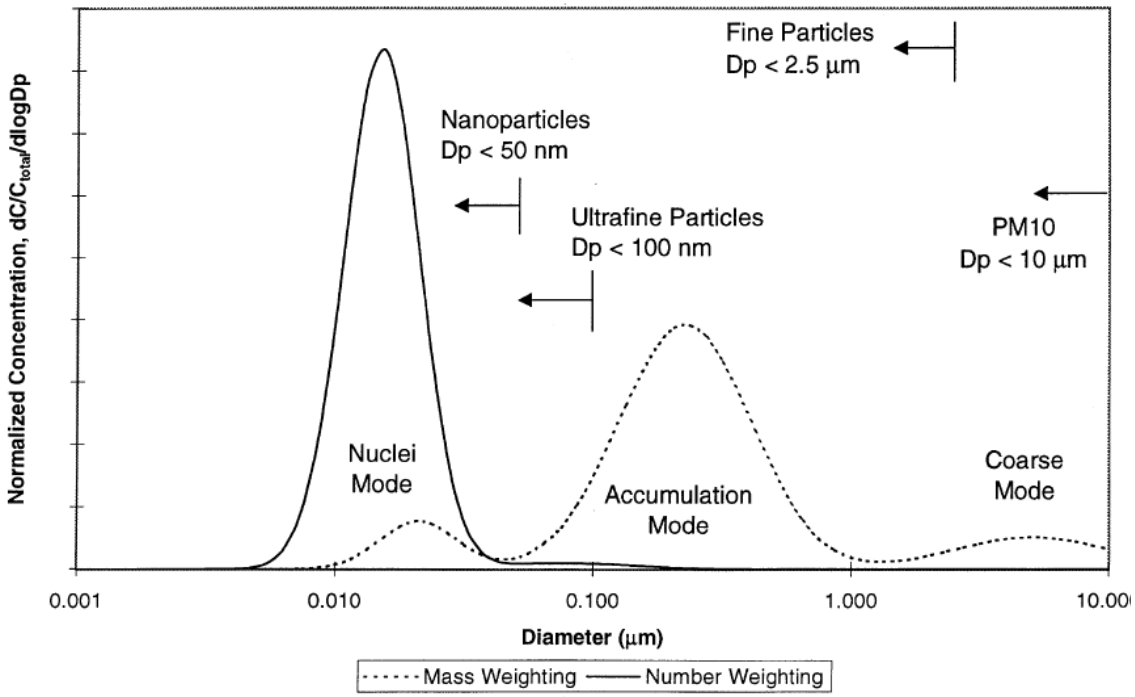

Figure 1.2 Typical diesel exhaust size distribution in terms of mass and number (Kittelson, 1998)

1.3 Emission Standards

Diesel engines were introduced to the roads of the United States in the 1940's and quickly dominated the trucking industry. They accounted for 36 percent of the heavy duty truck sales in 1960 and virtually 100 percent of sales in 1997 (EPA, 2002). Based on the epidemiological and toxicological studies, EPA and other agencies like the Mine Safety and Health Administration (MSHA) have imposed emission standards on diesel vehicles and machinery. The first standard on diesel engines was set in 1970 which was a smoke test and was not specific about the components of the diesel exhaust (EPA, 2002). In 1988, EPA set a particulate emission standard of 0.6 grams of particulate per brake horsepower-hour was established and this standard has been periodically tightened since then (EPA, 2002). There are separate standards for different types of diesel engines. For instance, non-road diesel engines

used in construction have completely different standards from highway light-duty diesel trucks. However, all of the standards have something in common in the fact that they are getting more stringent, and the focus of regulatory attention. Figures 1 and 2 show the DPM emission regulations for on-road heavy duty trucks set by EPA and the European Union Department of Environment. The strictest U.S. standard of 0.01 g/bhp-hr took effect on engines manufactured beginning in 2007 (Federal Registry, 2001).

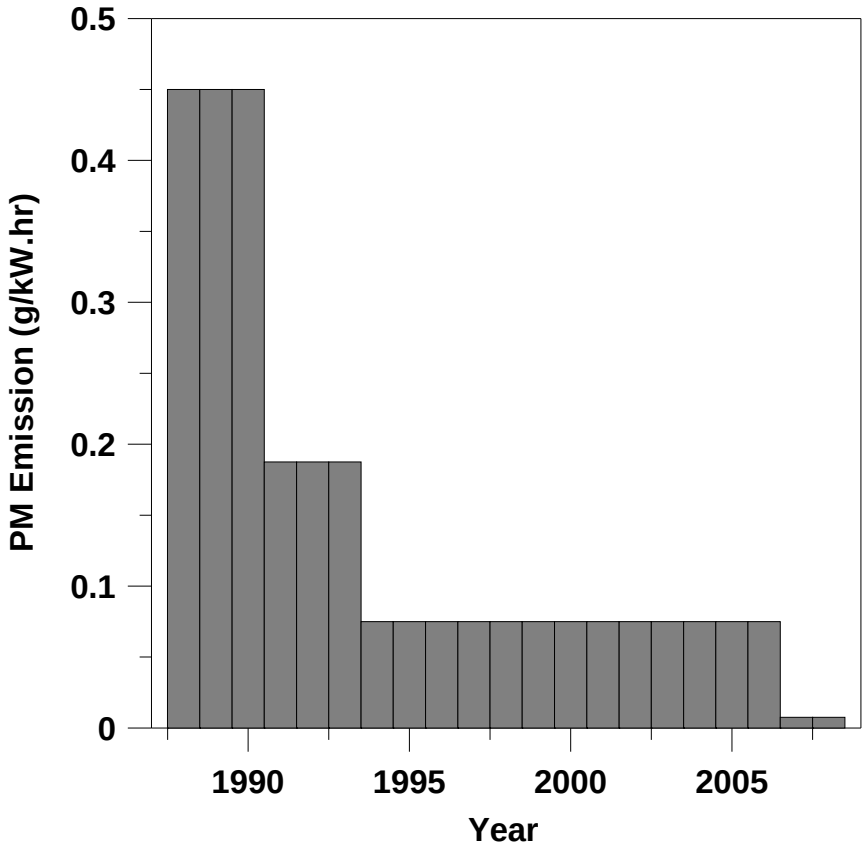

Figure 1.3 The gradual tightening of EPA DPM standards (EPA, 2002).

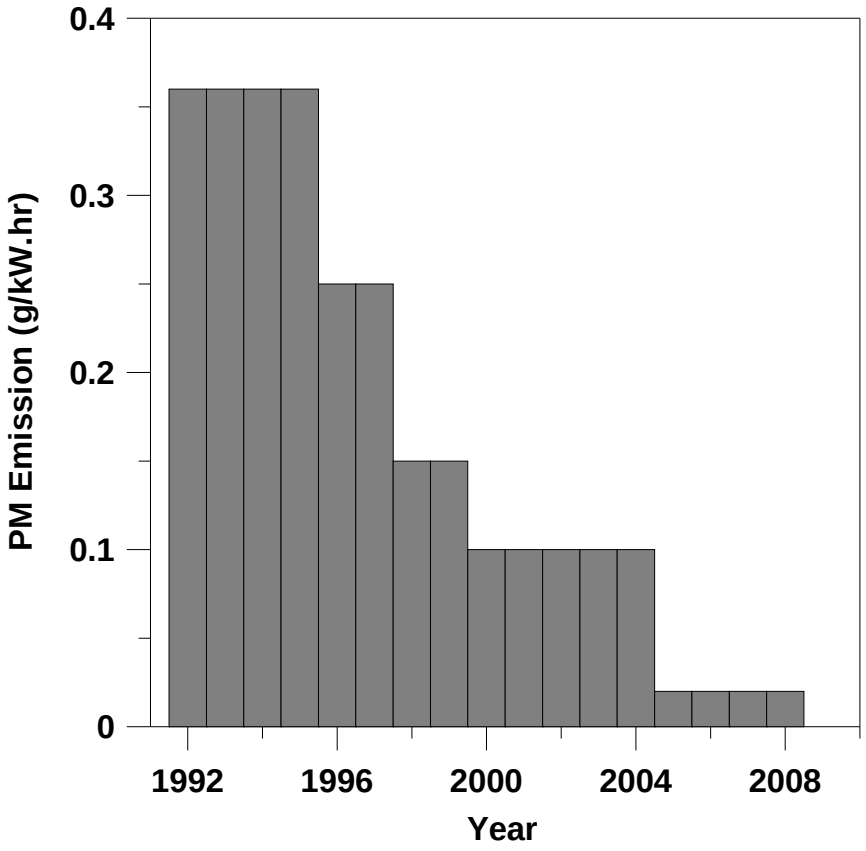

Figure 1.4 EU DPM Standards Trend (EU news, 2005)

1.4 Diesel Particulate Matter Emission Reduction Technologies:

1.4.1 Diesel Oxidation Catalysts (DOC)

Diesel oxidation catalysts use precious metals to enhance the destruction of some of the organics that comprise the soluble organic fraction (SOF) of diesel particulate, as well as gases such as CO and hydrocarbons (HC). DOCs are most effective when an engine is running at idle or at low loads and the levels of SOF on the diesel particulate can be high. To maximize the interaction of the exhaust components with the catalyst surface, a flow-through device with a high-surface area honeycomb structure is usually used. In two studies, EPA and California Air Resources Board (CARB) observed that the emission reductions produced by installed DOC

units to be 24 to 60 percent for PM, 50 to 90 percent for HC, and 45 to 98 percent for CO (EPA, 1999; CARB, 2000).

The main problem associated with the DOC is the high temperature needed for hydrocarbon oxidation, and the narrow temperature window for proper operation. DOCs convert SO_2 into SO_3 at temperatures above 300 ^oC whereas they need a minimum temperature of 200C to oxidize hydrocarbons (Guibet, 1999). SO_3 is a concern because it readily acts as a nucleation site for water and other vapors and causing a boost in the number of emitted particles. The use of Ultra Low Sulfur Diesel Fuel (ULSD) in the United States beginning in 2007 has significantly facilitated the employment of DOCs in diesel engines by reducing concerns about SO_3 formation. The installation of a DOC has been estimated to cost around $2,000 for heavy duty trucks and buses (Washington State SRP, 2003; EPA, 2003).

1.4.2 Particulate Traps

Mechanical filtration is the most straightforward way to separate suspended particles from a two-phase suspension. Mechanical filtration has been used for decades for environmental sampling, air cleaning, and industrial processes. The most developed technology for mechanical filtration of PM from diesel exhaust is known in the diesel industry as the diesel particulate filter (DPF). In any filter, pressure drop is a factor which contributes to the cost of system operation. There is a direct relationship between pressure drop and collection efficiency. Since fuel consumption is one of the most important factors in long-term costs of engine operation, it is very important to maintain as low a pressure drop as possible in any exhaust treatment device. This fact makes it difficult to design suitable filters for diesel engines because the filter must also have a very high efficiency to comply with demanding standards. DPF units must be sturdy

enough to tolerate the vibrations of the machinery, temperatures up to 400 ^{o}C during normal engine operation, temperatures up to1400 ^{o}C if the carbonaceous soot ignites, and also tolerate the stresses imposed by rapid temperature changes (Mayer, 2003).

None of the diesel filters remove the soot as a sieve removes large particles flowing in water. Instead, filtration mechanisms in diesel particulate filters rely on either shallow or deep bed filtration mechanisms. For instance, wall flow monolith filters, introduced by Corning, which are the most common type of mechanical filter on the market use surface filtration, in which a layer of soot deposits on the front edge of the filter and then that layer acts as a substrate to collect additional incoming particles. Commercialization of these filters began in the early 1980's. Figure 3 shows the structure of one of these filters, consisting of parallel channels of which half are closed at upstream end and the other half at the downstream end. This structure forces the exhaust to flow through the walls of the channels and the particles are collected on the walls. This layer of soot helps surface filters to have a very high efficiency but it also increases the pressure drop at the same time.

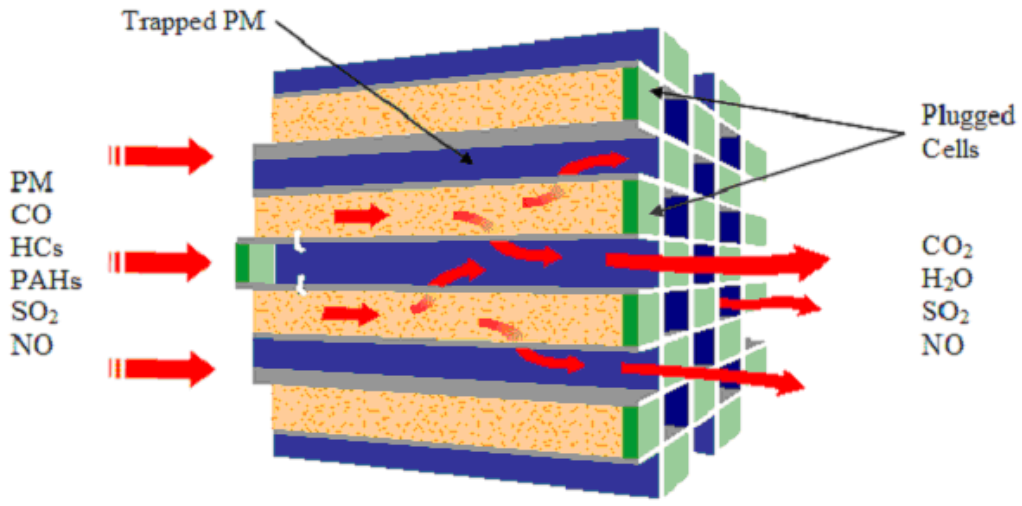

Figure 1.5 A typical diesel particulate filter (MECA, 2007)

1.4.2.1 Filter Regeneration

The particles that collect on mechanical filters must be removed periodically, otherwise the pressure drop through the filter will rapidly increase and eventually the filter will plug and fail. The process of removing particles from filters is sometimes known as filter regeneration. If a diesel particulate filter is not regenerated regularly, back-pressure can adversely affect the efficiency of the engine and create a substantial fuel penalty (Pattas *et al*, 1998). All of regeneration techniques for commercialized DPM filters are based on oxidizing the soot in situ, and converting it to CO_2, H_2O, and SO_2 gases. Since the ignition temperature of the soot is approximately 600 ^oC, standard diesel exhaust temperatures are insufficient to promote rapid DPM oxidation most of the time. Although the temperature of the exhaust can occasionally reach 750 ^oC, it is usually around Diesel exhaust temperatures are usually between 200 and 300 ^oC.

Two techniques have been employed to deal with the problem of diesel exhaust being too cool to reliably and consistently promote soot oxidation and filter regeneration: initiating soot oxidation with an auxiliary heat source (active regeneration), and reducing the ignition temperature of the soot by using catalysts (Neeft *et al*, 1996).

a) Non-catalytic Regeneration (Active Regeneration):

DPF regeneration is difficult because the temperature of diesel exhaust under most conditions is not hot to promote soot combustion to CO_2. Different methods have been attempted to increase the temperature of the exhaust or to heat components of the trap itself to initiate soot combustion. Burners which used a fine spray of diesel fuel to ignite the collected particles were successfully used in some experiments and an optimal firing time was proposed for them to minimize the fuel penalty (Higuchi *et al*, 1983; Wade *et al*, 1983). Nonetheless, burners were not

commercialized because of difficulties in controlling the flame properties and because incorrect regeneration timing could cause excess unburned fuel to accumulate on the filter structure and seriously damage the filter during the next regeneration sequence (Neeft *et al*, 1996).

Electrical heaters have been used to regenerate DPF filters. The needed energy came from the vehicle electrical system and the resulting fuel penalty was up to 5 percent, which was higher than that of fuel burners (Simon *et al*, 1985). Studies indicated that electrical heaters were difficult to control because of soot ignition control and flame propagation problems (Simon *et al*, 1985). A large amount of soot was needed to maintain high temperatures during a successful regeneration cycle and controlling the temperatures produced during regeneration was usually hard and often damaged the filter. In a study by Toyota, a complex electrical heating regeneration system was used and different methods to prevent filter cracking were investigated. The results indicated that the Toyota system was unlikely to prevent filter cracking. (Kobashi *et al*, 1993).

Another method to supply supplementary heat to the exhaust is by using the engine itself, a method known as exhaust gas throttling. By changing the air-to-fuel ratio, exhaust temperature can increased by several hundred degrees, and researcher have attempted to use the technique to ignitesoot collected in DPF units. Most commercialized DPF systems use gas throttling and air-to-fuel control for regeneration. However, regeneration using gas throttling can be difficult to control at very low speeds and it always results in a fuel penalty. Also, gas throttling reduces useful shaft output power (Garner *et al*, 1989).

b) Catalytic Regeneration (Passive Regeneration):

The power used to regenerate DPF's depends on the ignition temperature at which the soot starts to combust, and the heat requirement needed to maintain combustion. Lowering this temperature by using carbon oxidizing catalysts could result in easier combustion of the soot and easier regeneration of the filter. One commercial DPF system called the Continuously Regenerating Trap (CRT) was introduced by Johnson Matthey (Johnson Matthey Plc, London, UK). This system uses a specially formulated catalyst which converts nitrogen oxide gas (NO), which is present at moderately high levels in diesel exhaust, into nitrogen dioxide (NO_2), which is an extremely oxidizing compound. In the CRT, a catalyst converts NO to NO2, and the NO2 is used to oxidize (combust) the collected soot. These catalysts, however, can also oxidize SO_2 to SO_3 and therefore these systems are limited to areas where ultra low sulfur fuels are present. This system also uses a conventional DOC as pre-oxidizer which is another reason for its need of ultra low sulfur diesel (ULSD). Since ULSD has already been introduced in most developed countries, CRT can be used on many diesel engines. However, its bigger problem is its reliance on high levels of NO for the creation of NO_2 since future engines may not produce enough NO for soot combustion (Fino and Specchia, 2008).

Use of fuel-borne catalysts (FBC) is a relatively new technique in diesel particulate control. In this process, metal catalysts, usually iron, platinum, cupper, or cerium, are combined with the fuel. These catalysts are integrated with the soot during the combustion process and lower the oxidation temperature of the soot in a DPF Although this technology has been commercialized on a limit scale in Europe, it causes secondary emissions of metal oxides to the atmosphere. This system also results in the buildup of metal and metal oxide ash on the filter (Walker, 2004; MECA, 2005). A very complex combination of gas-throttling system and FBCs was introduced by Peugeot-Citroen in 2000 (Salvat *et al*, 2000). The pressure drop of the filter is

being controlled by a few sensors and as soon as the pressure drop increases, more diesel is fired in the engine to increase exhaust temperatures. Adding fuel-borne catalysts to the system assures a reasonable fuel penalty for the diesel engine. However, because of the increased ash production, the DPF need replacement every 80,000 km (Walker, 2004).

1.4.2.2 The Long-Term Potential of DPFs for Workplace Machinery and Industrial Vehicles

After more than 25 years of research on DPF's, some serious problems are still associated with their use in diesel engines. Even with the best regeneration methods, filters cause some back-pressure and increase the consumption of fuel. A study by Wade *et al* (1983), showed that DPFs operating with proper regeneration are still likely to experience some fuel penalty with an average penalty of approximately 3.3 percent. More recent studies show a backpressure range from 50-300 mbar and report increasing fuel penalty associated with increased backpressure up to 7 to 10 percent (Zelenka *et al*, 1996; Pattas *et al*, 1998; Salvat, 2000; Mayer *et al*, 2001).

The Peugeot-Citroen system to control soot emissions from some European passenger vehicles was first sold in 2001 and it is the most commercialized DPF in the world. It utilizes a DPF with fuel borne catalysts and has been employed on more than a million cars. But even after all this time, the high initial DPF costs and the maintenance and fuel penalty costs are ongoing challenges (Fino and Specchia, 2008).

The costs of installing a DPF system on a passenger vehicle have been estimated to range from 400 to more than a thousand dollars depending on the size of the engine (US Department of Energy, 2004). Because of the problems associated with wall-flow monolith filters, many companies pilot testing their use in the 1990's, removed these filters from their vehicles in 1999

(Heck *et al*, 2002). The recent PM emission standards are forcing manufacturers to again consider installing the devices on their engines. The European Union diesel particulate standards are also very strict and the majority of car producers, including Mercedes-Benz, Audi, Volks Wagon, and Opel, have already planned or are planning to incorporate filters into their diesel engine vehicles (Green Car Congress, 2005). Ford of Europe had to install DPF's on its products to comply with European Union environmental standards in 2005. Because of the pressure drop problems however, these filters have an average removal efficiency of only 30 to 40 percent (Green Car Congress, 2005).

In the non-road and occupational setting, there are also regeneration challenges with using mechanical filtration. Many non-road and machinery engines spend long periods of time idling or at low load, and under these conditions large amounts of soot are produced at low exhaust temperatures. The low temperatures make filter regeneration very difficult. (Pattas *et al*, 1995; MSHA, 2003b)

The catalytically-active mechanical filters, like CRT's, also face some very important challenges like the deactivation of catalytic active sites by certain compounds like sulfur and silicon, a process known as catalyst poisoning. The amount of sulfur in the fuel plays a significant role on the efficiency of all types of filters because production of SO_2 inhibits the conversion of NO to NO_2. A study sponsored by the U.S. Department of Energy, showed a 23 percent efficiency drop by increasing the sulfur content of the fuel and a more difficult regeneration due to increased soot ignition temperature (Department of Energy, 2000). In 2001, EPA established a standard lower the amount of sulfur in diesel fuel from 500 ppm to 15 ppm by 2007 (EPA, 2005). However, stationary diesel engines, e.g. emergency standby electric generator engines, and non-road machinery and vehicles can still use low sulfur diesel (EPA, 2004). Van

Setten *et al* (2001) referred to another problem known as catalytic loss. If catalysts can dissolve in the water introduced into engine by raining or washes, they might leave the exhaust pipe with water droplets.

Another important flaw with the use of mechanical filters is gradual plugging with ash. Ash consists of inorganic materials and has three main sources: lubricant oil, corrosion of the engine, and fuel additives, including fuel-borne catalysts. Ash cannot be burned during the regeneration of the filter and will accumulate in the DPF eventually resulting in plugging. At present, in commercialized and prototype systems, the ash is mechanically removed periodically during vehicle service, although unplugging can damage the catalytic coatings of filter (MECA, 2005). In recent field trials, continuously regenerating traps supposed to last for 700,000 kilometers, required maintenance or replacement every 100,000 to 200,000 kilometers (Walker, 2004).

Diesel particulate filters are usually made of brittle materials like ceramic which can crack due to material fatigue resulting from temperature fluctuations and mechanical stresses. Filter crack can significantly reduce the filter efficiency (Van Setten *et al*, 2001). Researchers have tried to solve this problem by better canning of the filter. However, canning itself can exert a high pressure on the filter and might cause mechanical stress (Van Setten *et al*, 2001). Strong temperature gradients on the filter can be created during regeneration cycles, and the ceramic structure of the filter can melt during an uncontrolled soot burn (Ohno *et al*, 2000; Heck *et al*, 2002). Van Setten *et al*, 2001 describe an example of mechanical filter failure and cracking, resulting in ceramic flakes from the filter going into the turbo charger and destroyed the radial turbine.

Because of the problems with filters and filter regeneration, some scientists believe that along-term solution to the problem of diesel particulate emissions has not been found and that improvements to diesel particulate capture technology are needed (Okubo *et al*, 2004; Zhang-Steenwinkel *et al*, 2004, Zheng and Keith, 2007). The Mine Safety and Health Administration (MSHA) stated that although particulate traps offer promising technology, "In-use deficiencies, secondary emissions, engine backpressure, DPF regeneration, DPF reliability and durability are major issues requiring additional research and engineering" (MSHA, 2003).

1.4.3 Electrostatic Precipitators:

In addition to filters and catalysts, electrostatic precipitators have been investigated by others as DPM removal devices. Electrostatic precipitators (ESPs) were invented in 1907 with the need to control air pollution from smelters. Now, ESPs are among the most widely used of all air pollution control devices. The combination of high efficiency and low pressure drop make them attractive particle collection devices. The large majority of ESP applications have been installed at large utilities and at heavy industry like steel mills and cement plants. A few efforts to miniaturize ESPs and use them on diesel engines have been attempted.

The very first study of this kind was performed by Faulkner in 1981 (Faulkner *et al*, 1981). As part of his work, Faulkner used thick needles as the charging electrodes. Deposition of soot close to the needles decreased the collection efficiency substantially and the ESP could not achieve high removal efficiencies (Faulkner *et al*, 1981). In another study, Masuda and Moon (1983) built a moving belt electrostatic precipitator and tested it on diesel exhaust. The moving belt was designed to remove the soot from the internal collection surface. Although they could capture 95 percent of the diesel soot, the complex design of the ESP appeared to prevent its

commercialization. Farzaneh *et al* (1994) built a wire-tube electrostatic precipitator using hexagonal tubes and tested it with diesel exhaust. The results showed 95% mass-based PM removal efficiency but a regeneration technique was never developed, and the research did not result in a commercial product (Farzaneh, 2005).

Saiyasitpanich *et al* used a cylindrical wet electrostatic precipitator (wESP), which used a film of water to remove the collected soot from the collecting tube of the ESP (Saiyasitpanich *et al*, 2006). The wESP was tested with a 75kW diesel engine under different loads, flow rates, and gas residence times. The wESP could achieve removal efficiencies above 95 percent, but the high removal efficiencies required a power consumption of 4100 watts (Saiyasitpanich, 2006). For comparison, the entire electrical system of long-haul tractor trailers typically produces approximately 5000 watts of electrical power for all their on-board systems.

In addition to the studies mentioned above, studies have been performed using electrostatic coronas (a.k.a. non-thermal plasmas) in diesel exhaust (Thimsen *et al*, 1990; Wadenpohl and Loffler, 1994; Ciach and Sonowski, 1996; Yao *et al*, 2004). The coronas were used to agglomerate the particles upstream of a standard mechanical filter improve the collection efficiency of the filter. These non-thermal plasmas were not used to charge the particles and then collect them with an electrical field as in standard ESP operation.

1.5 Objectives

Large-scale electrostatic precipitators are common at coal-fired power plants and on large industrial furnaces, and they show outstanding PM removal performance. They demonstrate very low pressure drop and high particle collection efficiency. However, ESPs have not been successfully miniaturized for diesel-powered sources, like trucks, construction machinery, or mining machinery. None of the experimental diesel exhaust ESPs investigated over the last 20 years has been successfully commercialized. The objectives of this research were to design, construct, and test a small-scale ESP and evaluate its performance to reduce emissions of diesel exhaust particulate. The target is to achieve a control efficiency of 90 percent.

The specific research objectives of this work were:

1- Determine the fundamental electrostatic properties of small-scale ESPs over a range of operating parameters. Investigate the onset voltage, voltage-current relationship, and sparkover voltage properties of the small-scale ESP, as a function of wire diameter and plate-to-plate distance. Compare the empirical data to the standard equations developed from large scale industrial ESPs.

2- Measure the mass concentration removal efficiency of the small-scale ESP as a function of wire diameter, plate-to-plate distance, and fuel type.

3- Measure the number concentration removal efficiency of the small-scale ESP as a function of wire diameter, plate-to-plate distance, and fuel type.

4- Investigate the mass and number concentration removal efficiencies of the small-scale ESP under different engine load conditions.

CHAPTER 2

FUNDAMENTALS OF ELECTROSTATIC PRECIPITATION

2.1 Introduction

The role of corona discharge and electrostatics in separating gases and airborne particles has been known since 1824 when Hohlfeld used corona discharge to clear smoke contained in a bottle (Hohlfeld, 1824). Successful industrial use of electrostatic precipitators (ESPs) started in 1906 with Cottrell's use of the technology to collect sulfuric acid, lead, and zinc oxide fumes from large industrial gas streams (Cottrell, 1908). ESPs are now among the most common particulate emissions control devices at coal-fired power plants and at industrial facilities such as cement plants and metal smelters.

Most particle control devices either redirect or somehow obstruct the flow to separate the particles. For instance, cyclones cause the whole flow to turn and separate particles with higher inertia. In mechanical filtration, the entire flow goes through a porous media, often constructed of fibers or porous foams, and the bending of the gas streamlines is the basis for separation. The process of redirecting the flow and the drag of the gas flow on the filter surfaces will cause a pressure drop, which can be substantial in many filtration devices.

In contrast, ESPs only exert electrostatic force on the particles. The gases are not redirected or turned in an ESP and therefore, they will have a comparatively lower pressure drop. As a result, the cost of operation for an ESP can be much lower than the cost of cyclonic or mechanical filtration systems. In addition, with proper engineering the removal efficiency of an ESP can be more than 99 percent for certain types of particulate which is remarkable considering the low pressure drop.

Figure 2.1 shows a diagram of a single stage electrostatic precipitator. The discharging electrode can be a needle or a wire and the collecting electrode can be a plate or a tube. During electrostatic precipitation, dirty air flows into the ESP and enters a high-voltage electric field generated by a series of wires and plates. Gas molecules are ionized in the intense electric field strength near the discharge electrode. The ionized gas molecules consist of both negative and positive components and the negative ions will migrate in the electric field toward the collecting electrode, effectively creating an electric current between the electrodes. On the way to the collecting electrodes, some of the ions will impact or diffuse to the surfaces of the incoming suspended particles and charge them. This process transfers charge from the ionized gas to the previously-uncharged suspended particles. The now charged particles will now move under an electrostatic force to the collecting plates. The particles will deposit on the collecting electrodes and at this point the gas has been cleaned of suspended particulate. The last step in practical ESP operation is the removal of the suspended particulate from the collecting electrodes (Parker, 1996). In this chapter, these steps will be discussed in details and the design process of an ESP will be explained.

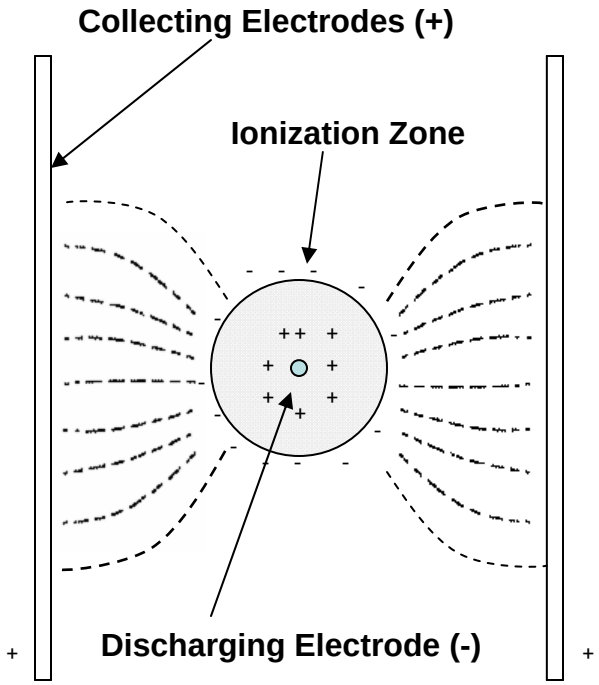

Figure 2.1 Schematic diagram of an electrostatic corona producing current (redrawn from Mizuno, 2000)

2.2 The Chemistry of Electrostatic Corona Formation

Formation of an electrostatic corona has two main prerequisites: an ionizable gas near the electrodes and a strong electric field for energizing the molecules. Many of the compounds found in air, either polluted or clean, are easily ionized in strong electric fields. For normal air in an electrostatic corona, the corona is the location of numerous chemical reactions, which produce a steady current of positive and negative ions (Hoeben, 2000):

[Chemical Reaction List for Corona Formation]

$H_2O + e^- \rightarrow OH + H + e^-$	dissociation	(2.1a)
$H_2O + e^- \rightarrow H_2O^+ + 2e^-$	ionization	(2.1b)
$H_2O^+ + H_2O \rightarrow H_3O^+ + OH$	dissociation	(2.1c)
$N_2 + e^- \rightarrow N_2^* + e^-$	excitation	(2.1d)
$O_2 + e^- \rightarrow O_2^* + e^-$	excitation	(2.1e)
$N_2 + e^- \rightarrow 2N + e^-$	dissociation	(2.1f)
$O_2 + e^- \rightarrow 2O + e^-$	dissociation	(2.1g)
$N_2 + e^- \rightarrow N_2^+ + 2e^-$	ionization	(2.1h)
$O_2 + e^- \rightarrow O_2^+ + 2e^-$	ionization	(2.1i)
$O_2 + e^- \rightarrow O_2^-$	attachment	(2.1j)
$O_2 + e^- \rightarrow O^- + O$	dissociative attachment	(2.1k)
$O_2 + O \rightarrow O_3$	association	(2.1l)
$H + O_2 \rightarrow HO_2$	association	(2.1m)
$H + O_3 \rightarrow HO_3$	association	(2.1n)
$N + O \rightarrow NO$	association	(2.1o)
$NO + O \rightarrow NO_2$	association	(2.1p)
$N_2^+ + O_2^- \rightarrow 2NO$	recombination	(2.1q)
$N_2 + O \rightarrow N_2O$	association	(2.1r)

The chemical reactions are for a negative corona happening in humid air. Using diesel exhaust as dielectric can result in more reactions due to additional chemicals in the exhaust like sulfur dioxide and sulfur trioxide. The chemical reactions formed during negative and positive corona are completely different. Due to these different formation mechanisms, negative coronas typically produce twice as much current as positive corona.

The polarity of the discharging electrodes specifies the type of the corona and the charge that will be imparted to the particles suspended in the gas being cleaned. If the discharge electrode is negative, then the corona will produce negative ionic current to travel from the discharge electrode through the air gap to the collecting electrode. Likewise, if the discharge

electrode is positive, then the corona will produce positive ionic current to travel from the discharge electrode to the collecting electrode. From the very first days of using electrostatic precipitation as a particle control means, negative corona showed superiority in terms of particle collection efficiency (Cottrell, 1908).

2.2.1 Positive Corona

Positive corona is usually used in small air purifiers that are common in American homes and offices. Low concentration of produced ozone makes this type of corona desirable for residential use. In positive corona, applying the strong electric field will move the electrons and ions which are already in the dielectric. Electrons have a very high mobility and will move very fast in an electric field. Consequent collisions of the electrons with the molecules will detach more electrons from neutral molecules and will form a primary electron avalanche. Also, photoionization removes more electrons from the molecules and forms a secondary avalanche. While the electrons are absorbed to the wire which is positive, the positive ions will move towards the collecting electrodes. Positive coronas in air have a smooth purple appearance evenly distributed along the discharge electrode.

2.2.2 Negative Corona

Negative corona is the type of corona which is usually used for particle collection in industry. The main differences between negative and positive coronas are in the ion types that travel the air gap. In positive corona, electrons move towards the discharging electrodes and positive ions move towards the plates; whereas in negative corona, the negative discharging electrode will repel the electrons and absorb positive ions. Due to high mobility of the electrons,

there is higher likelihood of complete air breakdown into plasma compared to positive corona. This breakdown will create continuous sparking which will hinder the operation of an ESP. Therefore, negative corona can only happen in gases with high electron affinities. In gases like O_2, after the electron leaves the highly-energized region close to the discharging electrodes, it collides and attaches to a molecule and forms a negative ion. These negative ions have much lower mobilities compared to electrons and these ions will conduct the electricity across the air gap.

Unlike positive corona, the appearance of negative corona is in form of non-uniform blue tufts and brushes all along the wires. Another difference between positive and negative corona is the audible pulse and the shake of the discharging electrode. All these phenomena are attributed to higher mass of positive ions which collide with discharging electrode. These collisions also detach more electrons from the wires which are believed responsible for high current seen in negative corona.

2.3 Fundamental Electrical Properties of an ESP

The ability of an ESP to remove suspended particles depends substantially on the quantity of charge imparted to the particles. Particle charging on the other hand is a function of the level of ionic current that the electrodes produce, which itself is dependent upon the voltage at which the ESP is operated.

There are two voltage endpoints that determine an ESP operating range. Onset voltage is the lowest voltage difference applied across the electrodes that produces an electric field sufficient to start the ionization of air molecules and produce a measurable ionic current. Sparkover voltage is the highest voltage that produces steady current output in an ESP, without

producing sparking at a rate that prevents operation. An ESP can only be operated at a voltage between these two endpoints. In between these voltages, there is a gradual increase in current production with increasing voltage, a trend known as the voltage-current relationship. Onset voltage, sparkover voltage, and the voltage-current relationship are collectively the fundamental electrostatic properties of the ESP and estimating them is an important component of ESP design.

2.3.1 Onset Voltage

The first comprehensive study on electrostatic coronas started in 1907 by F.W. Peek (Peek, 1911). This research was funded by General Electric and the results of were published in three manuscripts entitled "The Law of Corona" which described corona formation in detail and modeled it physically for the first time. The work included an extensive investigation of the strengths of electric fields required to start coronas, the onset electric field strengths Equation 2.2 shows the general form of Peek's onset electric field strength equation.

$$E_0 = \delta A + B\sqrt{\frac{\delta}{a}} \qquad (2.2)$$

Peek suggested values of $3*10^6$ V/m and $9*10^4$ V/m$^{1/2}$ for the empirical coefficients A and B. Although more recent researchers have suggested different coefficient values for onset voltage equation, their values were very close to the original ones proposed by Peek values and the general form of the equation remains unchanged (Robinson, 1978; Lowke et al, 2003). For the geometry of plate and wire ESPs, Equation (2.3) can be used to convert onset electric field to onset voltage:

$$V_0 = aE_0 Ln(\frac{\pi b}{2a}) \quad (2.3)$$

2.3.2 Sparkover Voltage

Sparkover voltage of the ESP (or in some references flashover voltage) is the voltage that the ESP cannot operate anymore due to extensive sparking. Peek's equation for sparkover voltage only holds for room temperature and does not take the effects of temperature and pressure into account. Empirical data has demonstrated that sparkover voltage is in fact a function of temperature and pressure, and modifications to Peeks sparkover relationship have been developed (Turner, 2000).

$$V_s = 30a(1 + 0.01\frac{b}{a\sqrt{a}})Ln(\frac{b}{a}) \quad (2.4)$$

$$E_s = 6.3 * 10^5 (\frac{273}{T} P)^{1.65} \quad (2.5)$$

2.3.3 Voltage-Current Relationship

Additional early work on electrostatic coronas was performed by J.S. Townsend, who described the voltage-current relationship in electrostatic systems (Townsend, 1915). Townsend's equation states that the relationship between applied voltage and consequent current depends on the diameter of the wire and the distance between the electrodes.

$$V = V_0 + aE_0\left[\left(\sqrt{1+\frac{2ib^2}{KE_0^2a^2}} - 1 - \ln\left(\frac{1+\sqrt{1+\frac{2ib^2}{KE_0^2a^2}}}{2}\right)\right)\right] \qquad (2.6)$$

Townsend equation's predicts a parabolic relationship between voltage and current, a trend that is observed in empirical experiments. Other researchers have offered alternative parabolic equations of the form shown in Equation 2.7 (Seaver, 1995; Mizuno, 2000).

$$i=MV(V-V_0) \qquad (2.7)$$

where M is an empirical constant. This equation is simpler than equation (2.6). However, the concepts rolled into the empirical constant A are representing quite a few parameters from the full Townsend equation, and it varies as a function of plate-to-plate distance, wire diameter, and dielectric constant.

Cooperman developed an approximation for the Townsend equation calculated the constant for low currents (Cooperman, 1952).

$$A = \frac{K}{b^2 Ln(4b/\pi a)} \qquad (2.8)$$

This equation is true if plate-to-plate distance is less than the distance between the rows of wires. This assumption is virtually always true in practice.

Another approximation was suggested by White for large currents (White, 1963).

$$i = \frac{K}{2b^2}\left[V - aE_0 Ln(\frac{b}{12a})\right]^2 \qquad (2.9)$$

There are numerous alternative methods to calculate the voltage-current relationship (Fazel and Parsons, 1923; McDonald et al, 1977; McLean et al, 1986; Talaie et al, 2001). However, in this study, Townsend's classic equation, equation (2.6) was used to compare the experimental data with theory. Also, equations (2.2) to (2.4) were used to calculate the other two fundamental electrical properties of the ESP.

2.4 Particle Charging

After corona discharge is established by strong electric fields near the discharge electrodes, there will be a flow of ionic current between the discharge and collecting electrodes. When the air gap between the electrodes is filled with suspended particles, the ions may collide with the particles and impart their charge to them. The ability of particles to accumulate charge is a function of many factors, including particle size, dielectric constant, and their residence time within the ESP. The physical mechanism of particle charging can be absolutely different depending on the size of the particle. The main charging mechanisms in a corona discharge are diffusion charging and field charging.

2.4.1 Diffusion Charging

Diffusion charging is the main mechanism for particles with a diameter less than 200nm (Hinds, 1999). These small particles are charged due to Brownian motion and random collisions

with air ions. An analytical equation for calculating charges on a particle after diffusion charging has been derived by White (White, 1963).

$$q(t) = \frac{d_p kT}{2e} Ln(1+\tau) \qquad (2.10)$$

In this equation, τ is a dimensionless parameter representing time that is defined by the following equation:

$$\tau = \frac{\pi d_p \bar{c}_i N_i e^2 t}{2kT} \qquad (2.11)$$

An alternative and more complex description of diffusion charging was proposed by Lawless, which requires numerical techniques to solve. (Lawless, 1996). Since diffusion charging is a stochastic phenomenon; particles will receive a distribution of charges, and there is always a probability for particles to receive significantly more or less charge than predicted by either Equations 2.10 or 2.11. However, in practice, after about three dimensionless time units, the charging process via diffusion becomes very slow (Turner, 2000).

2.4.2 Field Charging

Whereas diffusion charging is the dominant charging mechanism for very fine particles, the external electric field plays a direct role in charging particles bigger than 1μm. Particles of this size have sufficient size and surface area to be impacted by the rapidly moving ions that comprise the current in the air gap of the precipitator. Particles obtain charge when their path

intercepts lines of force in the electric field, since the ionic current follows these lines of force from the discharge to the collecting electrodes.

At a time *t*, the number of charges on the particle due to field charging can be calculated by the following equation:

$$n_t = \left(\frac{3\xi}{\xi + 2}\right)\left(\frac{Ed^2}{4K_E e}\right)\left(\frac{\pi K_E e K N_i t}{1 + \pi K_E e K N_i t}\right) \qquad (2.13)$$

2.4.3 Maximum Particle Charge – A Limit to Electrostatic Particle Collection

As particles collect charges in an ESP, they will acquire their own local electric fields causing nearby distortions in the external electric field being maintained by the electrodes (Figure 2.2). The magnitude of the local electric fields and distortions depends on the conductivity of the particles and the amount of charges they carry. The localized electric fields can negate the driving force for additional field particle charging, since the electric fields produced by the first several ions to impact on a particle surface will tend to repel ions of the same polarity. This reduces the rate of charging and finally at a specific charge, no additional charging occurs on the particles. This charge is known as saturation charge and can be calculated using the following equation (Hinds, 1999):

$$n_s = \left(\frac{3\xi_p}{\xi_p + 2}\right)\left(\frac{Ed^2}{4K_E e}\right) \qquad (2.12)$$

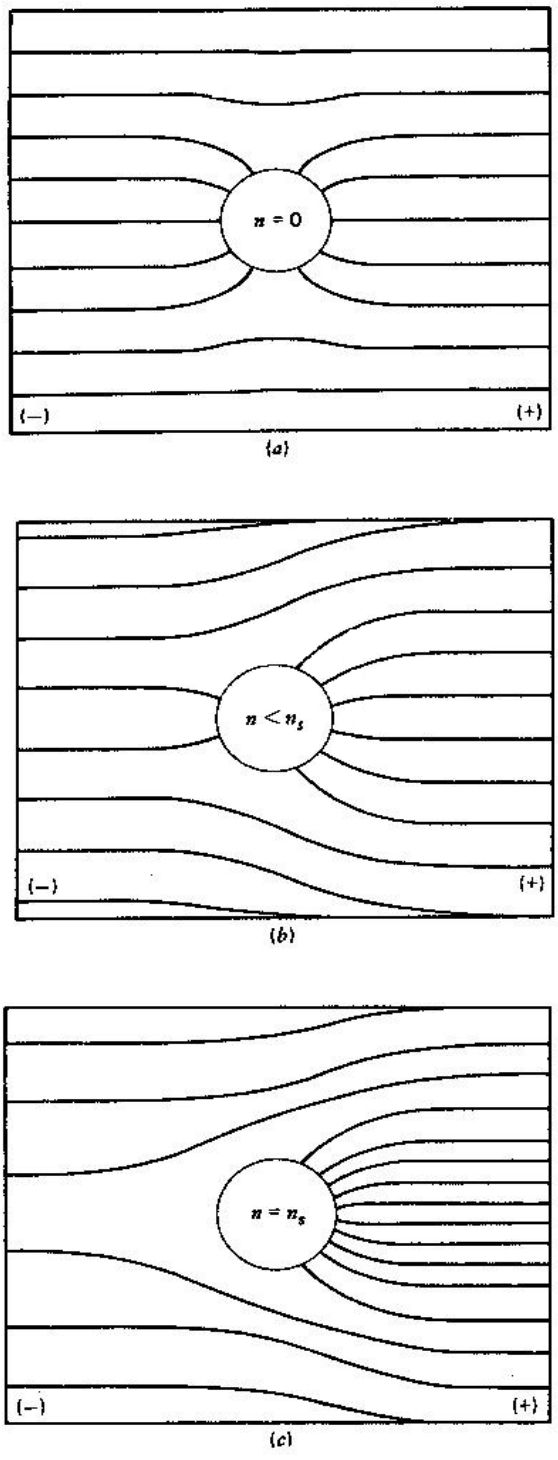

Figure 2.2 A conducting particle in a uniform field a) Uncharged particle b) partially charged particle c) Particle at saturation charge (Hinds, 1999)

2.4.4 Combined Charging

When the particle diameter is between 0.2μm and 1.0μm, both charging mechanisms are effective at putting charges on particles. A reasonable method to predict the charge on the particles in such situation is to simply add the charge by diffusion mechanism to the charge obtained by field charging mechanism. This method has been shown experimentally to provide a good approximation of the charges actually collected by particles (Turner, 2000; Unger, 2004).

An older analytical method, developed by Cochet, can also be used to calculate the quantity of charge collected by the particles as a result of the two methods (Cochet, 1961). Cochet assumes that if the charging time is infinite, particles of the same size will eventually collect the same charge.

$$q = \left\{ \left(1 + 2\frac{\lambda}{d_p} \right)^2 + \left(\frac{2}{1 + 2\frac{\lambda}{d_p}} \right) \left(\frac{\varepsilon_p - 1}{\varepsilon_p + 2} \right) \right\} \pi \varepsilon_0 d_p^2 E \qquad (2.14)$$

Other than these two analytical models, numerical models have been suggested to calculate the number of charges on the particles (Lawless, 1996). However, Sato suggested that adding up equations (2.9) and (2.12) agreed best with his experimental data (Sato, 1987).

2.5 Particle Migration

After suspended particles are charged in an electrostatic precipitator, the force exerted by the external electric field will move the particles towards the collecting electrode. This force can be much greater than other forces acting on particles, such as drag gravitational forces.

$$F = qE \qquad (2.15)$$

Where q is the sum of charge put on the particle during the charging process .

$$q=(n_F+n_E)e \tag{2.16}$$

The force moves the particles towards the electrode of the opposite polarity. i.e. in a negative corona precipitator, the particles obtain a net negative charge and the electrostatic force pushes them toward the positively charged collecting electrodes. Motion towards the collecting electrode is typically perpendicular to the main flow through the precipitator, so the motion towards the collecting electrode starts from zero and then accelerates until the electrostatic force is in equilibrium with the drag force on the particles. The drag force will depend on the turbulence regime of the particle motion. For particles with low net charge, or in weak electric fields, particle velocity might be in the Stokes regime, and terminal electrostatic velocity can be calculated using the following equation (Hinds, 1999):

$$V_{TE} = \frac{neEC_c}{3\pi\eta d_p} \tag{2.17}$$

For most practical electrostatic applications, particle motion is likely to be well outside Stokes regime, so terminal electrostatic velocity cannot be calculated analytically and numerical methods are necessary.

$$V_{TE}^2 = \frac{8neE}{\pi\rho d_p^2 C_D} \tag{2.18}$$

In practice, the equation can be easily solved using tables or graphical procedures (Hinds, 1999). At this point, the particle will travel at a terminal velocity until impaction on the collecting surface.

In addition to Hinds' equation for terminal electrical velocity, a new analytical method was developed based on equations suggested by Reist (Reist, 1993).

$$w = \left(\frac{\eta_g}{\rho_g d_p}\right) \log_{10}^{-1}\left(-5 + \sqrt{(12.1 + 9.1 \log R)}\right) \tag{2.19}$$

$$R = \frac{8qE\rho_g}{\pi\eta_g^2} \tag{2.20}$$

2.6 Particle Collection

Particle collection is the last step in removing suspended particles from a gas flow. The removal mechanism behind electrostatic precipitation is the collision of particles with a solid collecting electrode, causing the particles to deposit and thus removing them from the gas. Particles are held on to the collecting electrodes by a combination of van der Waals, electrostatic attraction, and surface tension forces. Although particle collection seems like a straight forward process, it can actually be very complicated. After particle deposition, there is always a possibility of detachment from the collecting plates. The process of particle detachment followed by resuspension in the gas stream is known as reentrainment. A very intense electric field coupled with particles with very low conductivity can cause a high-intensity localized electric field that can cause back corona and return the particles to the flow. Also, particles with very high conductivity can lose their electrostatic charge very quickly, reducing the force keeping them adhered to the collecting surface, and increasing the likelihood of detachment. Also, other factors like an increase in turbulence in the gas flow or the heat and vibration created during sparking events can lead to reentrainment.

2.6.1 Particle Collection in Laminar Flow

The turbulence regime of electrostatic precipitators can impact their performance. In large-scale industrial and utility ESPs, laminar flow in the precipitators is highly unlikely under normal operation, given the flow rates and channel sizes involved. However, for small-scale ESP units, where the plates-to-plate distances can be on the order of a centimeter, laminar flow is possible. In an ESP with laminar flow, the initially uncharged particles are moving in a straight line and turbulence of the flow does not disturb particle motion. Consequently, particle collection only becomes a function of motion in x and y directions. i.e. if migration velocity is large enough so that the particle moves fast enough in y-direction to hit the plates before leaving the ESP, it will be captured (Figure 2.2).

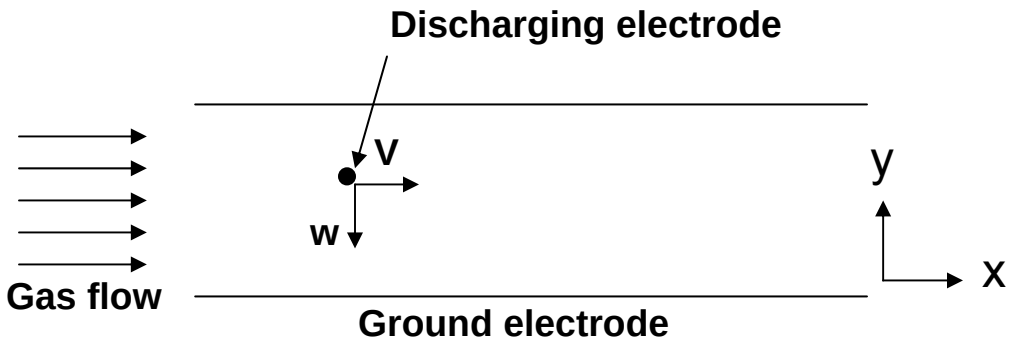

Figure 2.3 Particle motion in ESP with laminar flow (redrawn from White, 1963).

Therefore, the collection efficiency of the ESP will be defined by the following equation:

$$eff = 1 - (\frac{Lw}{bv}) = 1 - (\frac{Aw}{Q}) \qquad (2.21)$$

Theoretically, achieving an efficiency of 100 percent is feasible when the flow inside the ESP is laminar and the residence time is sufficient. Even for a precipitator operating under laminar conditions, Equation 2.21 will not completely describe performance, because it does not account for particle bounce and reentrainment.

2.6.2 Particle Collection in Turbulent Flow

When gas flow is turbulent, turbulent eddies make particle collection a more complicated process than the laminar case. Since the turbulent flow is dictating the 3D trajectories of uncharged particles, their paths before charging can be complex. The turbulent trajectory and the perpendicular velocity component created by the electrostatic migration will result in a probabilistic distribution of particle trajectories and particle positions in the precipitator.

A simple relationship was developed to describe the collection efficiency of an ESP under turbulent flow conditions, as a function of electrostatic, flow, and geometric parameters (Deutsch, 1922). In the relationship, it is assumed that at a short distance from the collecting plates, the collecting electric field is so strong that any particle which enters the region will be captured. Now, the problem of collection efficiency is reduced to calculating the probability of the particle entering the capturing zone.

Deutsch employed this approach to solve the problem and came up with his famous particle collection equation (Deutsch, 1922):

$$eff = 1 - e^{(-\frac{wA}{Q})} \qquad (2.22)$$

In addition to the assumption mentioned above, Deutsch assumed that precipitation electric field strength and migration velocity are constant near the collecting plates. White (1963) indicated that a few of the assumptions in obtaining equation (2.21) are reasonable assumptions. For example, because of the flow turbulence the particle concentration is probably uniform at any cross section. Also, gas velocity is uniform except near the walls. White suggested that if disturbing effects like reentrainment are reduced, the agreement between Deutsch and experimental data is very good (White, 1963). However, the Deutsch equation has been criticized by a few other scientists and alternative equations have been suggested (Matts and Ohnfeldt, 1964; Cooperman, 1970; Riehle and Lottler, 1994; Lowke et al, 1998).

$$Eff = 1 - e^{w_k (A/Q)^k} \qquad (2.23)$$

In this equation, w_k is average migration velocity and k is a constant between 0.4 and 0.6. k depends on the size distribution of the particles and other factors affecting collection efficiency.

White suggested using an approach close to Matts-Ohnfeldt equation for Deutsch equation (White, 1982). Instead of calculated migration velocity (w), effective migration velocity (w_e) will be used in Deutsch equation.

$$Eff = 1 - e^{-w_e (A/Q)} \qquad (2.24)$$

Effective migration velocity is in fact an empirical value which accounts for a lot of effects specific to a particular aerosol, size distribution being the most important one of them.

Therefore, using an empirical factor in the in Deutsch equation tends to improve its agreement with observational data.

CHAPTER 3

EXPERIMENTAL METHODOLOGY AND LABORATORY SET-UP

3.1 The Fundamental Electrical Properties of Small-Scale ESPs

The majority of the experimental studies on electrostatic precipitation have been performed with geometric scales appropriate for large industrial and utility precipitators, with plate to plate distances larger than 20 cm and wire diameters larger than 1 mm. Recently, some small-scale ESPs have been investigated or developed for applications like occupational particle sampling, household air purification, and diesel exhaust particle filtration (Farzaneh *et al*, 1994; Schaughnessy *et al*, 1994; Armendariz *et al*, 2003; Armendariz and Leith, 2003; Volkens and Leith, 2003). However, experimental data and empirically-based design guidelines for small-scale ESPs with thin wires and small electrode spacings are still comparatively few in number. It is difficult to ascertain the validity of the large-scale design models for designing small-scale units. The objectives of this portion of the research were to determine the fundamental electrostatic properties specific to small-scale ESPs over a range of operating parameters. Onset voltage, voltage-current relationship, and sparkover voltage properties of the small-scale ESP were measured as a function of wire diameter and plate-to-plate distance. The results were compared with the classical equations of electrostatic precipitation.

3.1.1 Design and Construction of the Prototype Small Scale ESP

With the lack of design guidance and performance data specific to small-scale precipitators, the traditional ESP guidelines developed for large industrial units were used as the starting point for the design of a small-scale ESP prototype. The ESP was sized to collect particulate from a flow of 0.6 actual m3/min of exhaust at a temperature of 120 ^{o}C from a diesel-powered electric generator. Based on published characterizations of diesel exhaust particulate, the mass median diameter was estimated to be 300 nm with a geometric standard deviation of 2.0 (Kittelson, 1998). The target mass collection efficiency for the diesel exhaust particulate was 90%.

The prototype was a single-stage unit with exterior dimensions of 21 x 21 x 33 cm, and it could be fitted with up to seven internal 150 x 250 mm collecting plates. The ESP shell and plates were constructed from 1 mm (18 gauge) 304 stainless steel. The plates were supported on two plate rails: 5 mm diameter steel rods that ran the width of the unit. Two shaft collars, 5 mm ID x 12 mm OD x 6 mm width, were welded to each plate and the shaft collar set screws were used to fasten the plates into position on the plate rails. With the shaft collar and plate rail system, the number and position of the plates, and the total collecting plate area could easily be adjusted. Figure 3.1 shows a diagram of the small-scale ESP.

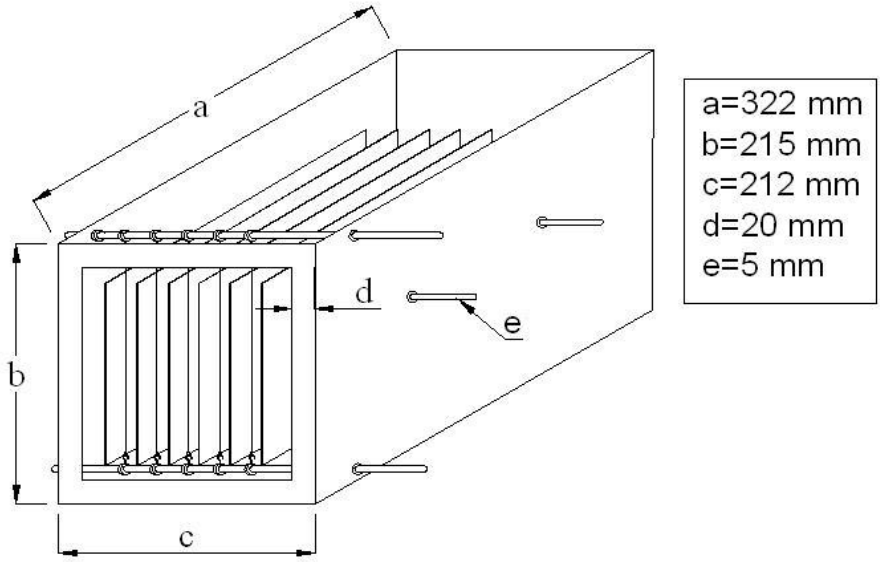

Figure 3.1 Dimensions of the prototype

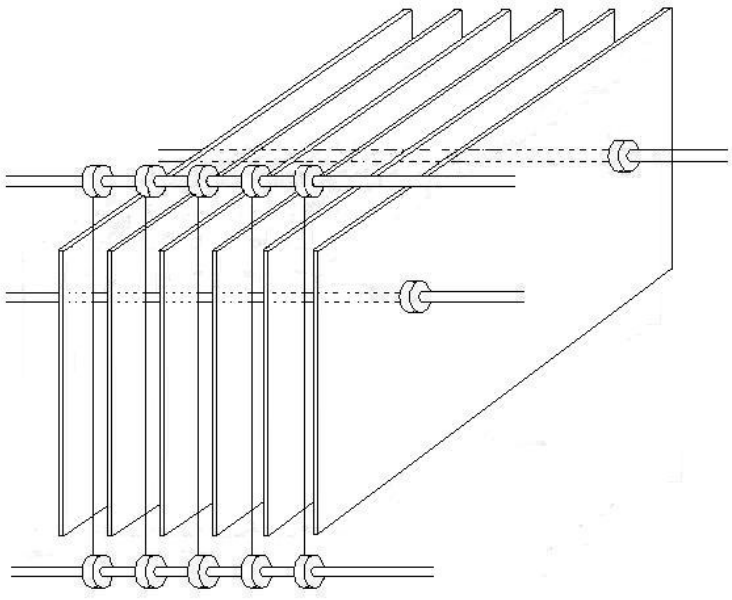

Figure 3.2 Rail system used to energize electrodes in ESP.

The charging electrodes for this ESP were straight wires constructed from 0.13 mm (0.005 inch), 0.20 mm (0.0080 inch), or 0.50mm (0.02 inch) diameter stainless steel wire. The wire diameters were verified by microscopic filar analysis. Each wires was cut to a length of approximately 20 cm and loops were made and secured on each end of the wire with pin contacts. The loops were attached to hooks on the shaft collars. The ESP was designed for up to five rows of wires, but a single row was used for this experiment. Two 5 mm diameter steel rods, 2 cm above and below the collecting plates, were used to hold the wires taut in the ESP. Shaft collars held the ends of each wire and allowed the user to easily change the wire positions. The same type of shaft collars used to secure the plates to the plate rails were used as the terminal ends of the corona wires. Two wire rails were used, one each on the top and bottom of the ESP. With this arrangement, wire and plate positions were easily changed between experiments, and the number of wires in the ESP could be changed with minor adjustments. Figure 3.2 shows the details of the plate rail and wire rail system of the ESP.

Teflon tubes were used to sheath the wire and plate rails to prevent contact between the rails and the outer shell of the ESP. Mylar sheets were used to insulate the internal surfaces of the ESP. Very high electrical resistance of mylar insured that random sparking from the electrodes did not energize the ESP shell.

3.1.2 Power Supply and Electrical Testing

The high voltage power equipment used for the investigation of the electrical properties of the small-scale ESP are shown in Figure 3.3. Two high voltage power supplies (HVPS) (Acopian, models P020HA3 and P010HA6, Easton, PA) were used to generate voltage difference between the wire and plate electrodes of up to 20,000 volts, with a maximum power

output of 60 Watts. The voltage output from the HVPS was externally controlled with a variable 12-volt DC power supply connected to the control terminals of the HVPS. Use of the variable 12-volt power supply allowed for control of the output from the HVPS at 50 volt increments. The output from the HVPS was monitored with two digital voltmeters connected to the HVPS monitoring terminals, one for current monitoring and one for voltage monitoring (Laurel Electronics, Model DPM, Costa Mesa, CA). Tests were performed with positive corona, i.e. with the positive HVPS lead connected to a wire rail, and also with negative corona, i.e. with the positive HVPS lead connect to a plate rail. Current outputs from the HVPS as small as 0.0001 mA (0.1 microamp) were detectable with the digital voltmeters. With approximately 20 to 100 cm of charging wire in the ESP during a test, the minimum detectible currents for each test ranged from 0.001 to 0.005 microamps/cm.

The electrical properties were investigated with a single wire diameter of 0.13 mm, and at plate-to-plate distances of 1.5, 2.0, and 2.5 cm, corresponding to plate-to-wire distances of 0.75, 1.0, and 1.25 cm. Then, a single plate-to-plate distance of 2.0 cm was used to investigate electrostatic properties at wire diameters of 0.13mm, 0.21mm and 0.50mm. The positions of the plates and wires were measured with high-precision calipers (Swiss Precision Instruments, Model 12-529-4, Garden Grove, CA). Experiments were performed with 3-plate/2-wire and 6-plate/5-wire configurations.

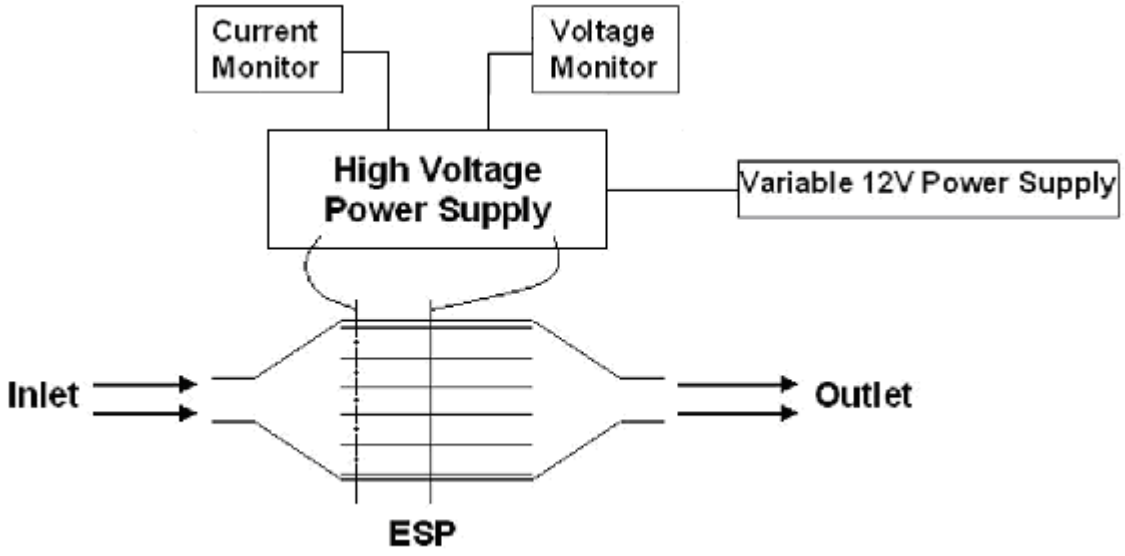

Figure 3.3 Setup of the high-voltage system

After setting the positions of the plates and wires and connecting them to the HVPS, the voltage supplied by the HVPS to the ESP was gradually increased from zero at approximately 250 volt increments. The lowest voltage setting with measurable current production (at least 0.0001 mA) was recorded as the onset voltage. Once the onset voltage was determined, the voltage was again increased at 50 volt increments. Sparks between the electrodes occasionally would occur at voltages beyond the onset voltage, and the frequency of sparking would increase with voltage. During sparking, the voltage was held constant until consistent current output resumed. The voltage which caused one or more sparks every two seconds was considered the sparkover voltage, and this was the upper end of the voltage-current experiment. The voltage and current data collected between the onset voltage and the sparkover voltage comprised a single voltage-current experiment. Five replicate voltage-current experiments were performed for each plate-to-plate distance and corona polarity.

3.2 Diesel Particulate Sampling and Analysis

With the worldwide recognition in the problem of diesel particulate emissions, and the geographic diversity of companies that manufacture diesel vehicles and diesel machinery, there have been many designs and configurations of diesel particulate sampling and analysis apparatus. A few studies have compared different methods of DPM sampling across numerous laboratories and found out that there were wide differences in methods in different laboratories which consequently affected the obtained results (Kittleson et al, 1999; Lyyranen et al, 2004). Although there is still not a unified method for DPM sampling used by all laboratories, the major goal of a sampling system is to obtain DPM that is representative of the environment of interest, be that DPM in the combustion cylinder, exhaust system, or DPM in the ambient or occupational atmosphere.

This objective of this portion of the research was to design and build a system for the generation, sampling, and analysis of diesel particulate matter. Because of the constraints imposed by working in an academic laboratory, there were considerations of both space and cost when designing the system, while at the same time not sacrificing the goal of building a system that would produce accurate results. One of the goals of the sampling system was to allow for the examination of mass concentration, number concentration, and size distribution with the same apparatus and only minor adjustments.

3.2.1 Diesel Particle Generation and Capture

The setup for the DPM generation, sampling, and analysis system is shown in Figures 3.4 and 3.5. The footprint of the entire system in the laboratory was only approximately 7m^2. Two

engines were used to produce the diesel exhaust. The main engine was a 5.5 kW diesel generator produced the diesel exhaust (Eastern Tools, model 178F) and the backup engine was a 6.5 kW generator (DUROPOWER, model 6500DES). Although the backup engine was slightly more powerful and produced a little more flow, the engines were actually very similar. Characteristics of the engines are listed in table 3.1.

Table 3.1 Characteristics of Diesel Generators

Model	178F	6500DES
Manufacturer	Eastern Tools	Duropower
Cylinder	1	1
Displacement (L)	0.296	0.418
Max. Power Output (kW)	5500	6500
Injection	DI	DI

Two lines of one inch galvanized steel pipe were used to transport the exhaust from the engine to the sampling lines and ventilation hoods. One line was the main line for sampling and analysis, and the second was a bypass line used for occasional maintenance or flow control. Two ball valves were used to adjust the flow that went through each line. The flow rate of the main line was measured using an orifice plate and a manometer, and temperature measurements were made at several locations using thermocouples. The sampling line was made from quarter inch stainless steel tubing which was introduced into the main line at an elbow, as shown in Figure 3.4. The sampling line was inserted 15 centimeters into the main line and parallel to the pipe walls. The sampling line flow was metered by a calibrated and laboratory made venturi meter.

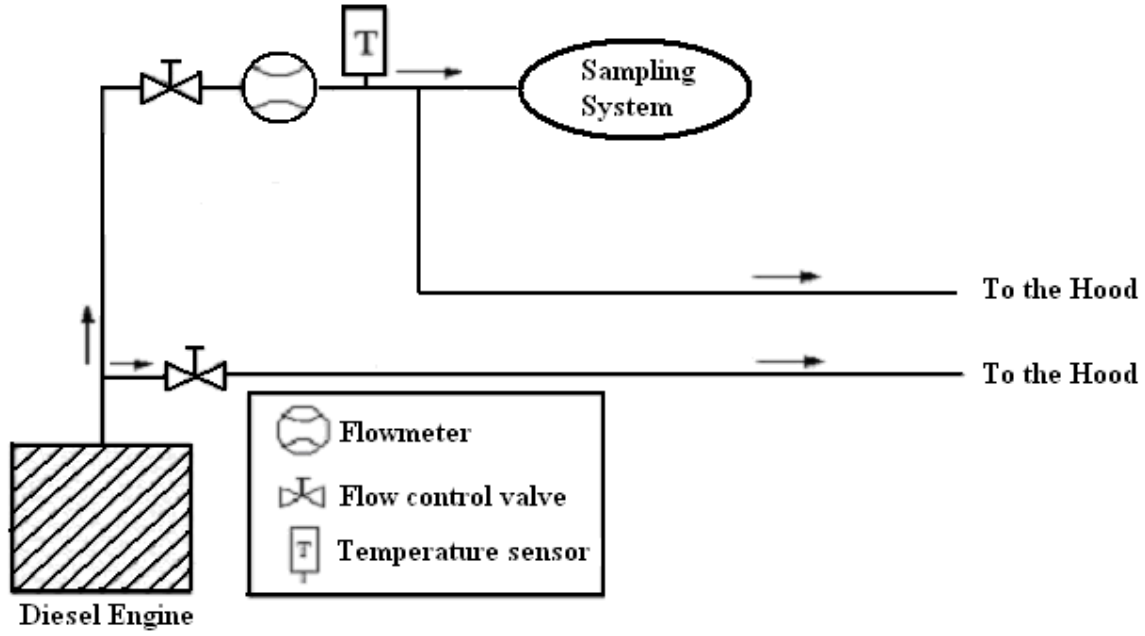

Figure 3.4 Exhaust transfer from the diesel generator to the hood

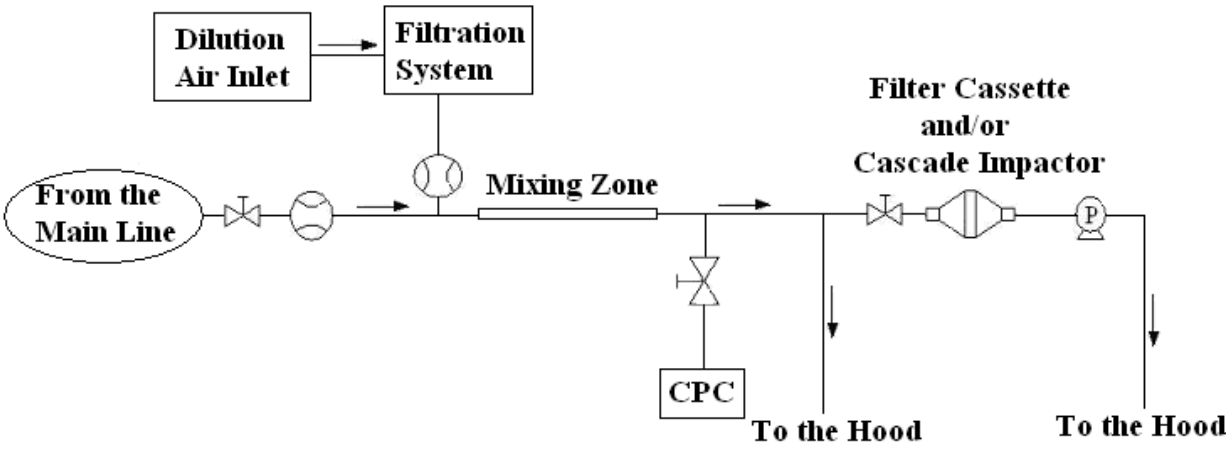

Figure 3.5 Sampling System for measuring mass concentration, number concentration, and size distribution

3.2.2 Dilution system

The sampling system was used for measuring three different DPM parameters: number concentration, mass concentration, and size distribution. Analysis of number concentration required a dilution ratio of at approximately 600:1 (clean air to diesel exhaust) to bring the number concentration and gas temperature into the operating range of the particle counting instrument being used. Mass concentration was determined by sampling exhaust directly onto pre-weighed filters without dilution. Size distribution was examined by sampling exhaust through a cascade impactor, which worked best with a dilution ratio of two to prevent rapid plugging of the final filter. This wide range of dilution ratio requirement meant that both dilution air flows and diesel exhaust flows had to be adjustable.

Dilution air was supplied by an air compressor, but because of the very high concentration of water mist aerosol in the compressed air, it was filtered using a four stage air purification system - rough particle filtering, fine particle filtering, activated carbon adsorption (Master Pneumatic Detroit Inc., Model BFC70H-2E9, Sterling Heights, MI), Drierite adsorption (Hammond Dierite Company, Model 207, Xenia, Ohio). This reduced the number concentration from approximately 200,000 particles per cm^3 to 0 to 1 per cm^3, below clean room particle standards. The diesel exhaust and dilution air were mixed in a section of 50 cm long, half-inch diameter pipe which was incorporated into the sampling system to increase the flow Reynolds number and mix the dilution air into the exhaust. The rest of the sampling system after the mixing zone, like the main lines, was made from one inch galvanized steel pipes. The residence time of the gases from the muffler to the point of dilution and mixing was less than 0.25 seconds. Other researchers have recommended residence times less than 0.25 seconds between the point

of particle exhaust and particle dilution, to minimize errors from the condensation of vapors into the particle phase (Kittleson, 1999).

3.2.3 Number concentration measurement

Number concentration was measured with a condensation particle counter (CPC, Kanomax Model 3800, Andover, NJ). The CPC can detect particles larger than 15nm and it samples at 700cc/min. The particle concentration upper limit of the CPC is 10^5 per cc, and the maximum recommended temperature of sampled aerosol is 35 ^oC. The dilution air acts to reduce the incoming concentration to less than the upper limit and also to reduce the temperature of the diesel exhaust from almost 90 ^oC at the sampling probe inlet to 25 ^oC at the CPC. A particle nephalometer (Met One Model 228, Grants Pass, Oregon), sensitive to particles larger than 500nm, was also used to sample the aerosol and provide information on coarse particle concentration. Pressure and temperature were both closely monitored upstream of the CPC and nephalometer to ensure conditions near 1 atm and below 35 ^oC during sampling.

3.2.4 Mass concentration and size distribution measurements

Mass concentration measurements were performed by sampling diesel exhaust through pre-weighed 47 mm Teflon membrane filters held in a stainless steel cassette. The mass gain in the filter was divided by the volume of exhaust sampled to obtain mass concentration. Different filters were tested for this experiment and Teflon membrane filters (Pallflex Membrane T60A20, East Hills, New York) allowed for high efficiency collection and consistent flow rate during sampling. Size distribution analyses was performed using a cascade impactor (SKC Model 225-370, Eighty Four, PA), which separated the particle mass into five size categories. All filters

used in the filter cassette and cascade impactor were weighed with a calibrated microbalance (Perkin Elmer, AD-6 Auto balance, Waltham, MA).

3.2.5 Initial Testing of the Sampling System

To test the initial configuration of the DPM generation, sampling, and analysis system, the exhaust from the diesel-powered generator was characterized several times over a period of 4 weeks. The mean mass concentration of the particles coming from the diesel generator was 170 +/ 30 mg/m^3. The mean total number concentration was $3.4*10^{13}$ +/- $1.3*10^{12}$ particles/m^3 (Low Sulfur Diesel used). Runs on different days produced similar results indicating that the sampling and analysis system had a high degree of precision. The size distribution of DPM from the generator showed that most of the mass concentration was contributed by particles with 250 nm or smaller diameters, in agreement to size distribution analyses obtained by other researchers. Experiments on dilution ratio ascertained that number concentration adjusted for dilution ratio did not vary when using dilution ratios from 600 to 800. This suggested that vapor condensation in the sampling lines was not biasing particle analyses. The total costs of the DPM generation, sampling, and analysis system, including electricity generator, CPC, microbalance, and piping, was approximately $24,500.

3.2.6 Measuring the Collection Efficiency of the ESP

The primary objective of this research is to reduce diesel particulate emissions through the development of electrostatic technology. Determining the effectiveness of any particle capture technology requires measuring its particle collection or removal efficiency. Before measuring collection efficiency or conducting other experiments, the engine and piping system

were warmed up by operating the engine for at least 60 minutes. If there was load on the engine, the warm up period consisted of two 30 minute parts with and without load on the engine.

The warm-up period was necessary for two main reasons. First, the composition of diesel exhaust during a cold start is different than the exhaust from a warm engine and this could affect particle removal efficiency. Secondly, after warm up, the temperature of the pipes and valves was generally constant and no longer changing. Tables 3.2 and 3.3 show how temperature and exhaust flow rate changed with time at different locations along the exhaust transport system. Both parameters were measured versus time with the engine running idle and at medium load. Point 1 was 1 meter away from the exhaust pipe. Points 2, 3, and 4 were 75 cm apart from each other and points 3 and 4 were monitoring the temperature before and after the ESP. Point 5 was the temperature at the point of sampling. The tables show that when the engine was running at idle, the ESP was collected the particles in exhaust temperatures ranging from 60 to 85 ^{o}C. However, with the medium load on the engine the temperature at the location of the ESP was usually greater than 100 ^{o}C.

Table 3.2 Temperature variation with time at different locations of the sampling system (engine running at idle). All temperatures are in ^{o}C.

Temperature after	Point 1	Point 2	Point 3	Point 4	Point 5	Flow (L/s)
0 minutes	22.7	22.6	22.8	22.4	22.3	7.2
10 minutes	89	75.5	63	45.5	23.5	7.4
20 minutes	95	90	75	50.8	23.2	7.4
30 minutes	97	95	82	51.5	23.5	7.4
60 minutes	97	95	85	56	25.5	7.4
90 minutes	99	95	86	59	25.4	7.4

Table 3.3 Temperature variation with time at different locations of the sampling system (engine running at medium load). All temperatures are in ^{o}C.

Temperature after	Point 1	Point 2	Point 3	Point 4	Point 5	Flow (L/s)
0 minutes	22.7	22.6	22.8	22.4	22.3	8.6
10 minutes	125	104	84	48	23	8.6
20 minutes	138	117	104	65	26	8.6
30 minutes	137	125	106	70	27	8.6
60 minutes	142	127	115	70	26	8.6
90 minutes	149	127	124	71	27	8.6

3.2.6.1 Measuring Collection Efficiency of the ESP – Number Concentration Basis

Measuring the collection efficiency of the ESP on a number concentration basis was performed by measuring the number concentration of particles just downstream of the ESP with the power supply to the ESP turned off (i.e. untreated number concentration), and measuring the concentration downstream with the power supply turned on (i.e. treated number concentration). In both cases, the CPC was used to measure number concentration. Particles in diluted untreated exhaust were analyzed for three minutes, followed by a one minute interval during which the ESP power supply was turned on, and then the CPC measured the treated number concentration for another three minutes. An alternating sequence of untreated and treated exhaust analyses was performed, and the overall number-based collection efficiency of the ESP was calculated using the following equation:

$$E_{number} = \frac{N_{untreated} - N_{treated}}{N_{untreated}} * 100 \qquad (11)$$

where E_{number} was the number-based removal efficiency of the small-scale ESP, $N_{untreated}$ was number concentration with the precipitator turned off, and $N_{treated}$ was number concentration with the precipitator on.

3.2.6.2 Measuring Collection Efficiency of the ESP – Mass Concentration Basis

Measuring the collection efficiency of the ESP on a mass concentration basis was performed with a procedure very similar to the one used to measure number concentration. Mass concentration was measured using pre-weighed Teflon sampling filters, with samples taken downstream of the ESP. Samples were taken, for ten minutes, with the power supply to the ESP turned off. Immediately after this untreated sample, the power supply was turned on and another ten minute sample was taken while the ESP was treating the exhaust. This procedure was repeated at least three times and three samples were taken with the power off, alternating with at least three samples taken with the power on. There was a five minute time interval, with the ESP off, between each pair of untreated/treated samples and the next pair. Based on these samples, the mass-based efficiency of the precipitator was determined for each sample with the following equation:

$$E_{mass} = \frac{M_{untreated} - M_{treated}}{M_{untreated}} * 100 \qquad (12)$$

where E_{mass} was mass-based removal efficiency of the small-scale ESP, $M_{untreated}$ was mass concentration with the precipitator turned off, and $M_{treated}$ was mass concentration with the precipitator on. Efficiency of the ESP at each voltage was determined by taking an average on all efficiency values associated with that voltage.

CHAPTER 4

RESULTS: FUNDAMENTAL ELECTRICAL PROPERTIES OF SMALL-SCALE ELECTROSTATIC PRECIPITATORS

4.1 Introduction to the Investigation of Small-Scale Electrostatic Properties

The pioneering work of Peek and Townsend, discussed in chapter 2, became the foundation for decades of research on industrial electrostatic precipitation. In addition to the fundamental research on corona formation and its properties and behavior in different gases; the practical design, construction, and operation of ESPs have received much attention. Government manuals, journal articles, and technical guidance documents published since the 1950's have properly focused on the issues necessary to successfully operate large industrial ESPs with capacities to treat tens to thousands of cubic meters per minute. Nonetheless, electrostatic precipitation has also been investigated or developed for small-scale applications like occupational particle sampling, household air purification, and diesel exhaust particle filtration (Faulkner et al, 1981; Masuda et al, 1983; Farzaneh et al, 1994; Shaughnessy et al, 1994; Volckens et al, 2002; Armendariz and Leith, 2003; Armendariz et al, 2003; Saiyasitpanich et al, 2006).

Although small-scale ESPs have many potential applications, the majority of the laboratory and industrial empirical data fundamental electrical properties is for large-scale industrial units. Table 4.1 shows a sample of some of the frequently-cited ESP

design literature and highlights some of its limitations in using the large-scale relationships for small-scale ESP design.

Table 4.1. Limitations of the Traditional ESP Literature for Small-Scale Unit Design.

Reference	Comment
White, 1955	Experimental data used pipes at least 10 cm in diameter
White, 1963	The smallest plate-to-plate distance was 4 cm
White, 1977	Wire-to-plate spacing values were between 20-30 cm
Oglesby and Nichols, 1978	Smallest plate-to-plate distance was 10 cm
Lloyd, 1988	Energization voltages were between 30kV-130kV
Parker, 1997	Typical plate-to-plate distances were 25-40 cm. Smallest unit described had 10 cm plate-to-plate
USEPA, 1998	Typical wire-to-plate distance was between 20 to 30 cm
Turner et al, 2000	Smallest flows evaluated were ~ 50 m^3/sec (100,000 cfm)

A prototype small-scale ESP was built to investigate the electrostatic properties of small-scale ESPs. The goal of this portion of the work was to develop data to guide the design of an ESP for diesel particle collection, and to also provide empirical data to future researchers of other small-scale applications. The three fundamental electrostatic properties investigated were the onset voltage, the voltage-current relationship, and the sparkover voltage. The parameters varied during the experiments included corona polarity, plate-to-plate distance, and wire diameter. In addition, a comparison was made between measured electrostatic properties and those predicted by the standard equations.

4.2 Effect of Plate-to-Plate Distance on Fundamental Electrical Properties

4.2.1 Empirical Results

Figures 4.1 and 4.2 show current production as a function of voltage for the small-scale ESP, for negative and positive corona, respectively, for three plate-to-plate distances. The curves show the mean values of five replicates at each plate-to-plate distance, 1.5, 2.0, and 2.5 cm. The error bands are drawn at +/- 1 standard deviation from the mean current value. The curves span the range from onset voltage to sparking voltage. Current production is normalized per unit length of wire.

The data indicated that current production decreased with increasing plate-to-plate distance at a constant voltage. For example, at 8000 volts with negative corona polarity, current outputs at 1.5, 2.0, and 2.5 cm plate-to-plate distances were 0.11, 0.03, and 0.01 mA/cm. This inverse relationship was in agreement with the trend predicted by equations (2.3) and (2.5) and by observations on large-scale units that show current inversely related to plate-to-plate distance. The data also indicate that the slopes of the voltage-current curves were inversely proportional to plate-to-plate distance, indicating that current production as a function of voltage increased more rapidly at smaller plate-to-plate distances than at larger ones.

The data also indicated that sparkover voltage increased substantially with increasing plate-to-plate distance, a trend expected from the standard equations and the data from industrial-scale units. In addition, positive corona sparkover voltages were always higher than negative corona values ($P < 0.05$).

The sparkover voltages were used with the onset voltage to determine the voltage operating ranges for each set of experimental parameters. The voltage operating range is essentially the maximum achievable voltage range over which steady current is produced and electrostatic precipitation is possible. The voltage operating range increased substantially with plate-to-plate distance across all tests.

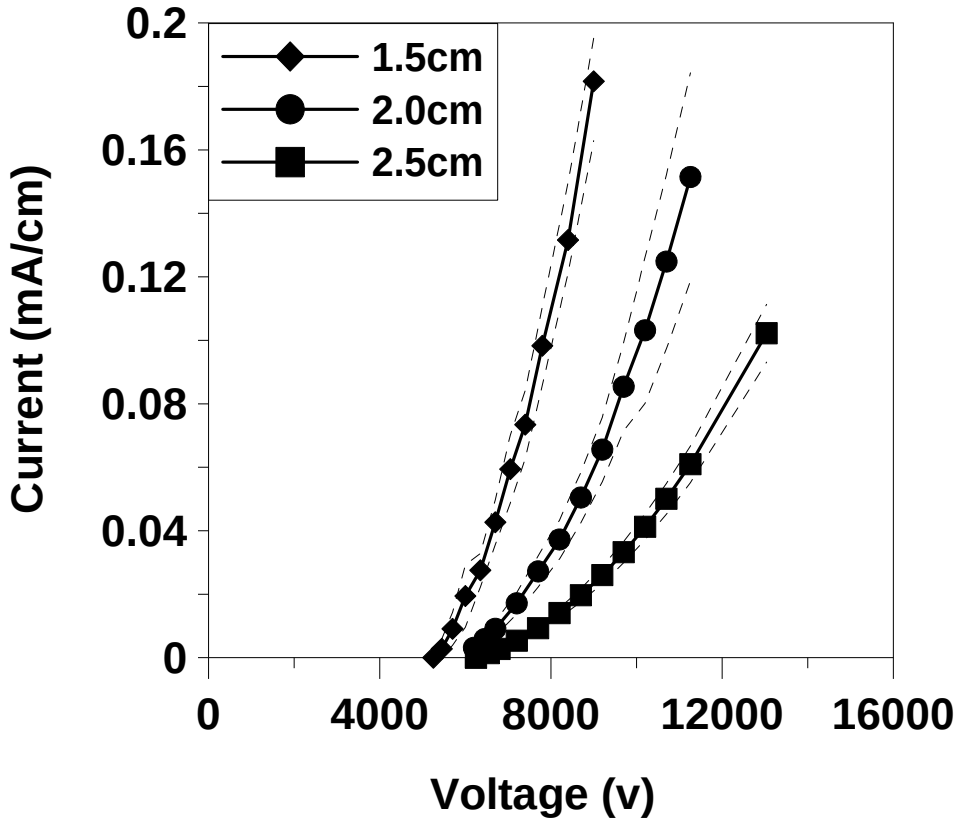

Figure 4.1 Effect of Plate-to-Plate Distance on Voltage-Current - Negative Corona.

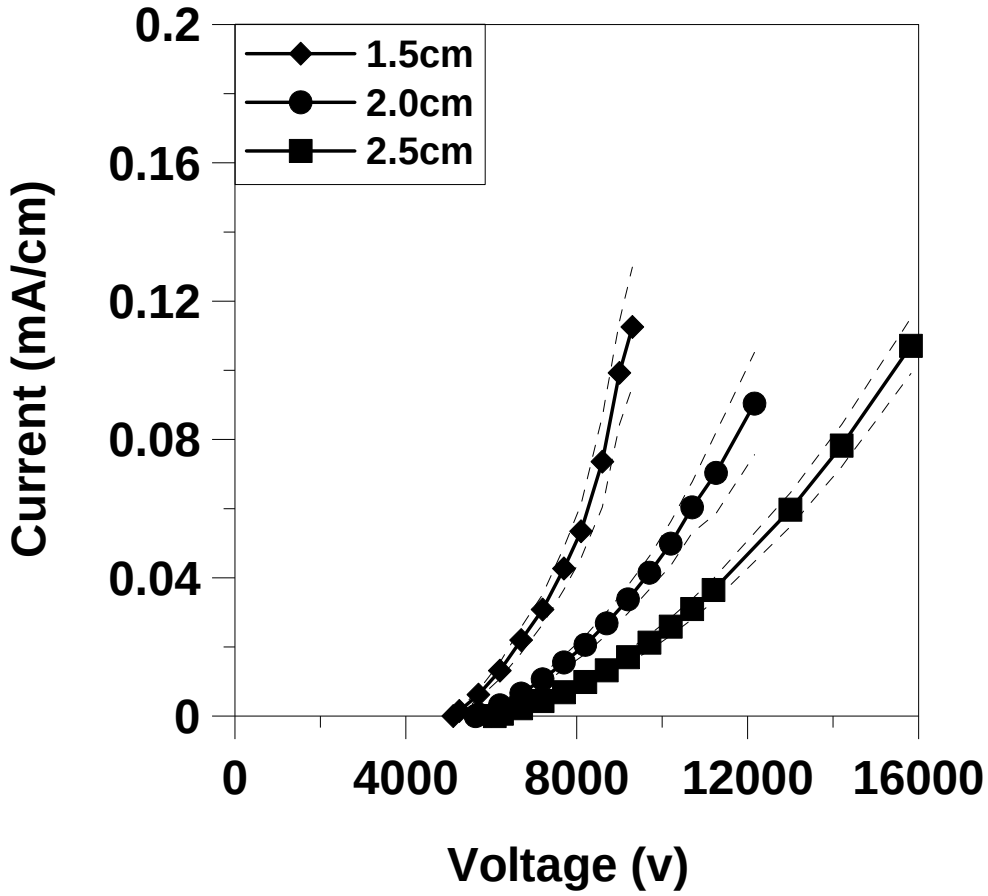

Figure 4.2 Effect of Plate-to-Plate Distance on Voltage-Current - Positive Corona

There were no significant differences in onset voltage between positive and negative coronas for the three plate-to-plate distances tested ($p \geq 0.1$). Current production began at approximately the same voltage regardless of whether negative or positive current was being produced. Since there were differences in the slopes of the voltage-current curves with corona polarity, with the negative corona experiments producing steeper curves, negative corona polarities consistently produced more current per applied voltage than the positive corona experiments ($P < 0.01$).

Analysis of the plate-to-plate distance and corona polarity data together indicates that the combination of negative coronas and small plate-to-plate distances produced the highest currents

in the ESP. For example, the current at 80 percent of sparkover voltage for negative corona and a 1.5 cm plate-to-plate distance (0.13 mA/cm) was 220% greater than the current for positive corona and a 2.5 cm plate-to-plate distance (0.06 mA/cm). Since negative coronas and small plate-to-plate distances produce the highest currents, these settings also would be expected to produce the highest ion densities, the maximum particle charging, and the highest particle collection efficiencies in small-scale ESPs.

4.2.2 Comparison of Experimental and Theoretical Electrical Properties

Table 4.2 summarizes the onset and sparkover voltages measured experimentally and the values predicted using traditional ESP relationships (i.e. using equations (2.2), (2.3), and (2.4), the empirically and theoretically determined equations for large-scale units). For both corona polarities, the measured onset voltages were not significantly different than the predicted values ($p > 0.1$). In this work, onset voltage was defined by the generation of at least 0.0001 mA of current.

Table 4.2 Experimental and Predicted Onset and Sparkover Voltages

Plate-to-Plate Distance (cm)	Corona Polarity	Onset Voltage (V_o) - volts			Sparkover Voltage (V_s) - volts		
		Exp.	Pred.	ΔV_o %	Exp.	Pred.	ΔV_s %
1.5	-	5300 +/- 230	5760	-8	7600 +/- 1100	12000	-37
	+	5100 +/- 67	5760	-11	8400 +/- 950	12000	-30
2.0	-	5800 +/- 320	6110	-5	10000 +/- 1300	17000	-41
	+	5600 +/- 100	6110	-8	11000 +/- 1400	17000	-35
2.5	-	6300 +/- 300	6380	-1	15000 +/- 700	21000	-29
	+	6100 +/- 160	6380	-4	16000 +/- 230	21000	-24

Exp. = experimental data
Pred. = perdicted values
Predicted values based on Equations (2.2) and (2.3) for V_o and on Equation (2.4) for V_s.
Percentage differences (Δ%) calculated as (experimental - predicted) / predicted x 100.
p-values determined for the significance of the difference between experimental and predicted values.

The measured sparkover voltage values were significantly lower than the theoretical values predicted with equation (2.4) ($p < 0.01$), with a mean difference of approximately 5000 volts. The lower than predicted values might have been a result of the difficulties in maintaining perfect wire alignment in small-scale units. A misalignment in a large-scale unit of 1 mm (i.e. the wire being 1 mm closer to one plate than another) would be less important in a large scale unit with plate to plate distances of 20 cm (200 mm), than in the current precipitator with plate to plate distances on the order of 2 cm. Accurately predicted onset voltages and lower than predicted sparkover voltages, meant that our small-scale wire-plate ESP had a smaller voltage operating range than would be predicted by the equations, whether the unit was operated with negative or positive corona current.

Along with the examination of onset and sparkover voltages, the differences between measured and predicted current production were examined. Equation (2.5) was developed by

Townsend to predict ESP current production and it was examined in this study to determine how well it predicted small-scale current production.

The experimental voltage-current data and the voltage-current data predicted with the Townsend equation (2.5) and Cooperman's low-current approximation (Equations (2.6) and (2.7)) are plotted in Figure 4.3. The error bars on the experimental data in Figure 4.3 are one standard deviation from the mean.

There were large differences in predicted voltage-current behavior depending on whether Townsend or Cooperman equations were used. For negative coronas, the slopes of the measured voltage-current curves were accurately predicted using the modified Townsend equation, but the low current approximation produced shallower curves, underpredicting current production as a function of voltage.

The standard Townsend equation is more complicated to use than the low current approximation of Cooperman, but it consistently generated more accurate predictions of current-voltage behavior. Cooperman's approximation consistently underpredicted current over the entire voltage operating range. The plate-to-plate distances and wire diameters of the ESP tested in this work were much smaller than the dimensions in typical industrial units. These small distances produce extremely high current densities. Typical current densities in industrial precipitators range from 0.05 to 1 mA/m^2 of collection plate area (McLean et al, 1986). For our small-scale ESP, the currents midway between the onset and sparkover voltages produced current densities of approximately 25 mA/m^2 plate area. The high currents produced by the small-scale ESP are a potential reason why Cooperman's approximation is inappropriate at these dimensions.

In addition, the data showed that the Townsend equation (equation 2.5) could accurately predict current production for the plate to plate distances on the upper end of those tested in the small-scale unit, but agreement was poorer for the smallest plate to plate distance.

To investigate the reasons why the Townsend equation worked well at some plate to plate distances but not others, several additional voltage-current tests were performed at larger plate-to-plate distances: 3.0, 4.0, and 5.0 cm. Then, sing the measured current production at each voltage and the known

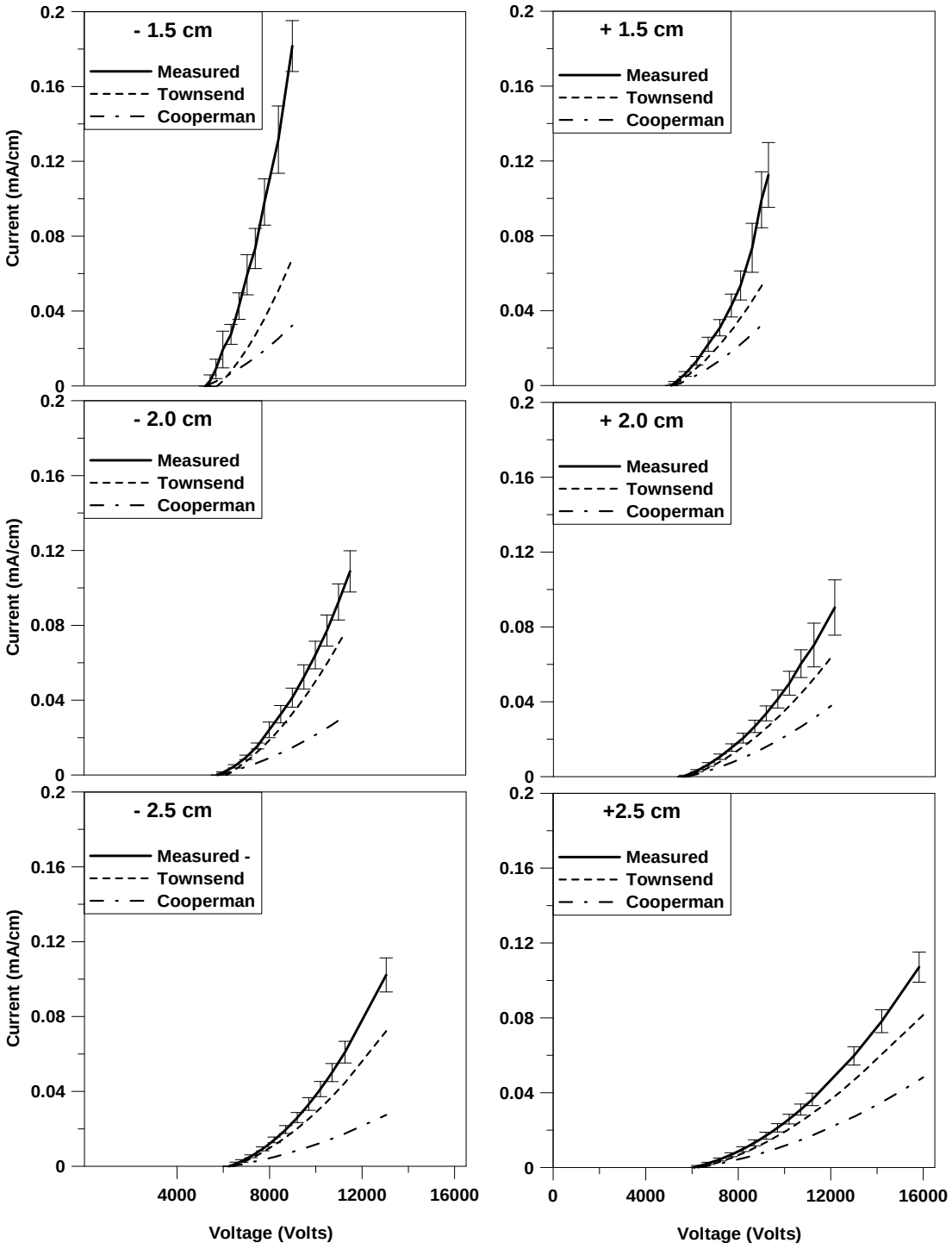

Figure 4.3 Comparison of measured and predicted voltage-Current trends. Data points are given for experimentally measured data, filled symbols are negative corona data points, and open symbols are positive corona data points. (a), (b), and (c) are negative corona currents, (d), (e), and (f) are positive corona currents.

known plate-to-plate distances, the Townsend equation was solved to determine the ion mobility value that produced the best agreement between predicted and measured current. Ion mobility is a physical parameter which describes the velocity of ionic motion in air as a ratio to the electric field strength in the area around the ions.

$$V = V_0 + aE_0\left[\left(\sqrt{1+\frac{2ib^2}{KE_0^2a^2}}-1-\ln\left(\frac{1+\sqrt{1+\frac{2ib^2}{KE_0^2a^2}}}{2}\right)\right)\right] \qquad \text{(2.6) repeated}$$

Figure 4.4 shows the electrical mobility values required to achieve perfect agreement between our empirical data and the Townsend equation. The data show that mobility values reach a minimum value at plate to plate distances larger than 4 cm. At plate to plate distances smaller than this, there was a gradual and then sharp increase in ion mobility.

Beyond plate to plate distances of 4 cm, the best agreement between predicted and measured current production was with mobility values of 1.2 cm^2/v.sec for negative ions and 1.6 cm^2/v.sec for positive ions. These values are in good agreement with the work of other researchers, including Charry and Kavet, who reported positive ion mobilities to range from 0.7 to 1.8 cm^2/v.sec and negative ion mobilities to range from 1.0 to 2.4 cm^2/v.sec (Charry and Kavet, 1987). In addition, Hinds (1998) recommended ion mobility values of 1.5 for both current polarities.

At plate to plate distance smaller than 4 cm, the apparent ion mobilities determined with the small-scale ESP were substantially greater than the values in the standard references. At a 1.5 cm plate-to-plate distance, the ion mobilities of the small-scale ESP were 4.7 cm^2/v.sec for

negative and 2.2 cm^2/v.sec for positive ions. The high mobility values at very small plate-to-plate distances is possibly due to a substantial proportion of the currents being carried either by free electrons, or small molecular weight primary ions. The number of free electrons and small ions in the ionizing region of an ESP is very high and at small plate-to-plate distance like 1.5 cm, the ionizing region is very close to collecting electrodes. This will cause a sharp increase in the value of mobility since free electrons and small ions have very high mobilities due to their extremely small masses (Hinds, 1998).

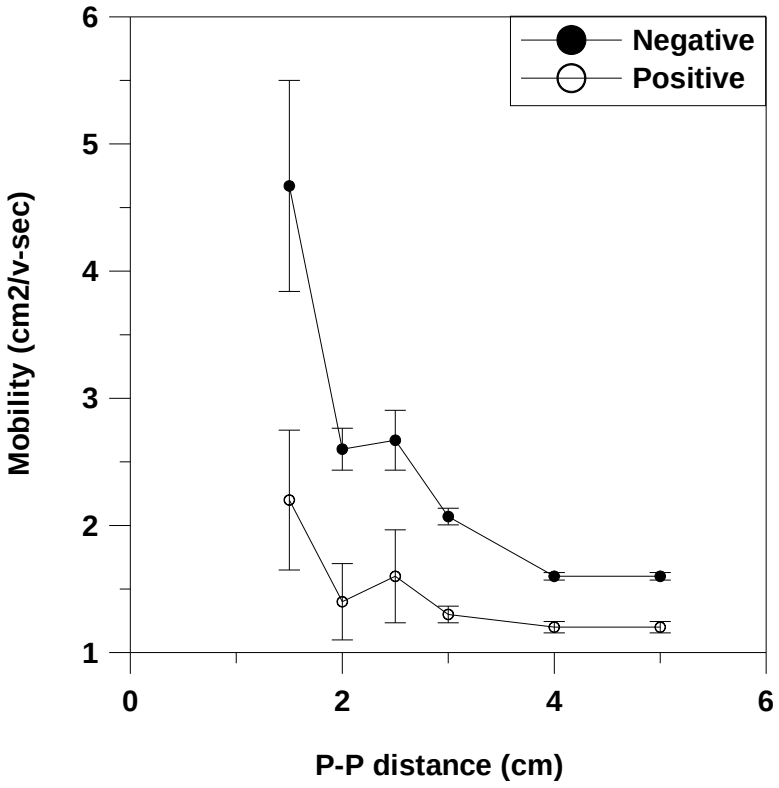

Figure 4.4 Calculated mobility versus plate-to-plate distance in small-scale ESPs

An important benefit of the design of the prototype unit was the extremely high current densities. Typical current densities in industrial precipitators range from 0.05 to 1 mA/m^2 of

collection plate area. For our small-scale ESP, the currents midway between the onset and sparkover voltages produced current densities of approximately 25 mA/m^2 plate area. In spite of the much higher current obtained by the small-scale ESP, theoretical and empirical equations which are developed based on large industrial ESPs can be used for small-scale ESPs to predict onset voltages and the voltage-current relationship if the electrical mobilities are properly adjusted to account for the importance of free electron current at the smallest plate to plate distances.

4.3 Effect of Wire Diameter on Fundamental Electrical Properties

4.3.1 Corona Current Production

Figures 4.5 and 4.6 show the voltage-current curves obtained for negative and positive corona, respectively, as a function of wire diameter. All of the curves are drawn from onset voltage to sparkover voltage, and current production is normalized per unit length of wire.

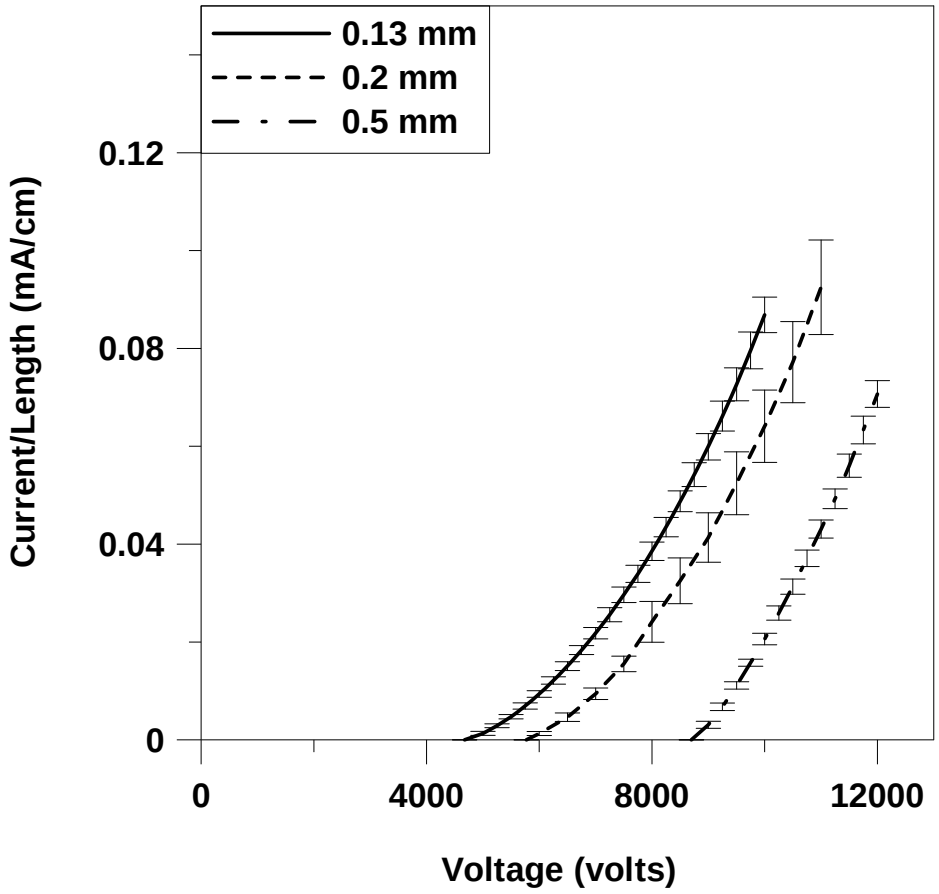

Figure 4.5 Voltage-current relationships for different wire diameters - negative corona

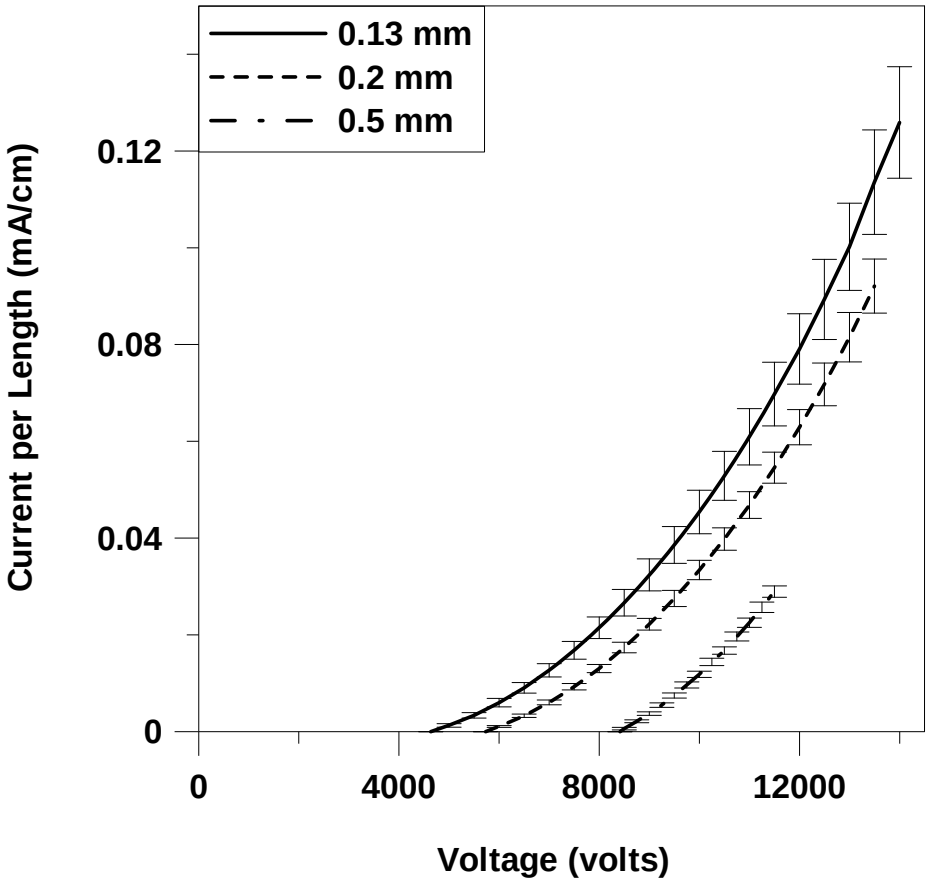

Figure 4.6 Voltage-current relationship for different wire diameters - positive corona

Current production showed an inverse relationship with wire diameter in both negative and positive cases. For instance, at 10,000 volts, a 0.5 mm diameter wire produced 0.021 mA/cm of current whereas a 0.13 mm diameter wire produced 0.11mA/cm. The data also indicate that negative corona produces higher current at a specific voltage compared to positive corona. Average negative corona current is approximately twice as much as positive corona current for all wire diameters tested in this experiment. The effects of wire diameter and corona polarity on current production were consistent with the predictions and observations of large-scale units.

In addition to the effects of wire diameter and corona polarity, current production in an ESP is also a function of wire roughness. White (1964) included a roughness factor *f* in the onset

voltage equation he developed, and recommended using a value of 0.5 for a scratched wire and 1.0 for a perfect wire.

$$V_0 = afE_0 Ln(\frac{\pi b}{2a}) \quad (4.1)$$

Figure 4.7 shows the SEM images of the 0.13mm, 0.2mm and 0.5mm wires tested. Multiple images were taken of each wire sample used. No substantial variation in roughness was observed for any of the wires. For comparison, Figure 4.8 shows images of manually sanded 0.2 mm and 0.5 mm wires.

4.3.2 Comparison of Onset and Sparkover Voltages

Table 4.3 shows experimental onset and sparkover voltages as a function of wire diameter. A direct relationship was observed between wire diameter and onset voltage. This is consistent with the predictions of equation (2.2). Paired T-tests performed on the experimental data showed no statistically significant difference in onset voltages with corona polarity for any of the wire diameters ($p > 0.1$). This is not the case with sparkover voltage which varied substantially between negative and positive corona. An inverse relationship between positive sparkover voltage and wire diameter was observed whereas negative sparkover voltages show a direct relationship with wire diameter.

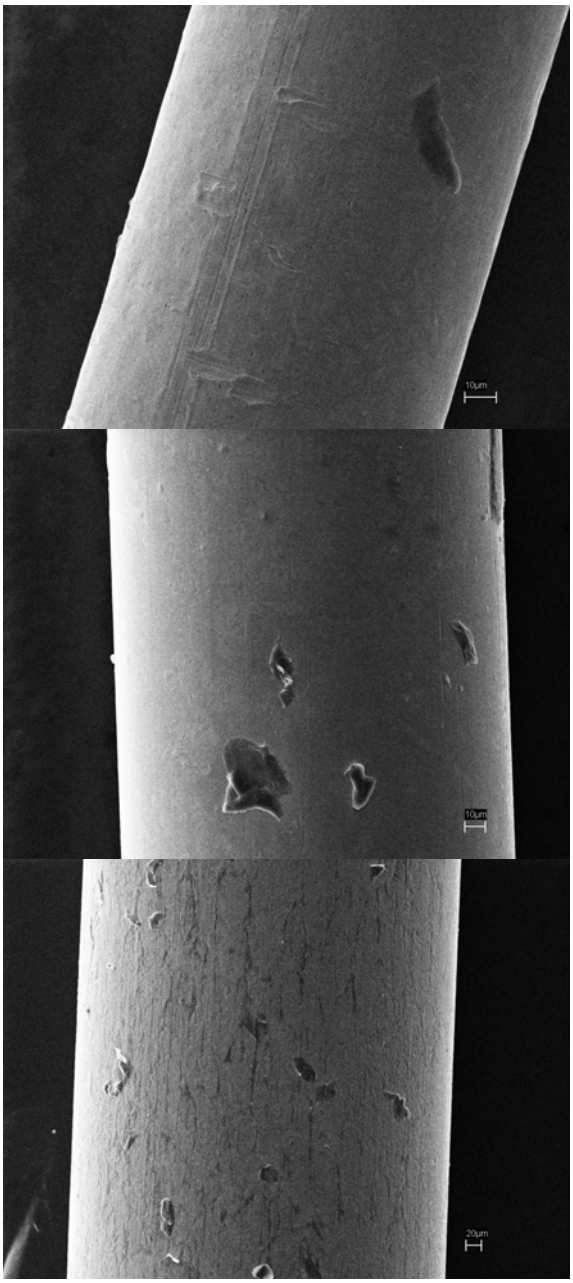

Figure 4.7 SEM images of different stainless steel wires. a) 0.13 mm b) 0.2 mm c) 0.5 mm

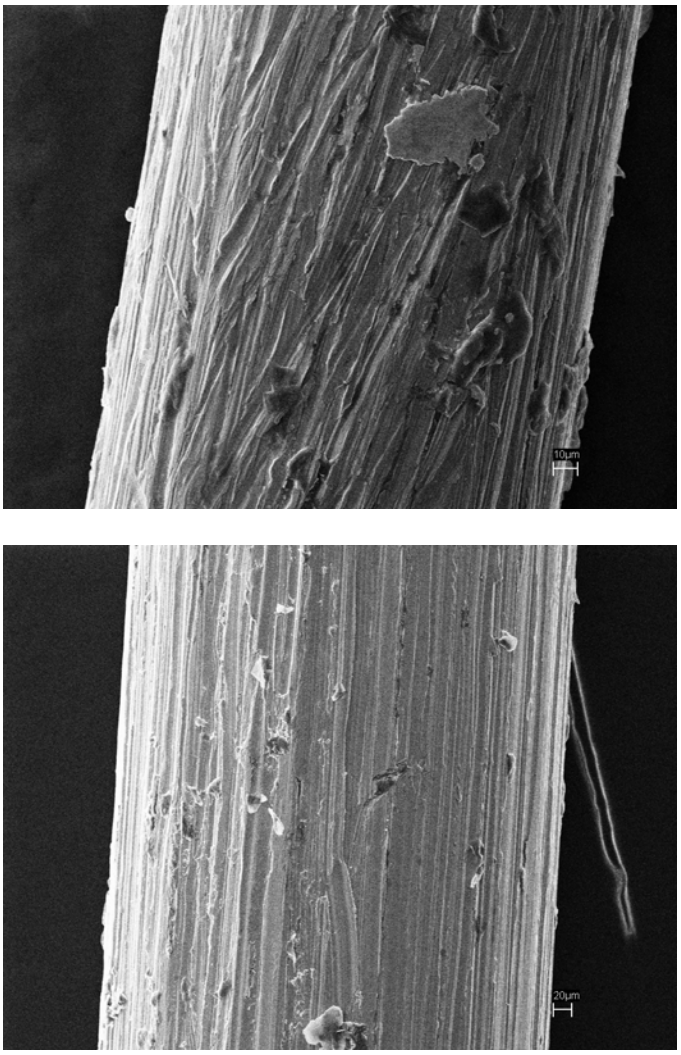

Figure 4.8 Manually scratched stainless steel wires a) 0.2 mm b) 0.5 mm

Table 4.3 Experimental onset and sparkover voltages for different wire diameters

Corona Polarity	Wire Diameter (mm)	Onset Voltage - volts			Sparkover Voltage – volts		
		Mean		SD	Mean		SD
-	**0.13**	4650	+/-	190	12670	+/-	500
-	**0.2**	5800	+/-	260	13390	+/-	730
-	**0.5**	8700	+/-	310	14290	+/-	510
+	**0.13**	4660	+/-	40	17700	+/-	430
+	**0.2**	5635	+/-	100	16800	+/-	1090
+	**0.5**	8410	+/-	250	15060	+/-	900

Many studies and reviews of large-scale ESP performance have indicated higher negative than positive sparkover voltages (Cottrell, 1908; White, 1963; Turner et al, 2000). However, in this work, positive sparkover voltages were substantially higher in all cases. The difference between negative and positive sparkover voltages seem to significantly decrease as the wire diameter increases. For instance, at 0.005 in, the difference is more than 5000 volts whereas at 0.02 in, it is only 800 volts. This suggests that there is a wire diameter above which, sparkover voltage will be higher for negative corona, and then the trends observed in large-scale units will be preserved.

Table 4.4 compares experimental results of onset voltage and sparkover voltage with the predictions made by equations (2.2) and (2.4). The results show that equation (2.2) can be used to closely estimate the onset voltage in small-scale precipitators with reasonable accuracy. Across all tested wire diameters, the results predicted by equation (2.2) are within five percent of the experimental onset voltages. Although the predicted sparkover voltage was close to experimental sparkover for 0.2 mm wire with positive coronas, consistent agreement was not observed.

Table 4.4 Experimental and theoretical onset comparison for different wire diameters

Corona Polarity	Wire Diameter (mm)	Onset Voltage – volts		Sparkover Voltage – volts	
		Experiment	Predicted	Experiment	Predicted
-	**0.13**	4650 +/- 190	5000	12670	21800
-	**0.2**	5800 +/- 260	6110	13390	16540
-	**0.5**	8700 +/- 310	9060	14290	10910
+	**0.13**	4660 +/- 40	5000	17700	21800
+	**0.2**	5635 +/- 100	6110	16800	16540
+	**0.5**	8410 +/- 250	9060	15060	10910

Predicted Onset-Onset voltage were calculated using equation (2.2) of Peek

Predicted Sparkover-Onset voltage were calculated using equation (2.4)

4.3.3 Comparison of Empirical and Theoretically Predicted Voltage-Current Trends

Figure 4.9 shows a comparison of empirical and theoretically predicted voltage-current trends. Equation (2.5) was used to predict current production as a function of voltage. One of the parameters needed to predict current production with equation 2.5 is the onset voltage. The onset voltages predicted by equation (2.2) were used with equation (2.5) to determine the predicted current production. Also, two different values of ion mobility were used to predict current production. A mobility value of 2.2 cm^2/v.sec, following the recommendation of White (1964), was used for predicting negative corona current, and for positive corona current, a value of 1.4 cm^2/v.sec was used (Charry and Kavet, 1987). As discussed earlier, the use of substantially higher ion mobility values for negative ions is appropriate in small-scale units since a significant fraction of the current might be carried from electrode to electrode by free electrons, which have substantially higher mobilities than typical negative air ions. With these parameters, good

agreement was obtained between empirical and predicted values, and predicted corona currents were typically within 20 percent of the experimental value for most tests. Even so, the empirical results consistently showed greater actual current production than would be predicted by the equations.

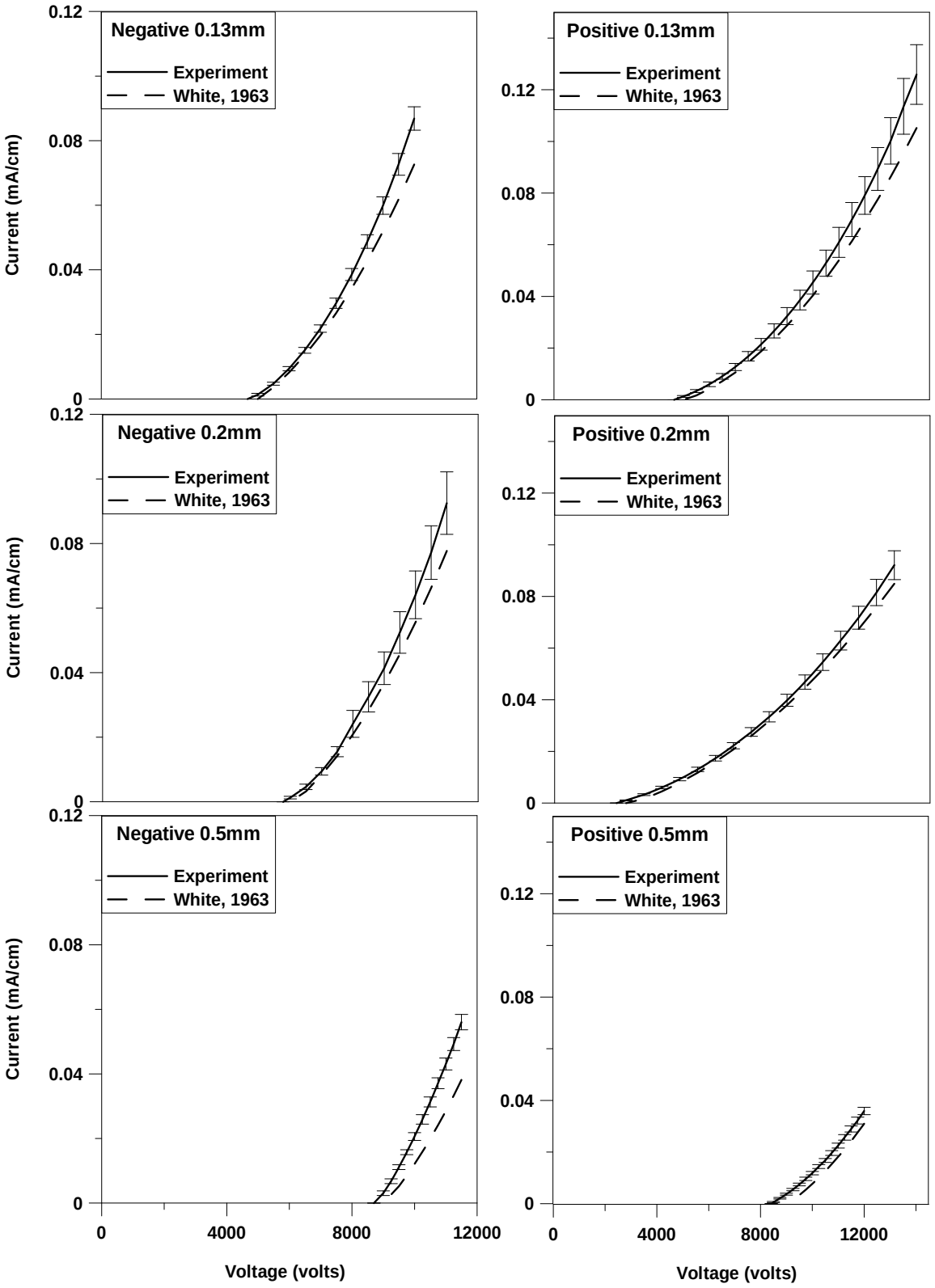

Figure 4.9 Comparison between experimental and theoretical current production

4.4 Onset Electric Fields and Voltages in Small-Scale Electrostatic Precipitators

Table 4.5 shows the complete set onset voltage data collected in these experiments, as functions of plate-to-plate distances, wire diameters, and corona polarities. The voltages applied between the charging and collecting electrodes are what is controlled by the high-voltage power supply system, but it is the electric field that is generated by the voltage which causes the ionization of gas molecules and the production of current. In plate-wire electrostatic precipitators, the relationship between electric field strength and applied voltage is described by equation (2.3):

$$V_0 = aE_0 Ln(\frac{\pi b}{2a}) \qquad \text{(2.3) repeated}$$

An important feature of equation 2.3 is that onset electric field strength is not predicted to be a direct function of plate-to-plate distance.

Table 4.6 shows the onset electric field strengths calculated with equation (2.3), derived from the onset voltages in Table 4.5.

Table 4.5 Onset voltages (volts) at Positive and Negative Corona Polarities. Mean values are shown, +/- 1 standard deviation.

plate-to -plate spacing (cm)	Onset Voltage (volts)											
	0.13 mm wire				0.2 mm wire				0.5 mm wire			
	Positive		Negative		Positive		Negative		Positive		Negative	
1	3750	+/- 46	3770	+/- 37	4585	+/- 79	4575	+/- 136	6155	+/- 6	6170	+/- 57
1.5	4330	+/- 70	4365	+/- 88	5215	+/- 24	5320	+/- 83	7465	+/- 102	7675	+/- 113
2	4615	+/- 59	4675	+/- 88	5705	+/- 47	5840	+/- 86	8210	+/- 98	8405	+/- 45
2.5	5075	+/- 62	5110	+/- 62	6135	+/- 74	6150	+/- 116	8975	+/- 74	9170	+/- 60
3	5380	+/- 14	5350	+/- 35	6555	+/- 35	6695	+/- 49	9480	+/- 45	9645	+/- 102
3.5	5725	+/- 24	5685	+/- 25	6970	+/- 21	7120	+/- 80	10020	+/- 72	10140	+/- 113
4	6085	+/- 59	6030	+/- 55	7415	+/- 55	7595	+/- 96	10695	+/- 73	10790	+/- 82
5	6895	+/- 17	6770	+/- 48	8285	+/- 15	8385	+/- 39	11870	+/- 22	12020	+/- 48
6	7750	+/- 57	7650	+/- 17	9190	+/- 25	9295	+/- 81	12955	+/- 73	13085	+/- 26

Table 4.6 Onset Electric Field Strengths (kV/cm) at Positive and Negative Corona Polarities. Mean values are shown, +/- 1 standard deviation.

plate-to -plate spacing (cm)	Onset Electric Field (kV/cm)											
	0.13 mm wire				0.2 mm wire				0.5 mm wire			
	Positive		Negative		Positive		Negative		Positive		Negative	
1	120.3	+/- 1.5	121	+/- 1.2	105.1	+/- 1.8	104.9	+/- 3.1	70.4	+/- 0.1	70.6	+/- 0.6
1.5	128.1	+/- 2.1	129.2	+/- 2.6	109.4	+/- 0.5	111.6	+/- 1.7	76.4	+/- 1	78.5	+/- 1.2
2	129.4	+/- 1.7	131.1	+/- 2.5	112.8	+/- 0.9	115.5	+/- 1.7	78.1	+/- 0.9	80	+/- 0.4
2.5	136.7	+/- 1.7	137.7	+/- 1.7	116.2	+/- 1.4	116.5	+/- 2.2	81	+/- 0.7	82.8	+/- 0.5
3	140.5	+/- 0.4	139.7	+/- 0.9	120	+/- 0.6	122.6	+/- 0.9	82.1	+/- 0.4	83.6	+/- 0.9
3.5	145.7	+/- 0.6	144.6	+/- 0.6	124.1	+/- 0.4	126.8	+/- 1.4	84	+/- 0.6	85	+/- 0.9
4	151.5	+/- 1.5	150.1	+/- 1.4	129	+/- 1	132.1	+/- 1.7	87.1	+/- 0.6	87.9	+/- 0.7
5	165.7	+/- 0.4	162.7	+/- 1.2	138.7	+/- 0.3	140.4	+/- 0.7	92.4	+/- 0.2	93.6	+/- 0.4
6	181	+/- 1.3	178.7	+/- 0.4	149.3	+/- 0.4	151	+/- 1.3	97.3	+/- 0.5	98.3	+/- 0.2

The data across all experiments indicated that there were no significant differences in onset voltage between positive and negative corona polarities ($P < 0.001$). As expected based on predictions and data from large-scale units, onset voltage significantly increased as a function of wire diameter. For instance, at 4.0 cm plate-to-plate distance, the onset voltage for 0.13 mm wire was approximately 6000 volts, but it was close to 11000 volts for 0.5 mm wire. Onset voltage

also increased with plate-to-plate spacing. However, the effect of plate-to-plate spacing was not as significant as the effect of wire diameter.

The onset electric field values from Table 4.6 were plotted and are shown in Figure 4.10. The figure shows the mean onset electric field strength values versus plate-to-plate distance. As expected, the data shows that onset electric field was a function of wire diameter, with lower onset electric field strength values for larger diameter wire. This trend is consistent with observations on large-scale units, for example, the results with 0.5 to 2.5 mm industrial-scale wires obtained by White (White, 1963).

However, the data in Figure 4.10 also showed that onset electric field strength was an apparent function of plate-to plate distance for a fixed wire diameter. A least-square linear regression indicates that the slope of the trends in onset electric field strength versus plate to plate distance were 11.4 kV/cm^2 for 0.13 mm wire, 8.5 kV/cm2 for 0.20 mm wire, and 5.5 kV/cm2 for 0.50 mm wire. This decrease in the slope suggests that the trend in onset electric field strength for thicker wires will be a straight horizontal line, perhaps because of the improved ability to maintain precise alignment with larger diameter wires.

A comparison was made between the experimental data and predictions made using equation (2.2), with values for the A and B coefficients suggested by Lowke et al (Lowke *et al*, 2003). Because the slopes of the empirical data decrease with wire diameter, there is better overall agreement between the predictions and the experimental data for the largest tested wire diameter (0.5 mm).

A possible explanation for the apparent dependence of onset electric field strength to plate to plate distance is that equation 2.3, which was used to covert the applied voltages to electric field strengths, may not be appropriate for the small wire diameters or plate-to-plate

distances used in these experiments. This explanation is supported by the fact that as the wire diameters increased and approached the diameters of wire electrodes in industrial units, the dependence of onset electric field to plate to plate spacing diminished.

Another factor that might explain the dependence of onset electric field strength on plate to plate distance is experimental artifact. Maintaining consistent wire-to-plate distances when the plates were closer together was more difficult than when the plates were farther apart. Small misalignments or surface features on the wires could bring wires close enough to one or both plates to substantially alter the electric field strength around the wires and result in lower voltages required to produce observable current. At a plate-to-plate distance of 1.0 cm, a deviation of 1 mm in wire alignment results in a 10 percent error in wire-to-plate distance, as opposed to an error of barely 2 percent when plates are 6.0 cm apart.

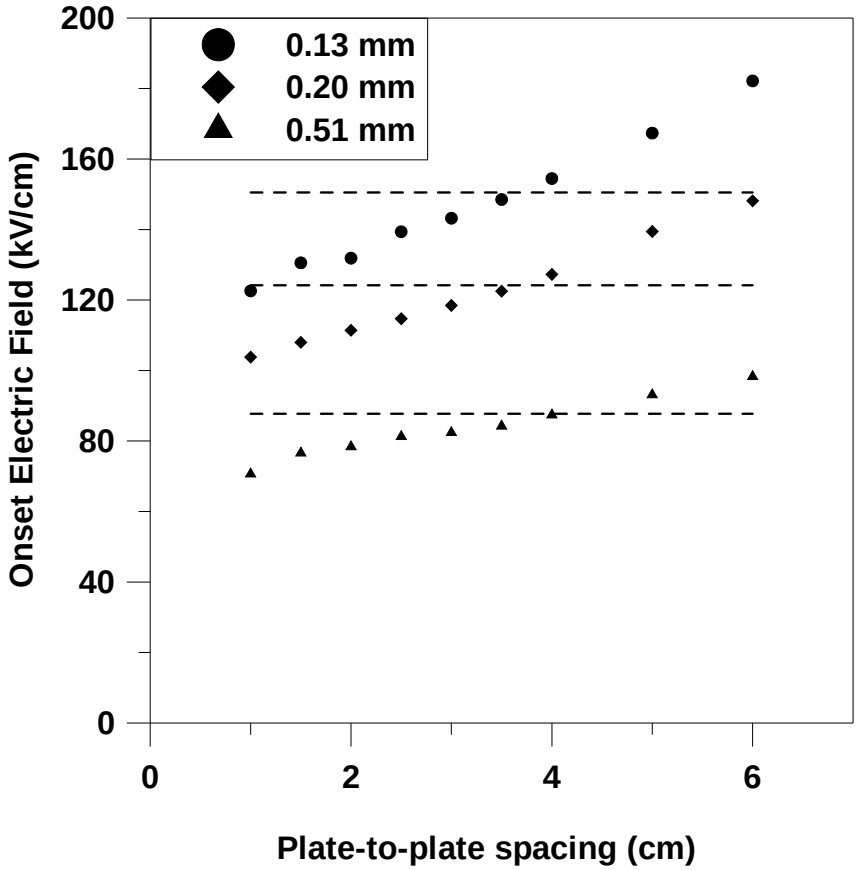

Figure 4.10 Experimental onset electric field strength versus plate-to-plate spacing. Predictions using Peek's equation (Equation 1) are shown as dashed lines.

CHAPTER 5

RESULTS: REMOVING DIESEL PARTICULATE MATTER WITH A SMALL-SCALE ELECTROSTATIC PRECIPITATOR

5.1 Introduction

Using electrostatic precipitation for diesel exhaust aftertreatment requires extensive design, experimental testing, and incremental improvements to achieve high performance. Although the idea of a device with virtually no pressure drop and high efficiency sounds appealing, there are several potential problems that need to be considered before applying the technology to diesel exhaust. Coarse particles are easily charged in a corona and strong electric field. However, almost all of the particles in diesel exhaust are under 100 nm in diameter. Most of the earlier studies on DPM collection with electrostatics mentioned in Chapter 1 do not provide data on fine particle collection, so it is unclear how well they worked on collecting these particles.

Regulatory environmental and occupational PM standards worldwide are on a mass concentration basis. Bigger particles dominate consideration of mass concentrations and mass collection efficiency of aftertreatment devices. However, most of the individual particles in diesel exhaust are quite small and number concentration efficiency will be an important indicator of the true benefits of any aftertreatment device. Recent studies on the health effects of nanoparticles further emphasize the importance of number

concentration measurements and number collection efficiency as being as important as mass concentrations (Oberdorster and Utell, 2002; Maynard and Kuempel, 2005). The particle sampling system designed at SMU to investigate DPM controls can measure mass and number concentration nearly simultaneously.

In addition to the importance of particle size in ESP performance and DPM health effects, the sulfur content of the particulate can play a significant role in the collection efficiency of the small-scale ESP. EPA mandated the use of ultra-low sulfur diesel (ULSD) fuel beginning in 2007 to facilitate the use of diesel particulate filters (EPA, 2005). At present, these filters are principally wall-flow filters, and high levels of sulfur in the fuel could lead to nucleation of more small particles. Stationary (non-mobile) and marine sources are still allowed to use fuel with higher levels of sulfur, so-called low sulfur diesel (LSD).

From electrostatic considerations, the electrical conductivity of diesel exhaust particulate depends on the sulfur concentration of the fuel to a large extent. Very high electron affinity of SO_2 molecules creates a much more conductive and easily charged material (White, 1963). Previous researchers have found that the chemical composition of DPM changes with engine load (Liang, 2006). This includes the partitioning of particulate carbon between the elemental form (i.e. black carbon) and the hydrocarbon form (i.e. organic carbon). Higher engine loads are associated with higher temperatures which are enough to burn most of the soluble organic fraction (SOF). Therefore, DPM consists of more elemental carbon at high engine load. Due to the dependence of composition on engine load, aftertreatment devices should be tested under different load conditions.

In this chapter, the results of tests of ESP performance with different load conditions, and the effects of fuel sulfur content on particle collection efficiency will be presented. After

addressing these two fundamental issues, a design improvement for the ESP will be discussed. The design improvement was developed by changing the geometry of the device.

Preliminary tests on the ESP showed very low removal efficiency of 10 to 20 percent for positive corona. These tests also showed that at plate-to-plate distances less than 3.5 cm, there is a very high probability of sparking. As a result, negative corona was used in the experiments in this chapter. Also, plate-to-plate distance was set to 3.5cm which seemed to have a high collection rate with minimum sparking.

5.2 Effect of Engine Load on ESP Performance

Diesel engines that power construction vehicles or run mining or welding equipment will alternate between low load and high load conditions during routine operation. During changes in engine load the exhaust flow rate, exhaust temperature, and the concentration and chemical composition of the DPM can change significantly. A series of experiments was performed to evaluate the collection efficiency of the ESP, at both idle and medium load conditions.

Exhaust from the diesel-powered electric generators was conducted through the ESP and then sampled and analyzed to determine number and mass collection efficiency. Tests were performed over a range of voltage settings to study the effect of current production on collection efficiency. At each voltage setting, number collection efficiency was determined by at least five replicate tests, and mass collection efficiency was determined by at least three replicates. For medium load conditions, four 500-watt construction work lights, with a combined draw of 2000 watts, were powered by the generator. These lights resulted in load conditions of 30 percent of engine's rated power, and 90% of the rated current output by the attached generator. All of the load-effect tests were performed using Low Sulfur Diesel (LSD).

Figure 5.1 shows the number removal efficiency of the ESP as a function of voltages. Results are shown for both idle and medium load conditions. The results indicate that at high voltages number removal efficiency was greater than 80% for medium load tests, and greater than 50% for tests at idle conditions. Number removal efficiency was substantially higher at medium load conditions than at idle. Both curves appear to flatten and reach maximum values as the voltage was increased.

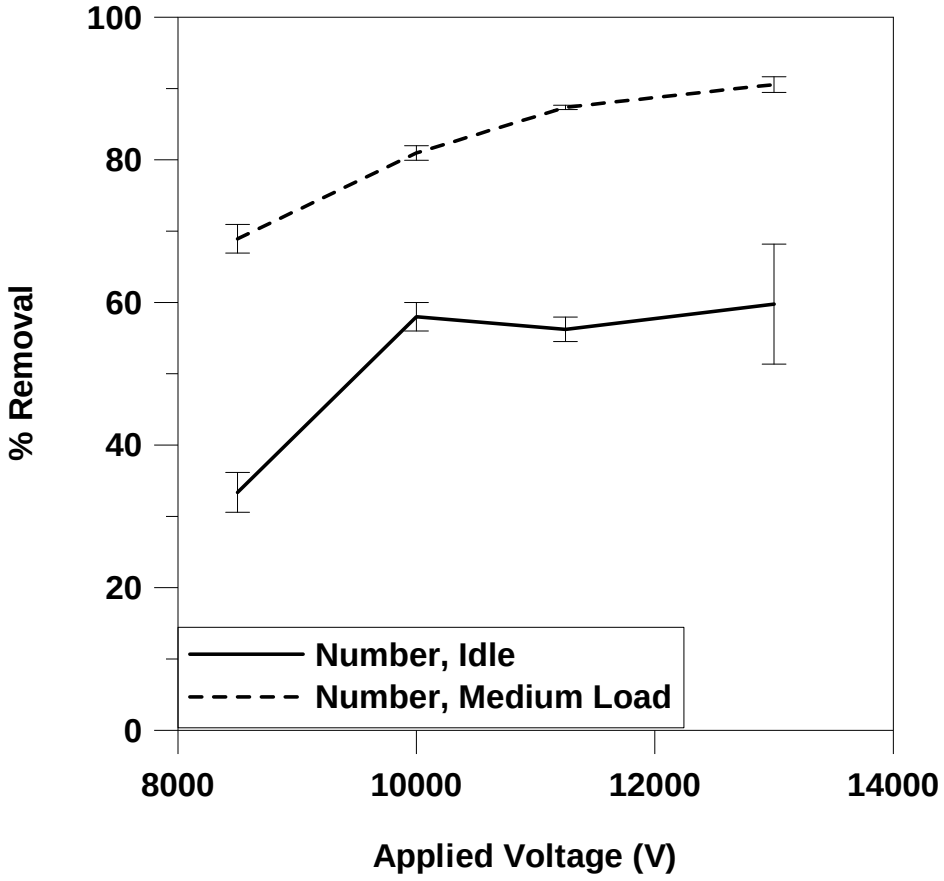

Figure 5.1 Number removal efficiency versus Voltage a) idle engine b) engine at medium load.

Figure 5.2 shows the mass removal efficiency of the ESP, at idle and medium load, as a function of voltage. The mean mass concentration of the particles in this experiment was 25 +/- 4.3 mg/m^3 when the engine was running idle. However, with the engine running at medium load, the average mass concentration decreased significantly and was around 3.6 +/- 0.8 mg/m^3. The figure shows no strong dependence of collection efficiency on applied voltage. Since mass concentration measurements are dominated by the few small particles flowing through the unit, and the charging and collection of these particles is easier than the collection of the small particles, the data indicate the possibility that large particles were being charged and collected as effectively as possible at all tested voltages.

Furthermore, above 10,000 volts sparking between the plates and wires was more frequent, interrupting the electric field and steady corona current output in the unit. Although the intermittent sparks were seen while the number tests were being performed as well, there was no drop in number removal efficiency. As explained in chapter 2, small particles are mostly charged by diffusion charging process whereas bigger particles are charged by field charging. When intermittent sparking occurs, the corona dissipates and the electric field decreases significantly for a fraction of a second. In this short time, smaller particles can still impart charge in the highly charged space inside the ESP. However, bigger particles leave the ESP since field charging is no longer in effect. As a result, intermittent sparking affects mass removal efficiency more than it affects number removal efficiency, hence the drops in mass removal curve occurs while number removal curve does not change significantly. In addition, sampling time for number concentration was shorter compared to mass tests. As a result of this shorter sampling time, the effects of sparking were not equally detrimental on these samples.

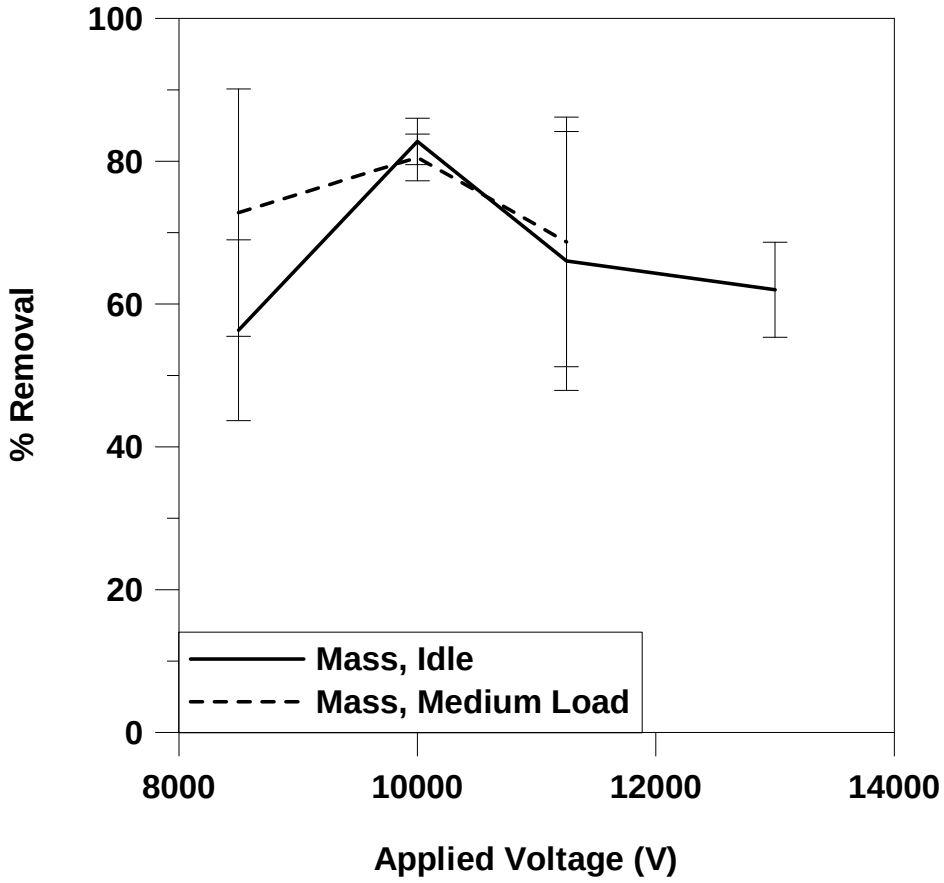

Figure 5.2 Mass removal efficiency versus Voltage a) idle engine b) engine working at medium load.

Previous researchers have documented that load changes on diesel engines can affect the particle size distribution and chemical composition of the DEP (Kittelson, 1998). Our own research suggested that this was happening, with the difference in collection efficiency between idle and medium load conditions. When the engine was running on LSD, medium load condition by itself reduced mass concentration by 85% compared to idle conditions and increased number concentration by more than 25 to 50%. This resulted in a shift in the size distribution curve towards smaller particles when the engine worked at medium load. The greater number removal efficiency of the ESP at medium load condition suggests that the ESP effectively captures the

nanoparticles prevalent at this condition, compared to the particles at idling conditions which have a more diverse size distribution.

5.3 Effect of Fuel Type on ESP Performance

Two types of diesel fuel were used in this experiment: Low Sulfur Diesel (LSD) and Ultra Low Sulfur Diesel (ULSD). Both fuels were purchased from commercial gas stations in Dallas area and were analyzed by an independent laboratory for their chemical and physical characteristics. The results of the analyses are shown in table 5.1. According to EPA regulations the concentration of sulfur in LSD fuel should have been less than 500 ppm, but the LSD was found to have an average concentration of 550 ppm. Also, table 5.1 shows that ULSD is slightly heavier and has a lower flash point compared to LSD.

Table 5.1 Chemical characteristics of the fuels used in the experiments

Distillation (ASTM D86), C	ULSD	LSD
IBP	179.4	193.3
10%	206.7	217.8
20%	-	240.0
30%	-	253.3
40%	-	265.6
50%	270.0	276.7
60%	-	287.8
70%	-	301.1
80%	-	315.6
90%	315.0	337.2
95%	-	350.0
EP	362.2	364.4
Recovery	-	98.5%
Residue	-	1.5%
Loss	-	0.0%
Gravity, API@60F (ASTM D1298)	37.7	33.4
Cloud Point (ASTM D2500)	-14.4	-10.5
Pour Point (ASTM D97)	-24.4	-17.5
Sulfur, ppm (ASTM D2622)	16	550
Flash Point C (ASTM D93, PMCC)	56.1	71

5.3.1 Effects of Fuel Type at Medium Load Conditions

Tests were performed to investigate the effects of fuel type and sulfur content on the particle collection efficiency of the ESP. The effects of fuel type on ESP mass collection efficiency were investigated at both idling and medium load conditions. In these tests, the engine was operated and the exhaust analyzed as previously discussed in section 5.2. Tests at medium load conditions were performed with the diesel generator operating at 30 percent of its rated power. Figure 5.3 shows the effects of fuel type on mass collection efficiency as a function of applied voltage.

When running on either fuel type, there was no significant trend in mass collection efficiency with voltage. The removal efficiency for ULSD tests varied between 50 to 60 percent.

The removal efficiency for the LSD tests was higher and varied between 70 and 80 percent. The differences in performance might be due to changes in the chemical structure of the exhaust and the DPM with changes in fuel type. The exhaust from the LSD tests likely had substantially more sulfur oxide content, decreasing the resistivity of the medium and making it easier for the negative ions to flow between the electrodes. Higher loads create higher exhaust temperatures, and other researchers have found that higher loads result in higher elemental carbon content in DPM, making the particle more conductive (Kittelson, 1998). SO_2 molecules have a high electron affinity which creates a much more conductive medium for the current to pass through (White, 1963). As a result, there is always a higher current of electricity between the electrodes when there is more sulfur oxide molecules present in the air. In some industrial applications the deliberate addition of water or sulfur to particulate is a way to increase conductivity and improve electrostatic precipitator performance. Therefore, with the engine running on LSD, higher corona currents were observed.

In addition, higher loads create higher exhaust temperatures which result in higher elemental carbon in the DPM. More conductive particles are another reason for the lead in efficiency with LSD. However, a combination of more conductive medium and more conductive particles caused more frequent sparking which prevented performing the tests at 13,000 volts.

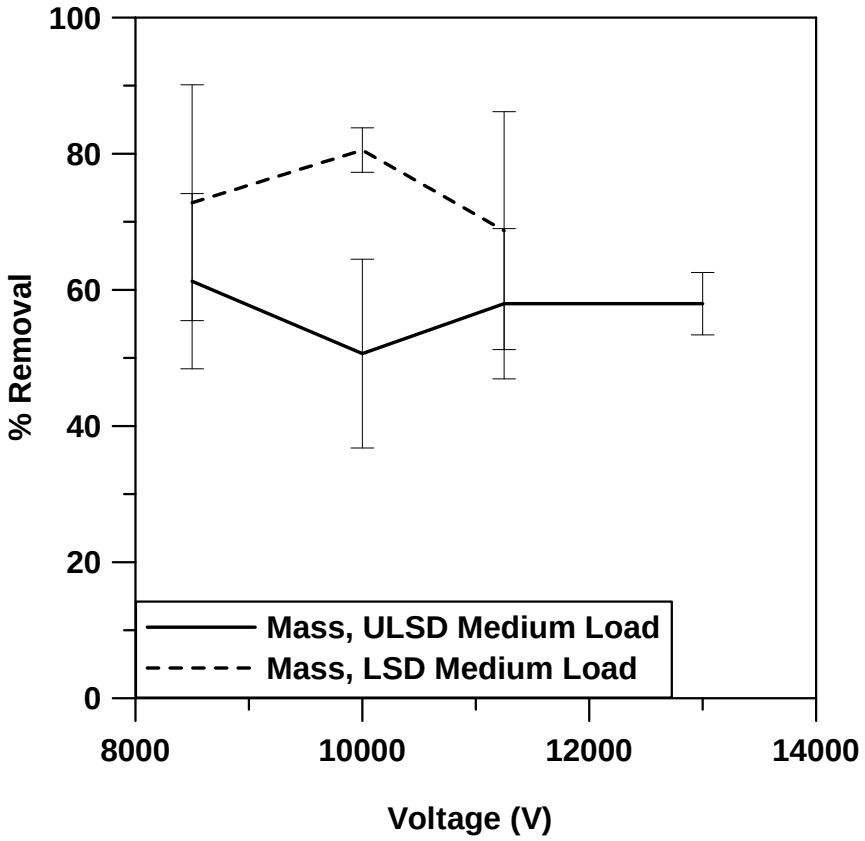

Figure 5.3 Effect of fuel type on the mass removal efficiency of the ESP with medium load on the engine

5.3.2 Effect of Fuel Type at Engine Idle Conditions

Figure 5.4 shows the effect of fuel type on the mass removal efficiency of the ESP at engine idle conditions. When the engine was running on LSD, mass collection efficiency peaked at 85 percent at 10,000 volts. The collection efficiency decreased at voltages above 10,000 volts was possibly due to the intermittent sparking of the ESP which increased in frequency substantially above this point. At the high extreme, operating the ESP at voltages above 13,000 volts was very difficult due to extensive sparking. When the engine was running on ULSD, collection efficiency was not a significant function of voltage, and collection efficiency was approximately 65 percent over a large span of voltages.

Other than the peak at 10,000 volts, the difference between the curves is not significant. However, average mass removal efficiency for LSD particles is slightly higher than that of ULSD particles. As explained in section 5.3.2, the reason for the difference between LSD and ULSD performance may have been due to the sulfur content of the exhaust. Exhaust generated during the combustion of LSD fuel may have had higher sulfur content than the exhaust generated during the combustion of ULSD fuel. It has been noted many times by others that the dielectric constant of the medium can affect particle charging (White, 1963; Parker, 1997). Since the tests in this section were performed on idle engine, elemental carbon content of DPM was not very high and particles were less conductive compared to medium load conditions. Therefore, the difference in efficiencies was not as substantial the one observed in figure 5.3.

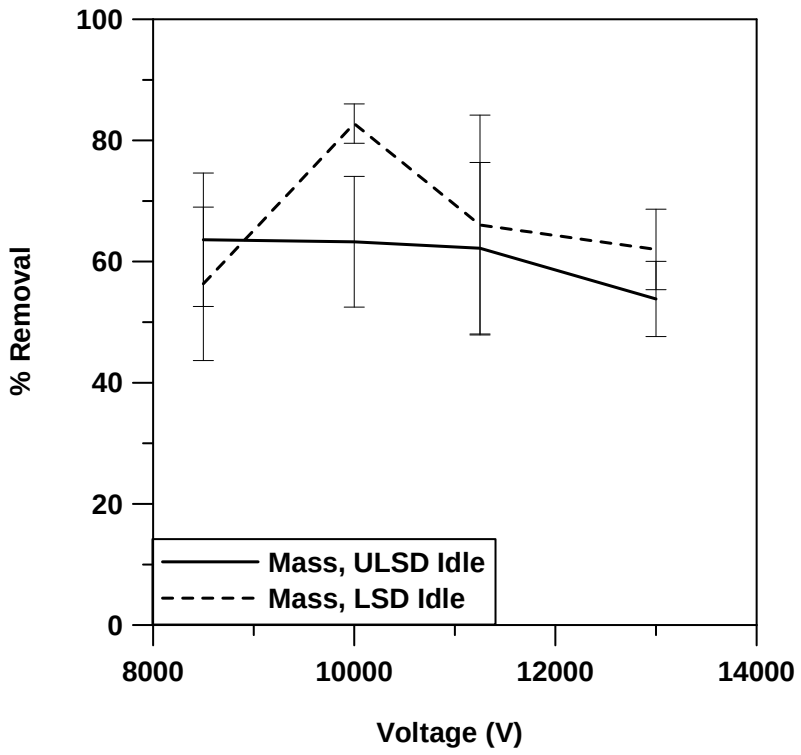

Figure 5.4 Effect of fuel type on the mass removal efficiency of the ESP when the engine is running idle.

5.4 Removal Efficiency of the ESP with an Innovative Design

The original design of the small-scale ESP showed moderate to high efficiency in removing particles from diesel exhaust both in terms of mass and number. However, wire breakage was an occasional problem during laboratory tests. As discussed in chapter 4, thinner wires produce more current than thicker wires. However, the very thin wires are more susceptible to breakage during operation. The combination of high temperatures, vibration, and the drag forces on the wires from the passing exhaust twice resulted in broken wires during tests.

To improve durability, a different wire configuration was developed. Instead of setting the wires perpendicular to the flow of the exhaust (vertical wires), the wires were positioned parallel to the exhaust flow (horizontal wires). The goal was to reduce the drag forces pulling on the wires to reduce the probability of wire rupture. In addition, the new configuration also added a few inches of total wire length in the ESP, which could potentially increase the removal efficiency of the unit. The new design is shown in Figure 5.5. A few changes were made to the ESP to enable the setup of horizontal wires. The rails in the original design that were used to energize the plates were removed and instead a new charging rod was positioned at the top of the box for to charge the plates. The plates were energized from the top of the box, to prevent the opportunities for short-circuiting between the now horizontal wires and the plate rails. Also, the rods which supported the wires were moved to the front and the back of the ESP, with at least one-inch distance from the plates. The new design was tested for mass and number removal efficiency under idle and medium load conditions. The fuel used in these tests was Ultra Low Sulfur Diesel fuel.

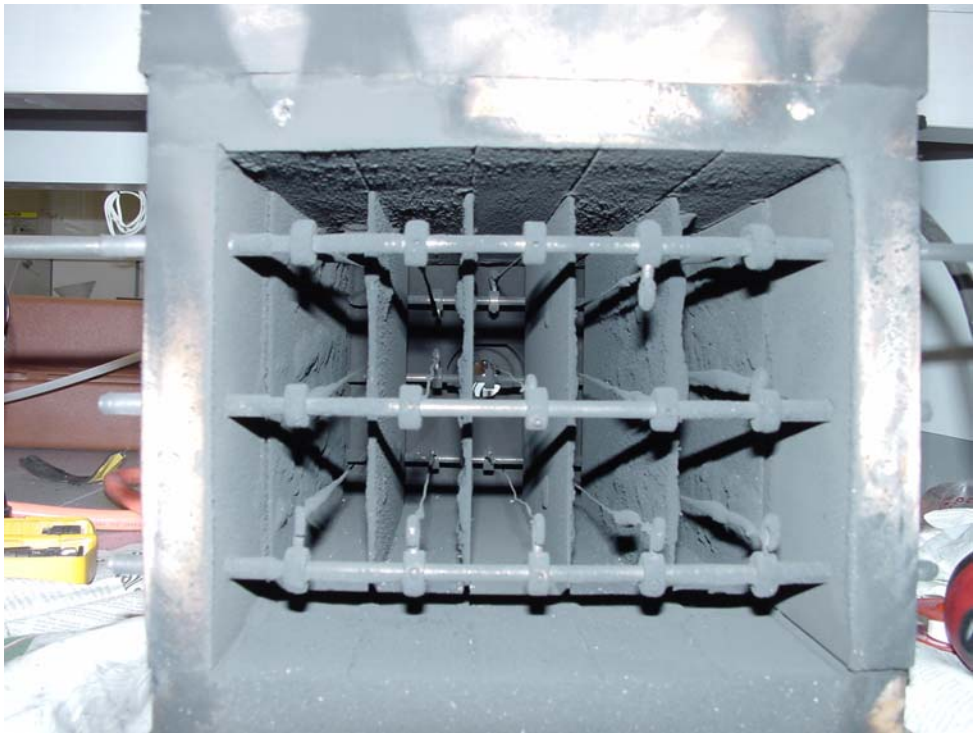

Figure 5.5 The new design of the ESP after soot collection-Front view.

5.4.1 Mass Removal Efficiency

The results of mass efficiency testing are shown in Figure 5.6. At idling conditions, the new ESP design showed substantial improvement in removal efficiency compared to the conventional design. While the vertical-wire ESP only showed a removal efficiency of around 65 percent at 10,000 volts, the horizontal-wire ESP removed more than 80 percent at this voltage. However, at medium load conditions the new ESP design was able to achieve removal efficiencies of 50 to 60%, approximately the same as the results with the original design. One of the main reasons for the improved performance was likely the greater length of wire between the plates in the new configuration compared to the original design. The greater wire length resulted in more current generation, and thus, power consumption was significantly higher. The

horizontal-wire ESP used 60 watts of power at 10,000 volts while the vertical-wire ESP consumed around 23 watts at the same voltage.

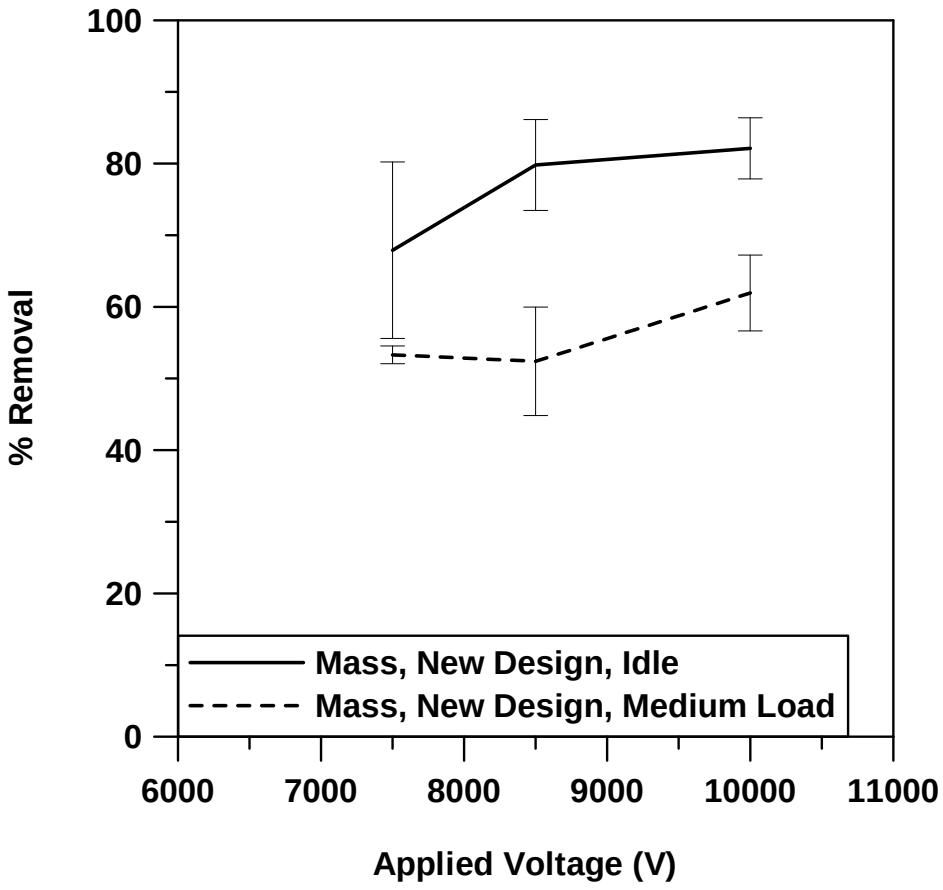

Figure 5.6 Mass removal efficiency of the ESP with a horizontal-wire design

Unlike the results obtained with the original ESP design (figure 5.2) the mass removal efficiency of the horizontal-wire ESP dropped when load on the engine increased. A drop in collection efficiency is predicted by the Deutsch equation, especially if collection efficiency is limited by residence time, although this behavior was not observed in the original configuration. Another possibility is that some particles were being transported through the ESP in exhaust that

was flowing in the weakest spots in the electric fields between the wires and plates, a condition known as "sneakage" (see Figure 5.7). In the original vertical-wire design, the flow was perpendicular to the wires and all the incoming particles had to pass through the high electric field zone near the wires. With the wires in a horizontal and parallel configuration, at a point halfway between the wires the electric field is at its minimum value, and particle that flow through these regions might not experience adequate particle charging, or sufficiently strong electric fields for particle migration to the plates.

In spite of the sneakage problem, when the engine is running idle, the newly designed ESP showed substantial improvement in removal efficiency compared to the conventional design. While the vertical-wire ESP only showed a removal efficiency of around 65 percent at 10,000 volts, the horizontal-wire ESP removed more than 80 percent of the mass. When the engine was running at medium load, the horizontal-wire ESP still showed higher removal efficiency, surpassing that of the vertical-wire by 10 percent.

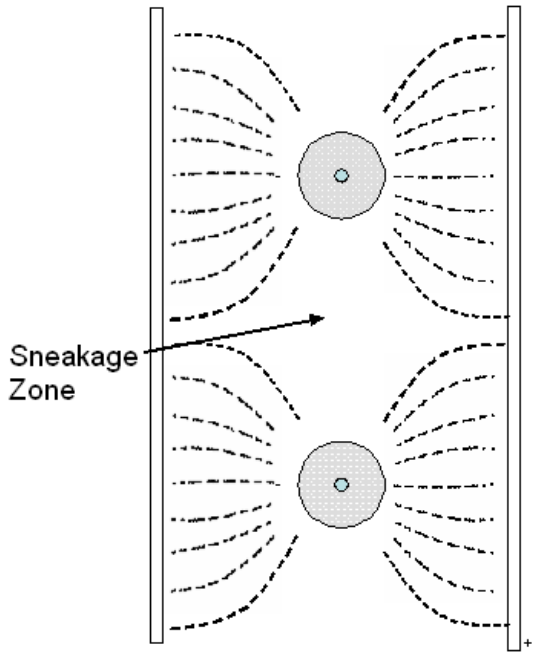

Figure 5.7 Sneakage zones in the new horizontal wire ESP design

5.4.2 Number Removal Efficiency

Figure 5.8 shows the number removal efficiency of the new ESP design under the two tested load conditions. Like the mass removal efficiency tests, the tests were run at voltages from 7500 to 10,000v. With the new design, the number removal efficiency curves were not significantly different. The number removal efficiencies for the two load situations are almost the same at 7500v and only around 10 percent higher at higher voltages. However, while comparing the two curves, it is also important to remember that number concentration is higher when the engine is running at medium load. i.e. although the ESP showed only a slightly better efficiency at higher loads, it collected many more particles at a higher flow. This result is a good indication of the effect of load on changes in the chemical composition and electrical conductivity of the diesel exhaust particles.

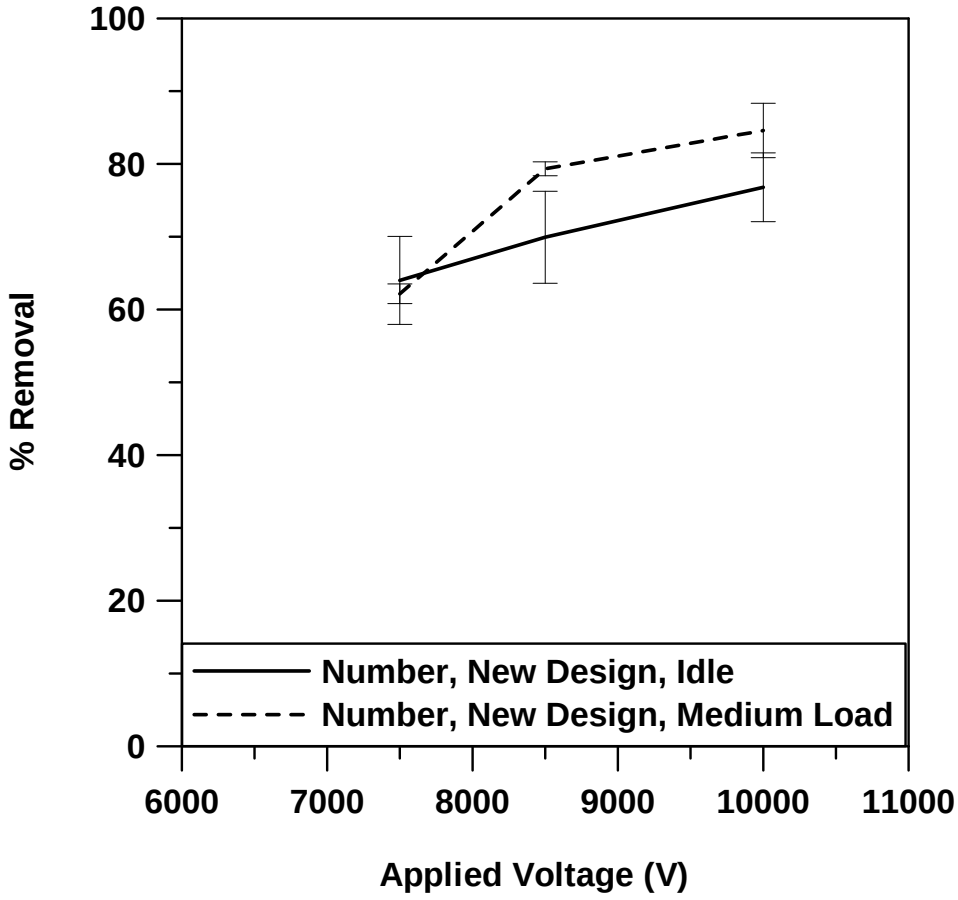

Figure 5.8 Number removal efficiency of the ESP with a horizontal-wire design

Due to higher conductivity of the particles, more current was produced while there was load on the engine. For instance, when the engine was running idle, the average produced currents were 3.0 mA for 8500v and 6.0 mA for 10,000 v. These currents were both increased by 16 percent on average when there was load on the engine. As a result, power consumption was also higher as a result of current production increases. However, the power needed for the ESP to operate at 8500v was around 30 watts which was still around 0.5 percent of the rated power of the generator being controlled.

5.5 Long-term Mass Removal

As a reliable aftertreatment device, the ESP should be able to work for a long time, under high temperature, without the need for frequent maintenance. New filters by Toyota use Ozone and active oxygen to burn the soot at a temperature much lower than its ignition temperature (Fino and Specchia, 2008). Our ESP showed very good self-cleaning properties for the corona wires, probably due to very high concentrations of ozone and active oxygen in negative corona. However, since carbon is a conductive material, even small accumulations of soot between the wires and plates can result in short-circuiting and thick accumulations on the plates could result in current suppression. Long-term tests were designed and performed on the ESP to investigate particle collection efficiency with time and to investigate the accumulation of soot inside the precipitator.

5.5.1 Experimental Methods for Long-term Tests

Long term tests were performed with the new ESP design, with wires parallel to the flow. An operating voltage of 8500 v was selected since it showed high removal efficiency with low power consumption during short-term tests. Plate-to-plate spacing of the ESP was set at 3.5 cm and 0.2 mm wire diameters were used for this experiment. The tests were performed using Ultra Low Sulfur Diesel.

Previous tests on mass concentration of the exhaust showed that when ULSD is used in the engine, a much higher concentration should be anticipated with load on the engine. Average mass concentration of the particles in the exhaust was 44.4 mg/m^3 +/- 12.1 mg/m^3 when the engine was running idle, compared to an average of 82.5 +/- 28.5 when there was load on the

engine. As a result, long-term tests were performed with medium load on the engine to investigate the performance of the ESP while continuously treating the exhaust with fairly high mass concentration.

Each long term test started with warming up the engine, idle for 30 minutes, and with medium load on the engine for 15 minutes. After the 45 minute warm up period, the load remained on the engine and the ESP was turned on. Mass samples were collected from the exhaust as soon as the ESP started operating and additional samples were taken each 60 minutes, for four hours. To create an extreme scenario, the ESP was not cleaned or moved for maintenance after each four hour test. i.e. tests were performed with plates and wires which were already covered with carbon particles.

To minimize the change in exhaust composition, no significant maintenance was performed on the engine during the tests. Current production of the ESP was precisely recorded during the tests to examine current trend with time and also the potential for sparking. Finally, additional safety measures were applied to ensure that the ESP was electrically separated from the rest of the system.

5.5.2 Continuous Mass Removal Efficiency of the ESP

Figure 5.9 shows the trend of mass concentration versus time with the ESP on. The figure shows that although standard deviation is relatively high at the beginning, most data points fall between 10 to 20 mg/m^3. The average mass concentration of all data points is 15.3 +/- 6.7 mg/m^3. This concentration, compared to the average concentration of the untreated exhaust at medium load, suggested a mass removal efficiency of 80.1 percent for the ESP at 8500v. This result is

higher than short-term test results observed in figure 5.5. However, experimental methods were very different in the two tests which make it difficult to directly compare the results.

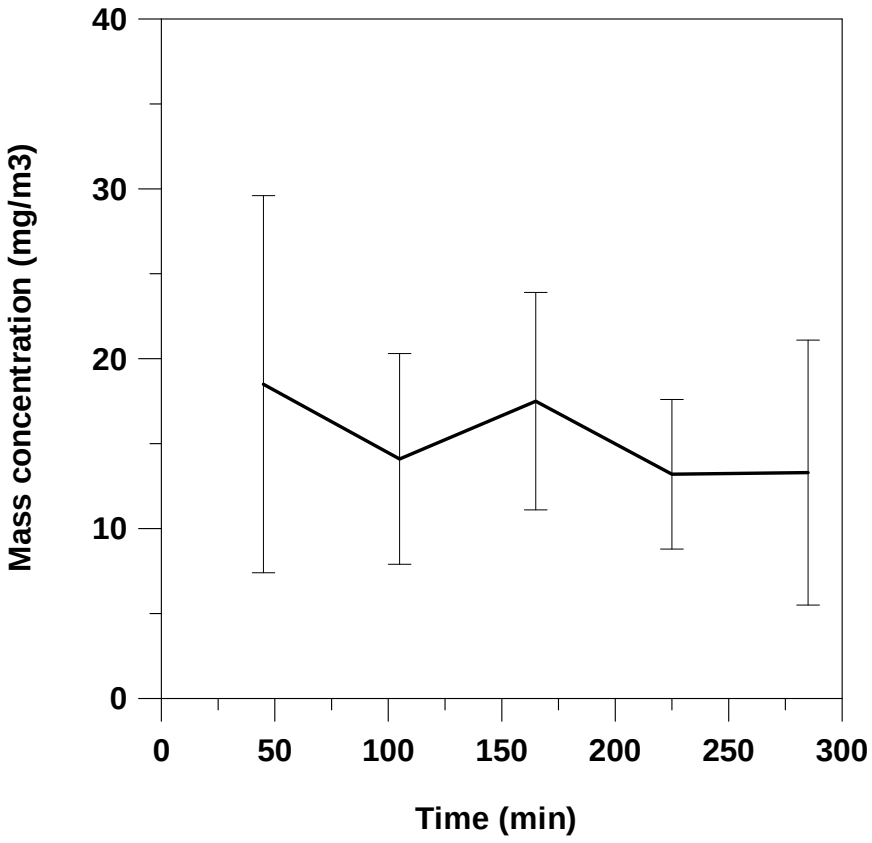

Figure 5.9 Mass concentration of the exhaust versus time. The ESP was on during the four hour tests.

Figure 5.10 shows the trend of current production versus time in the long-term tests. The results showed that a downward trend started for each curve after an hour and the current consistently went down after 60 minutes of ESP operation. Also, the current was significantly lower during the third test. While current production during the first test was close to 3.0 mA, it did not exceed 2.5 mA during the second test and showed a maximum of 1.5 mA in the third test.

Although current dissipation with time was expected due to deposition of the soot on the wires and plates, comparing figures 5.7 and 5.8 shows that this dissipation did not affect the performance of the ESP, suggesting that collection was not current-limited but perhaps limited by other factors.

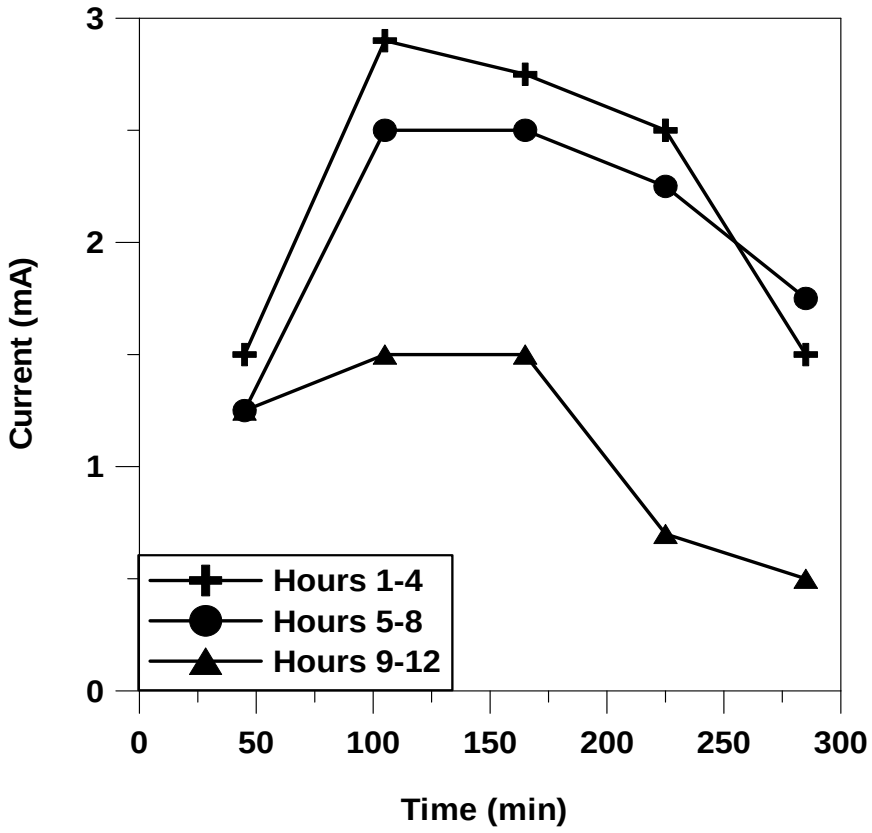

Figure 5.10 Current production of the ESP versus time. The ESP was on during the four hour tests.

Figure 5.11 compares the collection plates after soot collection for the two designs. Flow inlet in both cases was on the right side of the plates. Due to the fluffy nature of soot particles, taking a perfect picture of the plates was difficult. However, the pictures show that soot collection in both cases was more pronounced along the wires. Figure 5.9 also shows that the new design made more effective use of the collection plate area. There are three obvious thick

layers of soot deposition on the right side of the plate in figure 5.9b. This probably shows that the bigger particles were charged and collected in the first half of the ESP where the rest of the wire and collection plate lengths contributed more to removing smaller particles.

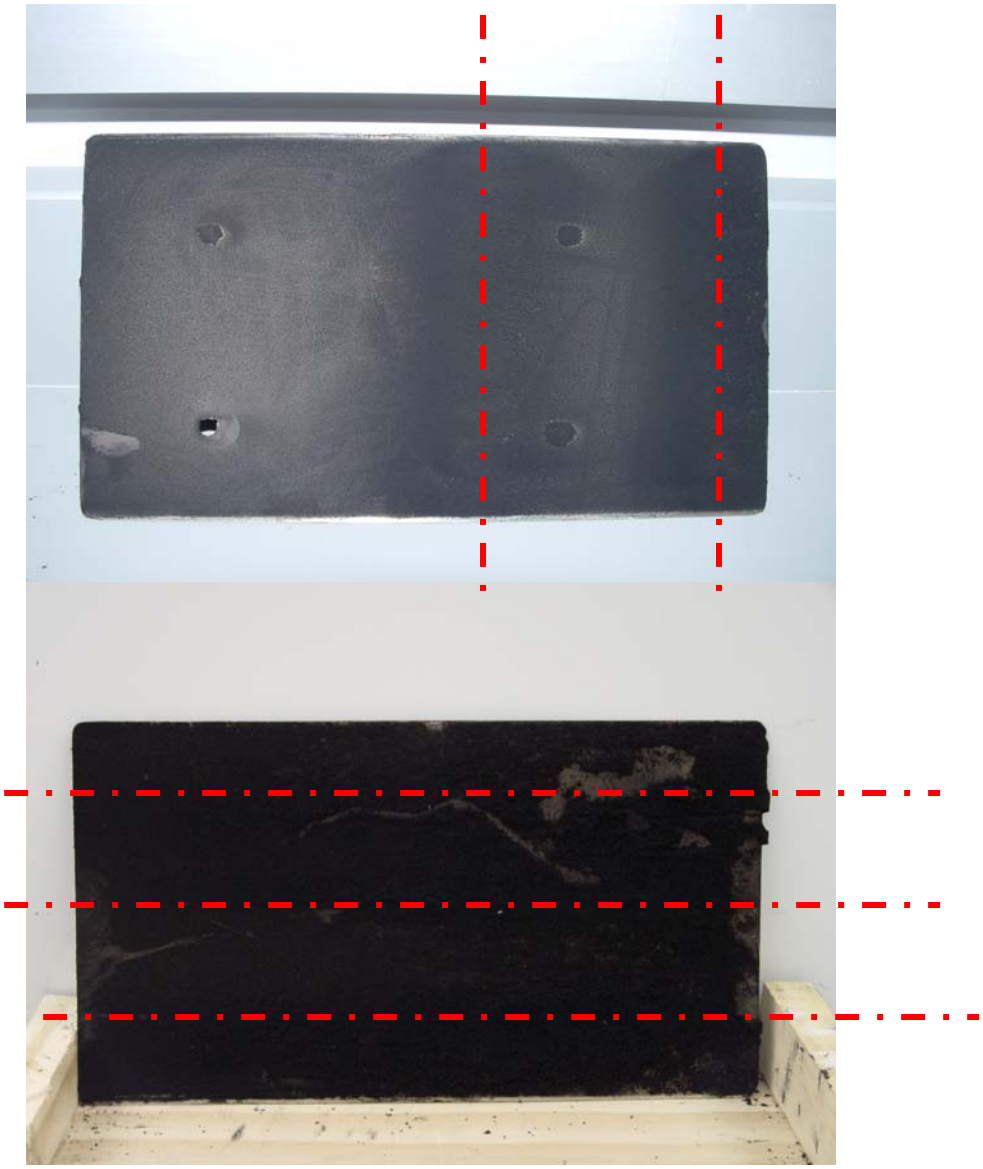

Figure 5.11 ESP collection plates after soot collection a) Original design after 8 hours b) New design after 16 hours. Approximate locations of wires are shown by dashed lines.

CHAPTER 6

CONCLUSIONS

A small-scale wire-plate electrostatic precipitator was designed, constructed, and tested to investigate the properties of small-scale precipitators, and develop an electrostatic control system for diesel exhaust particulate. To empirically investigate a gap in previous electrostatic experiments the ESP was built with wires thinner than 0.5 mm. In order to investigate small changes in ESP internal geometry, the ESP was designed so that plate-to-plate distances and corona polarities could easily be changed. This design enabled measuring fundamental electrical properties (FEP) of the ESP, including onset voltage, the voltage-current relationship, and sparkover voltage. The fundamental electrical properties experiments were performed in air and at room temperature and pressure.

A diesel exhaust particle generation, sampling, and measurement system was constructed to investigate the efficiency of a small-scale ESP collecting particles produced by 5.5 kW and 6.5kW diesel generators. Performance of the ESP was evaluated by measuring mass and number removal efficiency. Mass concentration sampling was conducted by sampling diesel exhaust through 47mm Teflon membrane filters in a metal filter cassette holder. Number concentration sampling utilized a condensation particle counter (CPC) that detected and optically counted particles above 15 nm. A dilution air

system was used to ensure the concentration of the particles and gas temperatures were within the operating limits of the CPC. The dilution air system used a four-stage filtration system, to produce ultra-purified dilution air. The findings of the study are as follows:

6.1 Fundamental Electrical Properties of the Small-Scale ESP

The fundamental electrical properties of the small-scale ESP were tested at different plate-to-plate distances with different wire diameters.

6.1.1 Effects of Plate-to-Plate Distance on FEP

Test results indicated that current production at a fixed voltage was inversely related to plate-to-plate distance. In addition, sparkover voltage and the voltage operating range increased with plate-to-plate distance. There were no significant differences in onset voltage between negative and positive corona tests, and negative coronas produced more current at a fixed voltage than positive ones. The combination of small plate-to-plate distances and negative coronas produced the highest currents within the ESP.

Comparisons were made between experimentally-measured electrostatic properties and predictions using fundamental electrostatic equations. There were no significant differences between measured onset voltages and predicted onset voltages. However, measured sparkover voltages were significantly smaller than predicted values. Voltage-current relationships for very small plate-to-plate distances could not be predicted using classic V-I equations and assumptions. The use of high ion mobility values, to account for the likely existence of a substantial amount of free electron current, allowed for good agreement between measured and predicted current production at even small plate to plate distances.

6.1.2 Effects of Wire Diameter on FEP

As expected from electrostatic theory, current production increased with smaller wire diameters. Also, onset voltages and onset electric field strengths decreased with smaller wire diameters. An unexpected result was that onset electric field strength was a function of plate-to-plate distance, a relationship that strengthened as wire diameter decreased. Sparkover voltages had an inverse relationship with wire diameter for positive polarity, and thus decreased with increasing thickness. Negative corona, however, had increasing sparkover voltages with increasing wire diameters. Test results showed that negative and positive polarities at the same wire diameter had the same onset voltage. Negative coronas, however, produced more current than positive coronas at a fixed voltage. Therefore, negative coronas with the use of very fine wires may be the ideal characteristics to generate the highest efficiencies for small-scale ESPs.

Theoretical predictions of electrostatic properties were compared with experimentally measured data using classical ESP equations. Measured onset voltages showed good agreement with those predicted by Peek's equation. Sparkover voltages obtained from experimental data were very different from predicted values and the operating span of the ESP could not be predicted by the equations. However, there was fairly good agreement between experimental current values and the current predicted by the Townsend equation, if the standard equations were modified for high ion mobilities.

Onset voltages of the ESP were measured with three very fine wires of 0.13 mm, 0.20 mm, and 0.51 mm diameter and over a range of plate-to-plate distances. Results show that for small-scale ESPs with very fine wires, the onset electric field strength varied from 70 to 181 kV/cm. As expected, the onset electric field strength was inversely related to wire diameter. In

addition, onset electric field strength showed an apparent positive dependence on plate-to-plate spacing, reflecting the precision of maintaining true wire-to-plate spacing in small-scale units or impropriety of the classical equations for ESPs with very fine wires.

6.2 Particle Collection Efficiency of the Small-Scale ESP

The small-scale ESP was tested under a variety of conditions to investigate and improve its ability to collect diesel exhaust particles. Preliminary experiments showed that at plate-to-plate distances less than 3.0 cm, sparking was highly likely to occur. Preliminary tests also showed that positive corona collection efficiency was poor on a mass basis. As a result, the ESP collection efficiency tests were performed at 3.5cm plate-to-plate distance with negative corona polarity.

6.2.1 Effects of Load Conditions on Collection Efficiency

Different load conditions result in different temperatures, flows, and DPM compositions which affect the performance of the ESP. A diesel powered electric generator was operated at idling and medium load conditions to examine the effects of load on collection efficiency. Low sulfur fuel with fuel sulfur concentration of 550 ppm was used in these first set of tests. The precipitator was tested over a range of voltages from 7500v to 13000 volts. Medium load tests were performed with 2000 watts of power being were drawn from the generator, which accounted for 30 percent of its rated power. The particle removal efficiency was measured in terms of both particle mass and particle number. Results showed a 30 percent increase in number removal efficiency when there was load on the engine. The ESP could remove above 90 percent of the particles in terms of number when there was load on the engine. Number removal

efficiency did not change significantly when the load was being drawn and reached its maximum of 80 percent at 10,000 volts.

6.2.2 Effects of Fuel Type on Collection Efficiency

Low-Sulfur diesel with a sulfur concentration of 550 ppm and Ultra Low Sulfur Diesel with a sulfur concentration of 15 ppm were fired in the diesel generator to investigate the effects of fuel type and sulfur content on collection efficiency. The mass removal efficiency of the ESP was obtained at different load conditions and the effect of fuel type on the removal efficiency was investigated. The ESP removed up to 85 percent of the mass in LSD case and up to 65 percent of the mass for ULSD. On average, mass removal efficiency of the ESP was 7 percent lower for idle and 18 percent lower for medium load when the engine was running on ULSD. However, the ESP was able to operate at higher voltage and higher current production with fewer sparks when ULSD was used. The efficiency reduction when using ULSD may have been due to lower conductivity of the particles when ULSD was used which made particle charging more difficult inside the ESP.

6.2.3 A New Design for the ESP

A new ESP configuration with horizontal wires was tested, with the goal to to reduce the possibility of wire breakage and improving precipitator performance. In the original ESP design, the wires were vertical, and the exhaust flow was perpendicular to the wires. However, the wires in the new design were parallel to the flow. Because of the horizontal orientation, additional wire length could be fitted within the precipitator, increasing the effective length of wires by 40

percent and resulting in increased current production. Mass and number collection efficiency of the new unit was tested, and the experiments were performed with ULSD.

The results showed around 85 percent of mass removal efficiency when the engine was running at idle conditions. With the engine operating at medium load, mass removal efficiency decreased by 20 percent. The drop in the mass removal efficiency was probably due to particles sneaking out of the ESP with increasing flow which was caused by the load. Number removal efficiency was approximately 75-85% with the new ESP design.

6.3 Suggested and Anticipated Future Work for Commercialization

1. Whereas this research was mostly focused on PM removal, some researchers have found that electrostatic coronas might be able to reduce emissions of NOx, VOCs, and other gases. More research on the effect of this small-scale ESP unit on gas cleaning properties would be a good next step.
2. The ESP showed very good performance in terms of both mass and number removal. In innovative design might involve coupling the ESP with a diesel particulate filter. A two-stage system like this might be very effective (99%+) and should be tested.
3. Biodiesel and other alternative fuels are slowly finding their way into the U.S. market. It might soon be important to investigate the removal efficiency of the ESP on engines running with alternative fuels, since the DPM from these fuels is likely to have a different chemical composition.

4 The tests in this research were run on small generators. More tests are necessary on bigger engines and the plate area should be modified for higher flow and higher concentration to obtain optimum removal efficiency.

5 The long-term commercial viability of the small-scale ESP or any other DPM collection device is dependent on an effective regeneration mechanism to remove the collected particles. Although the ESP showed potential self-cleaning wire properties, other options like covering the plates with a catalyst could be investigated.

CHAPTER 7

REFERENCES

Armendariz, A., Leith, D., (2003). A Personal Sampler for Aircraft Engine Cold Start Particles: Laboratory Development and Testing. *American Industrial Hygiene Association Journal*, *64*, 755-762.

Armendariz, A., Leith, D., Boundy, M, Goodman, R., Smith, L, Carlton, G. (2003). Sampling and Analysis of Aircraft Engine Cold Start Particles and Demonstration of an Electrostatic Personal Particle Sampler. *American Industrial Hygiene Association Journal*, *64*, 777-784.

Artaxo P., Oyola P., Martinez R. (1999). Aerosol composition and source apportionment in Santiago de Chile, *Nuclear Instruments and Methods in Physics Research Section B: Beam Interactions with Materials and Atoms, 150*(1), 409-416.

Brugge, D., Durant, J.L., Rioux, C. (2007). Near-highway pollutants in motor vehicle exhaust: A review of epidemiologic evidence of cardiac and pulmonary health risks. *Environmental Health*, *6*:23.

California Air Resource Board. (2000). *Diesel PM Control Technologies, Appendix IX*. Sacramento, CA.

Charry, J.M., Kavet, R.I. (1987). *Air Ions: Physical and Biological Aspects*. Raton, Florida: CRC Press, Boca.

Chuang, K.J., Chan, C.C., Chen, N.T., Su, T.C., Lin, L.U. (2005). Effects of Particle Size Fractions on Reducing Heart Rate Variability in Cardiac and Hypertensive Patients. *Environmental Health Perspectives, 113*(12), 1693-1697.

Ciach, T., Sosnowski, R.T. (1996). Removal of Soot Particles from Diesel Exhaust, *Journal of Aerosol Science, 27, Suppl. 1*, 705-706.

Cochet, R. (1961). Lois Charge des Fines Particules (Submicroniques) Etudes Théoretiques-Controles Récents Spectre de Particules. Coll.Int.la Physique des Forces Electrostatiques et Leurs Application. *Centre National de la Recherche Scientifique, 102,* 331-338.

Cooperman, P. (1960). A Theory for Space Charge Limited Currents with Application to Electrical Precipitation, *Transaction of American Institution of Electrical Engineers, 79*, 47-50.

Cottrell, F.G. (1908). *Art of Separating Suspended Particles from Gaseous Bodies*, U.S. Patent 895,729, August 11, 1908, 1-8.

Deutsch, W. (1922). Bewegung und Ladung der Elektrizitatstrager im Zylinderkondensator. *Annals of Physics, 68*, 335–344.

Dockery, D.W., Pope, C.A., Xu, X., Spengler, J.D., Ware, J.H., Fay, M.E., Ferris, B.G., and Speizer, F.E. (1993). An association between air pollution and mortality in six U.S. cities. *New England Journal of Medicine, 329*, 1753–1759.

Environmental Protection Agency. (1999). *Heavy-Duty Diesel Emission Reduction Project Retrofit/Rebuild Component* (EPA420-R-99-014). Boston, MA: Northeast States for Coordinated Air Use Management.

Environmental Protection Agency. (2002). *Health Assessment Document for Diesel Engine Exhaust, National Center for Environmental Assessment*. Washington, DC: Office of Research and Development.

Environmental Protection Agency. (2003). *Technical Highlights, Questions and Answers on Using a Diesel Oxidation Catalyst in Heavy-duty Trucks and Buses*. Washington, DC: Office of Transportation and Air Quality.

Environmental Protection Agency. (2004). *Final Regulatory Analysis: Control of Emissions from Nonroad Diesel Engines* (EPA420-R-04-007) Washington, DC: Office of Transportation and Air Quality.

Environmental Protection Agency. (2005). *Regulatory Announcement, Revisions to Motor Vehicle Diesel Fuel Sulfur Transition Provisions and Technical Amendments to the Highway Diesel, Nonroad Diesel, and Tier 2 Gasoline Programs*. Washington, DC. http://www.epa.gov/otaq/regs/fuels/diesel/420f05051.htm#background

European Union news. (2005). *policy positions & European Union actors online.* Retrieved in 2005 from: http://www.euractiv.com/Article?tcmuri=tcm:29-133325-16&type=LinksDossier

Evans, J.S., Tosteson, T., Kinney, P.L. (1984). Cross-Sectional Mortality Studies and Air Pollution Risk Assessment. *Environment International, 10*, 55-83.

Farzaneh, M., Allaire, M.A., Marceau, K., Lachance, P. (1994). Electrostatic capture and agglomeration of particles emitted by diesel engines. *Industry Applications Society Annual Meeting*, *Conference Record of the 1994 IEEE*, *2*, 1534 – 1537.

Farzaneh, M., Personal communication, August 2005.

Faulkner, M.G., Dubard, J.L., Gooch, J.P., McDonald, J.R., Abbott, J.H., Drehmel, D.C. (1981). Control Strategies for Particulate Emissions from Vehicular Diesel Exhaust. *Environmental International, 6*, 427-432.

Fazel, C.S., Parsons, S.R. (1924). the Current-Voltage Relation in the Corona. *Physical Review, 23*, 598.

Control of Air Pollution from New Motor Vehicles: Heavy-Duty Engine and Vehicle Standards and Highway Diesel Fuel Sulfur Control Requirements. 66 Federal Register 7,150 (January, 18, 2001)

Filleul, L., Rondeau, V., Vandentorren, S., Le Moual, N., Cantagrel, A., Annesi-Maesano, I., Charpin, D., Declercq, C., Neukirch, F., Paris, C., Vervloet, D., Brochard, P., Tessier, J.F., Kauffmann, F., Baldi, I. (2005). Twenty-Five Year Mortality and Air Pollution: Results from the French PAARC Survey. *Occupational Environmental Medicine, 62*, 453-460.

Finkelstein, M. M., Jerrett, M., Sears, M.R. (2004). Traffic Air Pollution and Mortality Rate Advancements Periods, *American Journal of Epidemiology, 160*, 173-177.

Fino, D., Specchia, V. (2008). Open Issues in Oxidative Catalysis for Diesel Particulate Abatement, *Powder Technology, 180*, 64-73.

Fraser, M. P., Yue, Z. W., Buzcu, B. (2003). Source apportionment of fine particulate matter in Houston, TX, using organic molecular markers, *Atmospheric Environment, 37*(15)*,* 2117-2123.

Garner, C.P., Dent, J.C. (1989). Microwave Assisted Regeneration of Diesel Particulate Traps, *SAE Technical Paper 890174*.

Garshick, E., Laden, F., Hart, J. E., Rosner, B., Smith, T. J., Dockery D. W., Speizer, F. E. (2004). Lung Cancer in Railroad Workers Exposed to Diesel Exhaust. *Environmental Health Prespectives, 112*(15), 1539-1543

Green Car Congress Diesel News (2005), Ford Expands Availability and Types of Particulate Filters in Europe, Retrived in 2005 from http://www.typepad.com/t/trackback/3070034

Guibet, J.C., Faure-Birchem, E. (1999). *Fuels and Engines: Technology, Energy, Environment*, (2nd edition), Paris, France: Editions TECHNIP.

Gurjar, B.R., Butler, T.M., Lawrence, M.G., Lelievel, J. (2007). Evaluation of emissions and air quality in megacities. *Atmospheric Environment*, doi:10.1016/j.atmosenv.2007.10.048

Heck, R.M., Farrauto, R. J., Gulati, S.T. (2002). *Catalytic Air Pollution Control – Commercial Technology,* (2nd edition). New York: Wiley Interscience.

Higuchi, N., Mochida, S., Kojima, M. (1983). Optimized Regeneration Consitions of Ceramic Honeycomb Diesel Particulate Filters. *SAE 830078.*

Hinds, W.C. (1999). *Aerosol Technology*: *Properties, behavior, and measurement of airborne particles*, (2nd edition), New York: Wiley Interscience.

Hoeben, W.F. (2000). Pulsed corona-induced degradation of organic materials in water. Ph.D. Thesis, Eindhoven University of Technology, The Netherlands, 2000.

Hoek, G., Brunekreef, B., Goldhohm, S., Fischer, P., Van den Brandt, P.A. (2002). Association between Mortality and Indicators of Traffic-Related Air Pollution in the Netherlands: A Cohort Study; *Lancet, 360*, 1203-1209.

Hohlfeld, M. (1824), Das Niederschlagen des Rauches durch Elektricitat; *Archiv fur dir gesammte Naturlehre*, *2*, 205-206.

Kim, J.J., Smorodinsky, S., Lipsett, M., Singer, B.C., Hodgson, A.T., Ostro, B. (2004). Traffic-related Air Pollution Near Busy Roads: The East Bay Children's Respiratory Health Study. *American Journal of Respiratory and Critical Care Medicine, 170*(5), 520-526.

Kittelson, D. B. (1998), Engines and Nanoparticles: a review. *Journal of Aerosol Science, 29*(5-6), 575-588.

Kittelson, D.B.; Arnold, M.; Watts, W.F. (1999). *Review of Diesel Particulate Matter Sampling Methods, Final Report*. Twin Cities Minnesota: Diesel Research Center, University of Minnesota, Twin Cities, Minnesota.

Kobashi, K., Hayashi, K., Aoki, H., Kurazono, K., Fujimoto, M. (1993). Regeneration Capability of Diesel Particulate Filter System Using Electric Heater, *SAE Technical Paper 930365*.

Krewski, D., Burnett, R., Goldberg, M., Hoover, K., Siemiatycki, J., Jerrett, M., Abra-hamowicz, M., and White, W. (2000a). Reanalysis of the Harvard Six Cities Study and the American Cancer Society Study of Particulate Air Pollution and Mortality. Part II: Sensitivity Analyses. Appendix F. Definition of metropolitan areas in the ACS Study. Cambridge, MA: Health Effects Institute.

Krewski, D., Burnett, R., Goldberg, M., Hoover, K., Siemiatycki, J., Jerrett, M., Abra-hamowicz, M., and White, W. (2000b). Reanalysis of the Harvard Six Cities Study and the American Cancer Society Study of Particulate Air Pollution and Mortality. Part II: Sensitivity Analyses. Appendix D. Alternate air pollution data in the ACS Study. Cambridge, MA: Health Effects Institute.

Krewski, D., Burnett, R., Goldberg, M., Hoover, K., Siemiatycki, J., Jerrett, M., Abra-hamowicz, M., and White, W. (2000c). Reanalysis of the Harvard Six Cities Study and the American Cancer Society Study of Particulate Air Pollution and Mortality. Cambridge, MA: Health Effects Institute.

Laden, F., Schwartz, J., Speizer F.E., Dockery, D. W. (2006). Reduction in Fine Particulate Air Pollution and Mortality: Extended Follow-up of the Harvard Six Cities Study, *American Journal of Respiratory and Critical Care Medicin, 173*, 667-672.

Lawless, P.A. (1996). Particle Charging Bounds, Symmetry Relations, and an Analytic Charging Rate Model for the Continuum Regime. *Journal of Aerosol Science, 27,* 191-215.

Liang, F. (2006). Composition and Formation Mechanism of Diesel Particulate Matter Associated with Various Factors from a Non-road Diesel Generator, PhD dissertation, Department of Environmental Engineering, University of Cincinnati, 2006.

Lipfert, F.W., Malone, R.G., Daum, M.L., Mendell, N.R., Yang, C.C. (1988). *A Statistical Study of the Macroepidemiology of Air Pollution and Total Mortality* (Report No. BNL 52122). Washington, DC: U.S. Department of Energy.

Lloyd, D.A. (1988). *Electrostatic Precipitator Handbook*. Philadelphia: Institute of Physics Publishing.

Lowke, J.J., D'alessandro, F. (2003). Onset corona fields and electrical breakdown criteria, *Journal of Physics D: Applied Physics, 36,* 2673-2682.

Lyyranen, J., Jokiniemi, J., Kauppinen, E., Backman, U., Vesala, H. (2004). Comparison of Different Dilution Methods for Measuring Diesel Particle Emissions. *Aerosol Science and Technology, 38*(1),12-23.

Mage, D., Ozolins, G., Peterson, P., Webster, A., Orthofer, R., Vandeweerd, V., Gwynne, M. (1996). Urban Air Pollution in Megacities of the World, *Atmospheric Environment, 30*(5), 681-686.

Manufacturers of Emission Controls Association, MECA. (2005). *Diesel Particulate Filter Maintenance: Current Practices and Experience*. Washington, D. C.

Masuda, S., Moon, J.D. (1983). Electrostatic Precipitation of Carbon Soot from Diesel Engine Exhaust. *IEEE Transactions on Industry Applications*, *IA-19* (6),1104-1111.

Matts, S., Ohnfeldt, P.O. (1964). Efficient Gas Cleaning with SF Electrostatic Precipitators. *SF Review, 6*(7), 105-122.

Mayer, A. (2003). *Encyclopaedic Article on Particulate-Filter-Systems, Particle-Traps*, Vienna, Austria: AKPF publications. http://www.akpf.org/pub/2003_particle_traps.pdf

Mayer, A., Nothiger, P., Zbinden, R., Evequoz, R. (2001). Particulate trap selection for retrofitting vehicle fleets based on representative exhaust temperature profiles. *SAE 2001-01-0187*.

Maynard, A.D., Kuempel, E.D. (2005). Airborne nanostructured particles and occupational health. *Journal of Nanoparticle Research, 7*, 587-614.

McDonald, J.R., Smith, W.B., Spencer, H.W., Sparks, L. E. (1977). A Mathematical Model for Calculating Electrical Conditions in a Wire-Duct Electrostatic Precipitation Device. *Journal of Applied Physics, 48*(6), 1977.

McLean, K.J., Lawless, P.A., Sparks, L.E., Ramsey, G.H. (1986) Negative Corona in Wire-Plate Electrostatic Precipitators. Part II: Calculation of Electrical Characteristics of Contaminated Discharge Electrodes, *Journal of Electrostatic, 18,* 219-231.

Mine Safety and Health Administration. (2003). *Diesel Particulate Matter Exposure of Underground Metal and Nonmetal Miners*; proposed rule, 30CFR part 57. Washington, DC: Federal Register.

Mine Safety and Health Administration. (2003b). *Diesel Particulate Matter (DPM) Control Technologies*, Washington ,DC: US Department of Labor. http://www.msha.gov/01-995/Coal/DPM-filterEfflist.pdf

Mizuno, A. (2000). Electrostatic Precipitation, *IEEE Transactions on Dielectrics and Electrical Insulation, 7*(5), 615-624.

Neeft, J.P.A., Makkee, M., Moulijn, J.A., Review Article: Diesel Particulate Emission Control, *Fuel Processing Technology, 47*, 1-69.

Oberdorster, G., Utell, M.J. (2002). Ultrafine particles in the urban air: To the respiratory tract–and beyond, *Environmental Health Perspective, 110,* A440–A441.
Oglesby, S., Nichols G. B. (1978). *Electrostatic Precipitation*. New York: Mercel Dekker.

Ohno, K., Shimato, N., Taoka, N., Santae, H., Ninomiya, T., Komori, T., Salvat, O. (2000). Characterization of SiC-DPF for Passenger Car. *SAE paper 2000-01-0185*.

Okubo, M., Kuroki, T., Miyairi, Y., Yamamoto, T. (2004). Low-temperature soot incineration of diesel particulate filter using remote nonthermal plasma induced by a pulsed barrier discharge. *IEEE Transactions on Industry Applications, Volume 40*(6), 1504 – 1512

Parker, K.R. (1997). *Applied Electrostatic Precipitation*; London: Blackie Academic Professional: London.

Pattas, K.N., Stamatelos, A. M., Kougianos, K. N., Koltsakis, G. C., Pistikopoulos, P. K. (1995). Trap Protection by Limiting A/F Ratio During Regeneration, *SAE Paper, Vol. 950366*.

Pattas, K., Kyriakis, N., Manikas, T., Pistikopoulos, P., Mustel, W., Rouverirolles, P. (1998). Parametric Study for a Ceramic Diesel Particulate Trap Applicaion on a Light Duty Truck. *International Jounal of Vehicle Design, 20*, 219-230.

Peek F.W. (1929). *Dielectric Phenomena in High-Voltage Engineering*. New York: McGraw-Hill.

Pope, C.A., Burnett, R.T., Thun, M.J., Calle, E.E., Krewski, D., Ito, K., Thurston, G.D. (2002). Lung Cancer, Cardiopulmonary Mortality, and Long-Term Exposure to Fine Particulate Air Pollution. *Journal of Americal Medical Association, 287*, 1132-1141.

Pope, C.A., Burnett, R.T., Thurston, G.D., Thun, M.J., Calle, E.E., Krewski, D., Godleski, J.J. (2004). Cardiovascular Mortality and Long-Term Exposure to Particulate Air Pollution: Epidemiological Evidence of General Pathophysiological Pathways of Disease. *Circulation, 109*, 71-77.

Pope, C.A., Dockery, D.W. (2006). Health effects of fine particulate air pollution: Lines that connect. *JAMA. 54*, 709-742.
Pope, C.A., Thun, M.J., Namboodiri, M.M., Dockery, D.W., Evans, J.S., Speizer, F.E., and Health, C.W. (1995). Particulate air pollution as a predictor of mortality in a prospective study of U.S. adults. *Americal Journal of Respiratory and Critical Care Medicine, 151*, 669–674.

Querol, X., Alastuey, A., Rodriguez, S., Plana, F., Ruiz, C.R., Cots, N., Massagué, G., Puig, O. (2001). PM10 and PM2.5 Source Apportionment in the Barcelona Metropolitan Area, Catalonia, Spain. *Atmospheric Environment, 35*(36), 6407-6419.

R M Harrison, R. M., Brimblecombe, P., Derwent, R.G., Dollard, G.J., Eggleston, S., Hamilton, R.S., Hickman, A.J., Holman, C., Laxen, D.P.H., Moorcroft, S. (1996). Airborne Particulate Matter in the United Kingdom. The Quality of Urban Air Review Group, May 1996, Birmingham, UK

Reist, P.C. (1992). *Aerosol Science and Technology, Second edition*. New York: McGraw-Hill Companies.

Robinson, M. (1978). Electrostatic Precipitation, in: *Electrostatic and its Applications*, New York: Wiley Interscience.

Saiyasitpanich, P., Keener, T. C., Lu, M., Khang, S. J., Evans, D. E., (2006). Collection of Ultrafine Diesel Particulate Matter (DPM) in Cylindrical Single-Stage Wet Electrostatic Precipitator. *Environmental Science and Technology, 40*, 7890-7895.

Salvat, O., Marez, P., Belot, G. (2000). Passenger Car Serial Application of a Particulate Filter System on a Common-rail, Direct-injection Diesel Engine. *SAE Paper, vol. 2000-01-0473*.

Sato, T. (1987). Charging process of Ine particles in unipolar ion Low. *Transactions on I.E.E. of Japan, 107*, 155–161.

Seaver, A.E. (1995). An Engineering Equation for Corona Devices. *IEEE Industry Applications Magazine, 1*(4), (1995) pp. 30-35.

Sharma, M., Agarwal, A.K., Bharathi, K.V.L. (2005). Characterization of exhaust particulates from diesel engine, *Atmospheric Environment, 39,* 3023–3028.

Shaughnessy, R.J., Levetin E., Blocker, J., Sublette K.L. (1994). Effectiveness of Portable Indoor Air Cleaners: Sensory Testing Results. *Indoor Air*, *4*, 179-188.

Simon, G., Stark, T. (1985). Diesel Particulate Trap Regeneration Using Ceramic Wall-Flow - Traps, Fuel Additives, and Supplemental Electrical Igniters, *SAE Paper No. 850016*.

Stayner, L., Dankovic, D., Smith, R., Steenland, K. (1998). Predicted Lung Cancer Risk Among Miners Exposed to Diesel Exhaust Particles. *American Journal of Industrial Medicine, 34,* 207-219.

Swietlicki, E., Puri, S., Hansson, H. C. (1996). Urban air pollution source apportionment using a combination of aerosol and gas monitoring techniques, *Atmospheric Environment, 30*(15)*,* 2795-2809.

Talaie, M.R., Taheri M. , Fathikalajahi, J. (2001). A new method to evaluate the voltage-current characteristics applicable for a single-stage electrostatic precipitator, *Journal of Electrostatics, 53*(3), 221-233.

Tan, P., Deng, K., Lu, J.X. (2004). Analysis of Particulate Matter Composition from a Heavy-duty Diesel Engine. *Proceeding of Institution of Mechanical Engineers, 218, Part D: J. Automobile Engineering.*

Thimsen, D.P., Baumhard, K.J., Kotz, T.J., Kittelson, D. B. (1990). The Performance of an Electrostatic Agglomerator as a Diesel Soot Emission Control Device, *SAE 900330*.

Townsend, J.S. (1915). *Electricity in Gases.* Oxford: Clarendon Press.

Trichel, G.W. (1938). The Mechanism of the Negative Point-to-Plane Corona Near Onset. *Physical Review 54*, 1078.

Turner, J.H., Lawless, P.A., Yamamoto, T., Coy, D.W., Greiner, G.P., McKenna, J.D., Vatavuk, W.M. (2000). Electrostatic Precipitators, in *Air Pollution Engineering Manual, (2nd edition)*. Air and Waste Management Association. New York: Wiley Interscience.

U.S. Department of Energy, Engine Manufacturers Association, & Manufacturers of Emission Controls Association. (2000). *Diesel Emission Control – Sulfur Effects (DECSE) Program, Phase I Interim Data Report No. 4: Diesel Particulate Filters –Final Report.* Washington, DC.

U.S. Department of Energy. (2004). *Diesel Particulate Filters, Market Introduction in Europe: Reviews and Status*. Washington, DC. http://www.eere.energy.gov/vehiclesandfuels/pdfs/deer_2004/session12/2004_deer_seguelong2.pdf

U.S. Environmental Protection Agency. (1998). *Stationary Source Control Techniques Document for Fine Particulate Matter* (EPA-452/R-97-001). Research Triangle Park, NC.

Unger, L., Bouland, D., Borra, J.P. (2004). Unipolar Field Charging of Particles by Electrical Discharge: Effect of Particle Shape. *Journal of Aerosol Science*, *35*, 965-979.
Van Setten, B.A.A.L., Makkee, M., Moulijn, J.A. (2001). Science and Technology of Catalytic Diesel Particulate Filters. *Catalysis Reviews, 43,* 489-564.

Vedal, S. (1997). Ambient Particles and Health: Lines that Divide. *Journal of Air & Waste Management Association, 47*, 551-581.

Volckens, J, Leith, D. (2002), Electrostatic Sampler for Semivolatile Aerosols: Chemical Artifacts. *Environmental Science and Technology*, 36, 4608-4612.

Wade, W.R., White, J.E., Florek, J.J., Cikanek, H.A. (1983). Thermal and Catalytic Regeneration of Diesel Particulate Traps, *SAE paper 830083.*

Wadenpohl, C., Loffler, F. (1994). Electrostatic Agglomeration and Centrifugal Separation of Diesel Soot Particles. *Chemical Engineering and Processing, 33*, 371-377

Walker, A.P. (2004). Controlling Particulate Emissions from Diesel Vehicles. *Topics in Catalysis, 28*, 165-170.

Washington State Educational Service Districts. (2003). *Washington State School Bus Retrofit Program Reference Manual* (Publication Number 03-02-016). http://www.pscleanair.org/programs/dieselsolutions/buses/ds_school_ref_man.pdf

White, H.J. (1963). *Industrial Electrostatic Precipitation.* Reading, MA: Addison-Wesley Publishing Company.

White, H.J. (1977). Electrostatic Precipitation of Fly Ash; *Journal of the Air Pollution Control Association*., *27,* 15-21.

White, H.J. (1955). Modern Electrostatic Precipitation. *Industrial & Engineering Chemistry research*, *47*(5), 932-939.

Yao S., Okumoto M., Madokoro K., Yashima T., Shimogami, J., Suzuki, E. (2004). Diesel particulate matter and NOx removal using a pulsed corona surface discharge. *American Institute of Chemical Engineers Journal, 50 (3),* 715-721.

Zelenka, P., Cartellieri, W., Herzog, P. (1996). Worldwide Diesel Emission Standards, Current Experiences and Future Needs. *Applied Catalysis B: Environmental 10*, 3-28.

Zhang-Steenwinkle, Y., Van der Zande, L. M., Castricum, H.L., Bliek, A., Van den Brink, R.W., Elzinga, G. D. (2004). Microwave-assisted Regeneration of a Perovskite Coated Ceramic Monolith Soot Trap. *Topics in Catalysis, 30/31*, 57-260.

Zheng, H., Keith, J. M. (2007). Averaging Theory for Diesel Particulate Filter Regeneration, *American Institute of Chemical Engineers, 53*(5), 1316-1324.

CHAPTER 8

PUBLICATIONS

Journal Articles

Armendariz AJ, Farnoud A, Boger W: [manuscript under revision] "Properties of Small-Scale Electrostatic Precipitators with Very Fine Wires," reviewed by the Journal of Occupational and Environmental Hygiene.

Armendariz AJ, Farnoud A: [manuscript under revision] "The Effect of Wire Diameter on Small-Scale Electrostatic Precipitators," reviewed by the Journal of Electrostatics.

Armendariz AJ, Farnoud A: [manuscript under revision] "Electrical Characteristics of Small-Scale Electrostatic Precipitators," reviewed by the Journal of the Air and Waste Management Association.

Proceedings

Armendariz AJ, Farnoud A, Huang C: [2008] "Using Electrostatic Precipitation to Control Diesel Exhaust Particulate Emissions," the Proceedings of the 12th Mine Ventilation Symposium, Reno, NV, June 9-11.

Farnoud A, Armendariz AJ: [2008] "Diesel Exhaust Treatment Using an Electrostatic Precipitator," proceedings of the Air and Waste Management Association Annual Conference, Portland OR, June 24-27.

Farnoud A, Armendariz AJ: [2007] "Fundamental Electrical Properties of a Small-Scale Electrostatic Precipitator," the proceedings of the American Association for Aerosol Research Annual Conference, Reno, Nevada, September 24-28.

Farnoud A, Armendariz AJ: [2007] "A Compact System for the Generation & Sampling of Diesel Particulate Matter," proceedings of the American Association for Aerosol Research Annual Conference, Reno, Nevada, September 24-28.

Farnoud A, Armendariz AJ: [2007] "Electrostatic Control of Particulate Emissions from Diesel-Powered Machinery," proceedings of the American Association for Aerosol Research Annual Conference, Reno, Nevada, September 24-28.

Farnoud A, Armendariz AJ: [2007] "Design and Performance of a Small-Scale Electrostatic Precipitator for Diesel Particulate Control," proceedings of the Annual Conference of the Air and Waste Management Association, Pittsburgh, PA, June 26-29.

Farnoud A, Armendariz AJ: [2007] "A Compact System for the Generation and Sampling of Diesel Exhaust Particulate," Proceedings of the Annual Conference of the Air and Waste Management Association, Pittsburgh, PA, June 26-29.

Dissertations

Farnoud A: [2008] Electrostatic Removal of Diesel Particulate Matter, Ph.D. Thesis, Southern Methodist University.

CHAPTER 9

INCLUSION AND MATERIALS STATEMENTS

(1) This project has not involved the use of human test subject. Therefore, the gender and minority inclusion provisions of PHS-2590 are not applicable.

(2) This project has not involved the use of adult or child test subjects. Therefore, the inclusion of children provisions of NIH and PHS398 are not applicable.

(3) This project has resulted in the development of empirical data on the electrostatic properties of small-scale electrostatic precipitators. The PI is actively working to publish the data in relevant peer-reviewed journals. Much of the data has already been presented at scientific conferences and is available in the proceedings for those conferences. In addition, the data is included as a core component of the dissertation of Ali Farnoud, the doctoral student who worked on this project. His dissertation is available from the Southern Methodist University Central Library. The PI and Dr. Farnoud are eager to share the data and the other results of their study with interested researchers.